TAMPEREEN TEKNILLINEN YLIOPISTO
TAMPERE UNIVERSITY OF TECHNOLOGY

Jonna Paajaste

GaSb-Based Gain and Saturable Absorber Mirrors for Lasers Emitting at 2–2.5 µm

Julkaisu 1182 • Publication 1182

Tampere 2013

Tampereen teknillinen yliopisto. Julkaisu 1182
Tampere University of Technology. Publication 1182

Jonna Paajaste

GaSb-Based Gain and Saturable Absorber Mirrors for Lasers Emitting at 2–2.5 µm

Thesis for the degree of Doctor of Science in Technology to be presented with due permission for public examination and criticism in Tietotalo Building, Auditorium TB104, at Tampere University of Technology, on the 28th of November 2013, at 12 noon.

Tampereen teknillinen yliopisto - Tampere University of Technology
Tampere 2013

ISBN 978-952-15-3193-4 (printed)
ISBN 978-952-15-3198-9 (PDF)
ISSN 1459-2045

Abstract

The GaSb material system enables reaching the 2–3.5 μm wavelength range, which is important for many applications. Optically-pumped semiconductor disk lasers are attractive for producing high-power, high-brightness laser radiation with the wavelength controlled by the selection of materials. Such lasers can be quite compact, offer good beam quality, and produce ultra-short pulses by mode-locking with a semiconductor saturable absorber mirror.

This thesis is concerned with the development of GaSb-based heterostructures for novel laser sources (i.e. semiconductor disk lasers) operating at 2–2.5 μm wavelengths, with both continuous wave and pulsed operation. In particular, the thesis includes new results concerning the development of GaSb/(AlGaIn)(AsSb) semiconductor disk lasers emitting high-power with broad wavelength tunability of about 50–150 nm. The broad tunability has been achieved by employing quantum wells with different operation wavelengths with asymmetric positioning in the microcavity.

GaSb-based nonlinear saturable absorber mirrors were also studied and novel techniques related to their fabrication are presented. A semiconductor saturable absorber mirror was successfully used to mode-lock a high-power disk laser at 2 μm wavelength. Naturally fast absorption recovery of the absorber mirror was discovered and several techniques to control it were studied. Unlike for more conventional absorber materials, low-temperature growth revealed no relation to absorption recovery time. Instead the absorption recovery time could be changed by tailoring the strain and energy band structure in quantum wells and by using an optical cavity design with surface proximity quantum wells.

Acknowledgements

The work presented in this thesis was carried out at the Optoelectronics Research Centre (ORC), Tampere University of Technology, during the years 2006–2013. The work has been supported in part by the National Graduate School of Material Physics, The Finnish Founding Agency for Technology and Innovation (TEKES), the European Union, the Academy of Finland, Finnish Foundation of Technology (TES), Jenny and Antti Wihuri Foundation, and the Technology Industries of Finland Centennial Foundation.

I would like to start by thanking my Ph.D. supervisor Prof. Mircea Guina for his enthusiasm, the professional knowledge in the field, and for securing the funding required for my work. I gratefully thank my supervisor and the team leader of the SSMBE10-2 group, Dr. Soile Suomalainen, who has supported me all the way from an undergraduate student, to my master's degree, and finally to my dissertation. Thank you for always having time for my questions and for having good ideas when I needed the guidance.

I also wish to acknowledge Emeritus Prof. Markus Pessa for giving me the opportunity to work at ORC, and for creating an environment that encourages researchers for high level research and new innovations. I thank Dr. Pekka Savolainen for managing ORC well, and making it easy for me to do my job. For the same reason I also want to acknowledge the work of Anne Viherkoski and Eija Heliniemi concerning all the administrative issues.

My publications have been a result of very intense team work. Special thanks go to my dear colleague Riku Koskinen for solving endless problems with me, spending endless hours at the lab with me, and listening to my endless yapping for seven years! I also want to thank Dr. Antti Härkönen and Dr. Lasse Orsila for both the facts and the fun, no topic is off-limits with these guys. I am also grateful to Antti for his excellent work

with our SDLs and all the help with the publications. I wish to acknowledge the work of Christian Grebing and Jukka-Pekka Alanko concerning the mode-locking experiments and the work of Jussi Rautiainen on SDL characterization. I thank Prof. Oleg Okhotnikov and Jari Nikkinen for our co-operation on the 2.5 μm SDL. I am grateful to Teemu Hakkarainen for all the help in trying to understand the Auger recombination and for Dr. Antti Laakso for providing the energy level simulations. I also wish to acknowledge Prof. Günter Steinmeyer and Prof. Uwe Griebner for their work on our SESAM publications, the pump probe measurements and the mode-locking experiment performed at the Max Born Institute, Berlin.

One of the most significant resources of ORC is the positive atmosphere and the high team spirit. I would like to thank everyone at ORC, and I start with the people who introduced me to semiconductor science and technology, Dr. Mika Saarinen, Dr. Jari Lyytikäinen, Dr. Antti Tukiainen, and Dr. Tomi Leinonen. I want to express my gratitude also to the rest of the "younger" generation of MBE group not already mentioned: Ville-Markus, Arto, Sanna, Janne, Miki, and J-P, for being the best colleagues one can have. I also wish to thank all the users of Semipub and Voltti; our discussions have been marvellous, mind-blowing, eccentric or sometimes even simply tasteless, but they kept me going, together with the terrible coffee.

I am also grateful to my parents for encouraging me to study, and for supporting me even when my choices were not always what you expected. I thank my sister Jutta for always being one of my best friends and an ally in life, no matter what. Big thanks also to all my friends, you are the best! Finally I wish to thank my significant other, "il mio lui" Miika, for being the voice of reason for me; never putting me down, but always lifting me up, helping me to find my courage all the way to my doctorate.

Pisa, Italy, 2013
Jonna Paajaste

Contents

List of Publications

This thesis is a compendium, which contains some unpublished material, but is mainly based on the following papers published in open literature.

[P1] J. Paajaste, S. Suomalainen, R. Koskinen, A. Härkönen, M. Guina, M. Pessa, "High-power and broadly tunable GaSb-based optically-pumped VECSELs emitting near 2-μm", *Journal of Crystal Growth*, Vol. 311, No. 14, pp. 1917–1919, (2009)

[P2] A. Härkönen, J. Paajaste, S. Suomalainen, J.-P. Alanko, C. Grebing, R. Koskinen, G. Steinmeyer, M. Guina, "Picosecond passively mode-locked GaSb-based semiconductor disk laser operating at 2 μm", *Optics Letters*, Vol. 35, No. 24, pp. 4090–4092 (2010)

[P3] J. Paajaste, J. Nikkinen, R. Koskinen, S. Suomalainen, O.G. Okhotnikov, "Power scalable 2.5 μm (AlGaIn)(AsSb) semiconductor disk laser grown by molecular beam epitaxy", *Journal of Crystal Growth*, Vol. 323, No. 1, pp. 454–456, (2011)

[P4] J. Paajaste, S. Suomalainen, R. Koskinen, A. Härkönen, G. Steinmeyer, M. Guina, "GaSb-based semiconductor saturable absorber mirrors for mode-locking 2 μm semiconductor disk lasers", *Physica Status Solidi C*, Vol. 9, No. 2, pp. 294–297, (2012)

[P5] J. Paajaste, S. Suomalainen, A. Härkönen, U. Griebner, G. Steinmeyer, M. Guina "Absorption recovery dynamics in 2 μm GaSb-based SESAMs", *Journal of Physics D*, **Revised October 2013**

Author's contribution

The work presented in this dissertation is a part of teamwork which has involved semiconductor crystal growth, material characterization, sample processing, laser characterization and theoretical simulations. The author's main contribution in all the papers has been the design, fabrication, and characterization of the semiconductor heterostructures. A more detailed description of author's contribution on research work and preparing the scientific papers is given below.

In [P1] the author designed and fabricated the laser gain mirrors and performed the preliminary material characterization. The author wrote the first draft of the paper, refined it with help of co-authors and was also the corresponding author.

In [P2] the author fabricated the laser and semiconductor saturable absorber mirror material and did the preliminary material characterization. The author helped the co-authors to refine the paper.

In [P3] the author designed and fabricated the laser gain material and did the preliminary material characterization. The author wrote the first draft of the paper, refined it with help of co-authors and was also the corresponding author.

In [P4] the author designed and fabricated the semiconductor saturable absorber mirror material, designed measurements, conducted most of them and analyzed the results. The author wrote the first draft of the paper, refined it with help of co-authors and was also the corresponding author.

In [P5] the author designed and fabricated the semiconductor saturable absorber mirror material, designed measurements, conducted most of them and analyzed the results. Author wrote the first draft of the paper, refined it with help of co-authors and was also the corresponding author.

List of Abbreviations and Symbols

Ag	Silver
Al	Aluminium
AlAs	Aluminium-arsenide
AlAsSb	Aluminium-arsenide-antimonide
AlGaAs	Aluminium-gallium-arsenide
AlGaAsSb	Aluminium-gallium-arsenide-antimonide
AlGaSb	Aluminium-gallium-antimonide
AR	Antireflective
As	Arsenic
Au	Gold
BF	Birefringent filter
BEP	Beam equivalent pressure
CHCC	A type of auger recombination
cw	Continuous wave
DBR	Distributed Bragg reflector
DFB	Distributed feedback laser
FP	Fabry–Pérot
FWHM	Full width at half maximum
Ga	Gallium
GaAs	Gallium-arsenide
GaInAsSb	Gallium-indium-arsenide-antimonide
GaInNAs	Gallium-indium-nitride-arsenide

GaInSb	Gallium-indium-antimonide
GaN	Gallium-nitride
GaSb	Gallium-antimonide
hh	Heavy hole
HR	High reflective
In	Indium
InGaAs	Indium-gallium-arsenide
InGaAsP	Indium-gallium-arsenide-phosphide
InGaP	Indium-gallium-phosphide
InP	Indium-phosphide
IR	Infrared
LD	Laser diode
lh	Light hole
LIDAR	Light detection and ranging
MBE	Molecular beam epitaxy
MIR	Mid-infrared
OC	Output coupler
OP-SDL	Optically-pumped semiconductor disk laser
ORC	Optoelectronics Research Centre
OSA	Optical spectrum analyzer
PL	Photoluminescence
QD	Quantum dot
QW	Quantum well
RF	Radio frequency
RPG	Resonant periodic gain
RT	Room temperature
RWG	Ridge waveguide laser
SDL	Semiconductor disk laser

Sb	Antimony
so	Spin split-off
SESAM	Semiconductor saturable absorber mirror
SHG	Second-harmonic generation
Tm,Ho:YAG	Thulium,Holmium-doped yttrium-aluminium-garnet
Tm:YAG	Thulium-doped yttrium-aluminium-garnet
VCSEL	Vertical-cavity surface-emitting laser
VECSEL	Vertical-external-cavity surface-emitting laser
XRD	X-ray diffraction

Symbols, Greek alphabet

α	Absorption coefficient
α_0	Unsaturated absorption coefficient
$\Delta\lambda_{99\%}$	Bandwidth of $R \geq 99\%$ reflectivity band
ΔR	Modulation depth
ε_{ZZ}	Strain
λ	Wavelength
λ_B	Bragg wavelength
λ_{OP}	Operation wavelength
λ_{SB}	Stopband center waelength
τ_{rec}	Absorption recovery time
τ_1	Absorption recovery time fast component
τ_2	Absorption recovery time slow component
ϕ	Phase

Symbols, other

C_{i}	Weight factor corresponding to activation energy E_{acti}
E_{acti}	Activation energy for carrier escape
E_{C}	Conduction band energy
E_{V}	Valence band energy
F_{sat}	Saturation fluence
I	Intensity of light
I_{sat}	Saturation intensity
I_{Auger}	Auger recombination current
L	Cavity length
M^2	Beam quality factor
N	Number of DBR layer pairs, $N = 1, 2, 3, ...$
P	Optical power
Q	Quality factor of a laser cavity
R	Reflectivity
R_{S}	Reflectance maximum at saturation
T	Temperature
T_{QW}	Quantum well growth temperature
c	Speed of light in vacuum
d	Thickness, nonlinear coefficient
d_{eff}	Effective nonlinear coefficient
k	Boltzmann's constant
m	An integer, $m = 1, 2, 3, ...$
n	Refractive index
n_{high}	Refractive index of high index layer
n_{low}	Refractive index of low index layer
n_{eff}	Effective refractive index
t	Time

Chapter 1

Introduction

After the first laser was invented by T. H. Maiman in the 1960's [1], the evolution of lasers has been rapid [2, 3], having a major effect on our everyday lives. However, while already commercialized, the laser development is still ongoing. The existing applications have uncharted potential and the development of new techniques and designs related to lasers and nanotechnology enable the realization of new innovations. For new applications the development of lasers requires the right combination of wavelength, power, efficiency, size, and spectral features.

The development of optoelectronic components at mid-infrared wavelength region has recently attracted more attention due to many emerging applications. For example, at the wavelength range of 2–5 μm there exist many fundamental absorption lines of atmospheric pollutants and residual gases of industrial processes. The absorption can be monitored by using spectroscopic techniques and light sources and detectors operating at this wavelength range [4, 5]. Adding to the importance of environmental issues, the 2–3 μm wavelength range offers solutions also for many other fields such as medical applications, light detection and ranging, and free space optical communication [4, 6].

The available semiconductor materials for lasers and detectors to cover the mid-infrared wavelength range are quite limited. Table 1.1 presents the state-of-the-art results prior to this work for the 2–3 μm semiconductor lasers, revealing clearly that the GaSb/(AlGaIn)(AsSb) material group is dominant. This is due to the narrow bandgap that is common in these heterostructures but nearly inaccessible for other semiconductor

material groups [7].

Besides the narrow band gap, the GaSb material system provides many other advantages for device developments, such as the use of lattice-matched distributed Bragg reflectors (DBRs) comprising layers with a high refractive index contrast. Such DBRs have an exceptionally broad stopband ($\sim$300 nm [8]) and require a relatively small number of layer pairs to achieve high reflectance. The broad stopband makes GaSb-based vertical-cavity lasers highly interesting for spectroscopic applications requiring a wide tuning range.

Table 1.1: State of the art lasers for 2–3 μm by the year 2008. (Semiconductor disk laser (SDL), Distributed feedback laser (DFB), Ridge waveguide laser (RWG) and Laser diode (LD))

λ (μm)	Power / T (W) / ($^\circ$C)	Laser type	QW / Barrier / Waveguide	Ref.
2	5 / -15	SDL	GaInSb / AlGaAsSb	[9]
2.33	0.6 / -18	SDL	GaInAsSb / AlGaAsSb	[10]
2.6	0.002 / 5	DFB	GaInAsSb / AlGaAsSb	[11]
2.8	0.008 / RT	RWG	GaInAsSb / GaSb / AlGaAsSb	[12]
3	0.130 / RT	LD	GaInAsSb / AlGaInAsSb / AlGaAsSb	[13]

Very compact electrically pumped edge emitting lasers, i.e. laser diodes (LD) have been developed [14–16] and are available commercially. Yet, such lasers have modest performance in terms of output-power and beam quality. Alternatively, an optically pumped semi-conductor disk laser (SDL) [17] provides a good quality, nearly diffraction-limited beam and output powers much higher than a single-mode laser diode. Compared to VCSELs, the well-established vertical cavity surface emitting lasers, the SDLs are more advantageous in terms of fabrication complexity; there is no need for doping associated with electrical injection and their processing is more straightforward. Moreover, the external cavity configuration enables the use of intra-cavity filters for wavelength tuning [8, 18] and semiconductor saturable absorber mirrors (SESAMs) for pulsed laser operation via mode-locking. Prior to this work, the operation of high-power SDLs was achieved at low temperatures and the tuning range was not explored.

In addition of continuous wave *cw* SDLs, GaSb-based material system enables the development of SESAMs at mid-IR wavelengths and consequently pulse generation via mode-locking or Q-switching. While still being an emerging technology, currently there is not much information available on the properties and growth technology of GaSb-based SESAMs. For the development of laser sources exploiting SESAMs, the control of absorption recovery times is essential [19] and thus the study of GaSb-based SESAMs is needed.

The first aim of this thesis was to develop GaSb-based gain mirrors for SDLs. The other important challenge pursued in the work concerned the fabrication of SESAMs for mode-locking SDLs and a systematic study of their ultrafast non-linear response. Collateral developments, not included in the thesis, have concerned development of 2 μm LDs [14], development of SESAMs for a Q-switched solid state laser [20], and use of 2 μm SESAMs in mode-locked solid-state lasers [21, 22].

This thesis is structured to serve as an introduction to the development of mid-infrared GaSb-based SDLs and SESAMs. A summary of the research reported in the five original research papers, included as part of the dissertation, is presented. First, the physics and technology related to GaSb-based heterostructures are explained in Chapter 2. In Chapter 3, the results on high-power and broadly tunable SDLs, part of [P1] and [P3], are summarized. The techniques presented in [P4] and [P5] to control absorption recovery time in GaSb-based SESAMs, are discussed in Chapter 4. Some examples of ultrashort pulse generation ([P2] [23]) are shown in Chapter 5 and finally, the main results are summarized in Conclusions.

Chapter 2

Physics and technology of GaSb-based optical devices operating at 2–3 μm

This chapter introduces the main characteristics of the (AlGaIn)(AsSb) material group and the basic concepts concerning heterostructure fabrication by molecular beam epitaxy (MBE). The design and theory of GaSb-based SDLs and SESAMs are also presented.

2.1 Near mid-IR materials

The III–V semiconductor material system (AlGaIn)(AsSb) establishes a firm platform for optoelectronic devices operating near the mid-infrared spectral range (2–3 μm). Figure 2.1 represents energy gaps and lattice constants for several semiconductor material groups with varying compositions. Some common ternary compounds are presented by the lines connecting the binary compounds. With the right combination of material and composition, both lattice constant and operating wavelength can be chosen to suit nearly any application of choice. As it can be seen from the figure, for infrared wavelength range, the (AlGaIn)(AsSb) material system is a good choice.

Nearly all materials in the scope of this thesis are lattice-matched to a GaSb substrate, meaning that their compositions are selected to minimize the strain in the heterostructure. $Ga_xIn_{1-x}As_ySb_{1-y}$ can be used as a direct bandgap gain material, either lattice-matched or as an intentionally strained layer covering emission/absorption from 1.7 μm to over

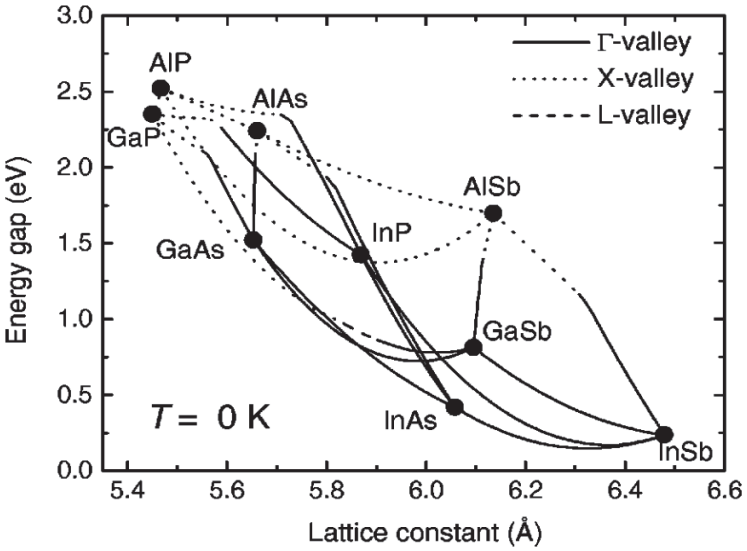

Figure 2.1: The dependence of the bandgap energy and lattice constant in III–V semiconductor materials. Reprinted with permission from [7]. Copyright 2001, AIP Publishing LLC.

3 μm. It has always a direct band gap independent from the In-composition, which is essential for optoelectronic devices. In terms of fabrication simplicity, binary and ternary compounds are usually favored, but the use of quaternary compounds increases the degree of freedom to control parameters such as energy gap and strain. Figure 2.2 presents the energy band edge positions for $Ga_xIn_{1-x}As_ySb_{1-y}$ as a function of In-composition. As shown in the figure, the band alignment of $Ga_xIn_{1-x}As_ySb_{1-y}/Al_xGa_{1-x}As_ySb_{1-y}$ heterostructure varies with In-composition and the strain. Hence, compressive strain is favoured especially at longer wavelengths, since it ensures better carrier confinement for all In-compositions.

As $Ga_xIn_{1-x}As_ySb_{1-y}$ is a typical gain material, the GaSb and $Al_xGa_{1-x}As_ySb_{1-y}$ materials are often used as the mirror, barrier and waveguide materials. Al_xGa_{1-x}-As_ySb_{1-y} materials are suitable for the barrier and waveguide layers of III-Sb-based semiconductor lasers because of their larger energy gap and smaller refractive index which is beneficial especially in mirror structures. One of the reasons for choosing $Al_xGa_{1-x}As_ySb_{1-y}$ is that the barrier and cladding layers are normally quite thick and need to be grown lattice-matched to GaSb. In $Al_xGa_{1-x}As_ySb_{1-y}$ the lattice-matching is

achieved for $(AlAs_{0.08}Sb_{0.92})_x(GaSb)_{1-x}$ compositions.

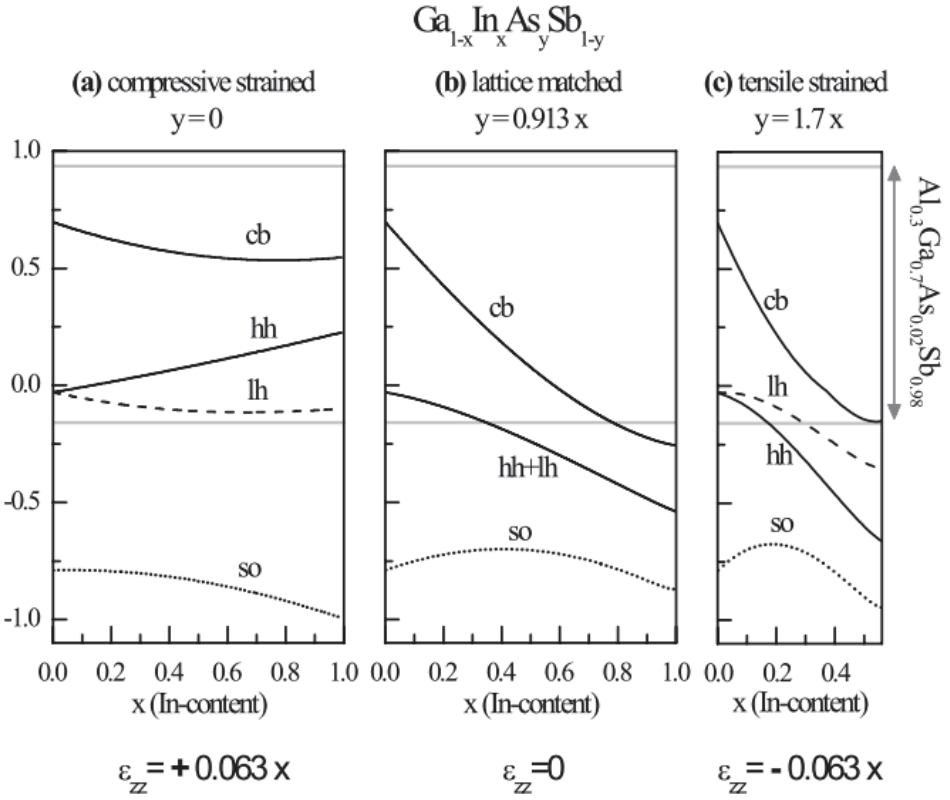

Figure 2.2: Relative position of energy bands in $Ga_xIn_{1-x}As_ySb_{1-y}$/GaSb for different lattice strain and In-composition. Notations cb, hh, lh, and so stand for conductance, heavy hole, light hole and spin split-off bands respectively. ε_{ZZ} is lattice strain represented as a function of In-fraction. Reprinted with permission from [24]. Copyright 2006, Springer.

Besides lattice mismatch, in the case of $Ga_xIn_{1-x}As_ySb_{1-y}$ and $Al_xGa_{1-x}As_ySb_{1-y}$ compounds, there is also a miscibility gap that needs to be considered. Miscibility gap is a group of compositions that cannot achieve a permanent ordered structure. These compounds are metastable depending on the growth temperature and material composition. An example of miscibility gap for $Al_xGa_{1-x}As_ySb_{1-y}$ is shown in Figure. 2.3. As it can be seen, it has a strong growth temperature dependence and thus for $Al_xGa_{1-x}As_ySb_{1-y}$ it is essential to choose the growth temperature and composition in the right manner. Miscibility will manifest itself mainly as generic greyness since there is no ordered crys-

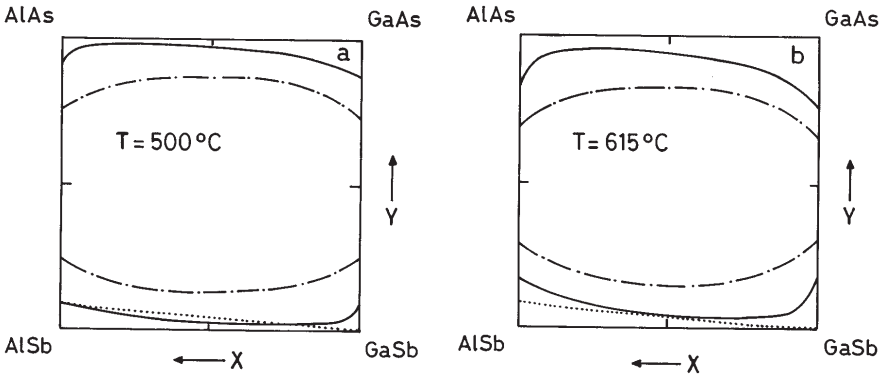

(a) (b)

Figure 2.3: The miscibility gap of quaternary $Al_xGa_{1-x}As_ySb_{1-y}$ for two temperatures. Point line indicates lattice-matching condition to GaSb, solid and point–dash line the boundaries of miscibility. Reprinted with permission from [25]. Copyright 1992, Elsevier Limited.

talline structure. The greyness is visible to human eye under polarised light at fixed angles and also when viewed with an optical microscope. It can also be verified by measurements such as high resolution x-ray diffraction (XRD).

2.2 Molecular beam epitaxy of GaSb

Many techniques can be used for semiconductor fabrication, the choice depending on the desired structure complexity, layer thicknesses and required interface quality. Molecular beam epitaxy (MBE) is a crystal growth technique in which a flux of atoms or molecules is directed to a heated single crystal substrate in ultra-high vacuum (UHV) (pressure $< 10^{-9}$ mbar). In UHV conditions, the atoms incorporate at the surface as a result of physical mechanisms and chemical reactions and repeat the lattice structure of the underlying single crystal substrate. The desired growth mode is Frank van der Merwe, i.e. layer by layer –growth, when the layer thicknesses in heterostructures are defined by atomic layer precision [26]. With thin layers of few nanometers or even less, sharp and precise interfaces are essential to maintain the desired pure layer structure. A detailed review of MBE technology for different material systems has been recently published

in [27].

The semiconductor structures presented in this work were grown using a conventional solid source molecular beam epitaxy reactor (VG ten-port V80H). A schematic of a MBE system is presented in Figure 2.4. Elemental In, Al and Ga together with As_4 and Sb_4 were used as group III and V sources respectively. The group V constituents were cracked into As_2 and Sb_2 using high temperature cracking tubes. All structures were grown on an n-GaSb (100) wafer.

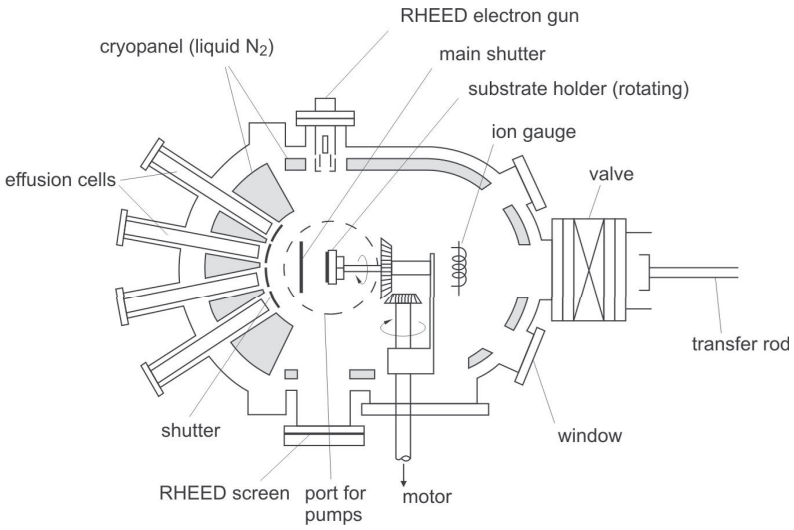

Figure 2.4: MBE reactor schematic. Reprinted with permission from [28]. Copyright 2009, Springer.

In MBE growth, the most important growth parameters that can be regulated during the process, are the grown materials, substrate temperature, and the atomic fluxes on the substrate (and thus the growth rate). The temperature of the substrate determines the reactions at the surface via its role on Arrhenius activated reactions and mechanisms [26]. The optimal temperature depends on the grown material and for GaSb based materials, the temperature varies from 480–500 °C for In-compounds, around 560 °C for GaSb, and temperatures a bit over 600 °C for Al-compounds.

The growth rate in MBE is governed by the atomic flux of group III species, and the growth is performed in group V overpressure. Typically, the growth rates are in the order

of one μm per hour. The beam equivalent pressure (BEP) ratios of V/III fluxes measured at the gauge depend on the grown material: for GaSb they are around 5–6, for Al-compounds 20 or higher. During growth, the group V flux is always present for temperatures over 300 °C. Also for both quaternary systems in this thesis ($Ga_xIn_{1-x}As_ySb_{1-y}$ and $Al_xGa_{1-x}As_ySb_{1-y}$), the III-V material is always grown with a group V overpressure, which is why for several group V constituents, the mutual composition has to be calibrated to find the correct combination of material source fluxes and growth temperature.

2.3 Semiconductor disk lasers

The semiconductor disk lasers (SDLs), also known as vertical-cavity surface-emitting lasers (VECSELs), are a new class of laser sources that have been developed rapidly during the last decade [17, 29]. In an SDL, the cavity is formed vertically by a semiconductor heterostructure including a semiconductor mirror, i.e. gain mirrors, and one or more external mirrors.

Such lasers have emerged at the frontier between the simple directly-emitting semiconductor lasers and the more complicated solid-state lasers. The simplicity to engineer the emission properties of semiconductors is thus combined with the functionality of solid-state lasers enabled by the use of external cavity elements. Ultimately, this concept renders possible emission in a broad wavelength range with high output power scalable up to 100 W [30], high beam quality, capability to fill spectral gaps that cannot be reached by traditional solid state disk lasers (i.e. current wavelength coverage is from 240 nm [31] to 5000 nm [32] but not without gaps), and broad wavelength tuning (i.e. easily several tens of nm but could be as high as 150 nm for GaSb SDLs [P1]). The state of the art results for SDLs are shown in Figure 2.5.

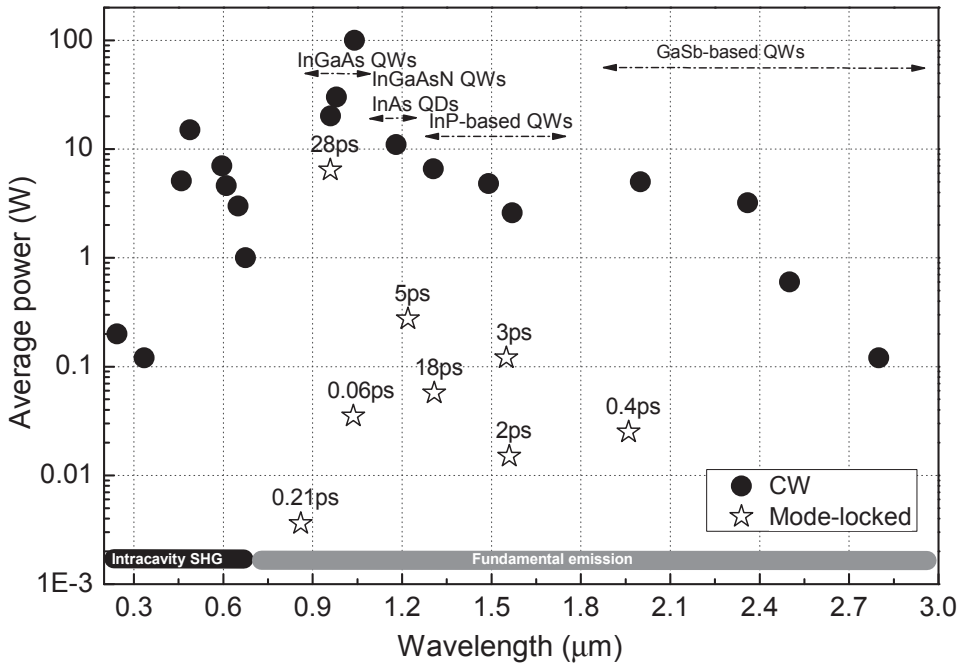

Figure 2.5: Selection of SDL results showing the maximum average power reached at different wavelengths. InGaAs(N)-based gain materials dominate the results up to 1.3 μm, above which InP-based and GaSb-based QWs are used. Only SDLs incorporating single gain chips are included. Pulse durations related to mode-locked results are given in picoseconds. [31, 33–52][P2–P3]

2.3.1 Design of the GaSb gain mirrors

An SDL gain mirror consists of a distributed bragg reflector mirror (DBR), an active region and a window layer as shown in Figure 2.6. The window layer material has a larger energy gap than the active region, thus preventing carrier migration to the surface and losses caused by surface recombination as well as adding to the efficiency in active region recombination. The active region can comprise, for example, bulk material [53], quantum dots (QDs) [54] or quantum wells (QWs), latter of which are studied here.

The DBR is a high quality multilayer thin film, which reflects radiation only at its stopband wavelength region, which can be tailored to the desired wavelength by modifying the layer thicknesses. A DBR stack consists of layers of two materials with high

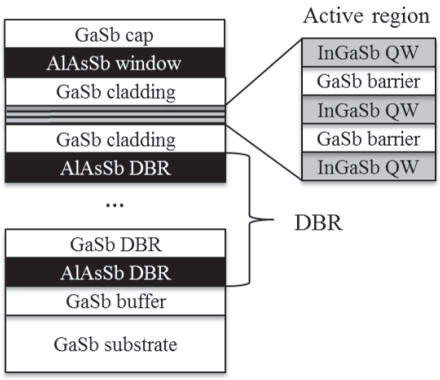

Figure 2.6: Schematic of an example SDL mirror design. The number of DBR layers and QWs may vary.

n_{high} and low n_{low} refractive indices and precise layer thicknesses. The optical thickness of each layer is a quarter of the desired operating wavelength and the operation is based on the constructive interference of Fresnel reflected waves from the layer interfaces [55]. When reflecting from the lower refractive index material, the wave exhibits a phase shift of 180 degrees while the reflection for high refractive index material does not cause a phase shift [55]. The overall interference from all the interfaces will result in a total reflectance R:

$$R = \left[\frac{1-(n_{\text{low}}/n_{\text{high}})^{2N}}{1+(n_{\text{low}}/n_{\text{high}})^{2N}}\right]^2 \tag{2.1}$$

where N is the total number of layer pairs. The width of the stopband, i.e. spectral region of high-reflectivity, can be obtained from

$$\Delta\lambda_{SB} = \frac{2\lambda_{\text{SB}}\Delta n}{\pi n_{\text{eff}}} \tag{2.2}$$

where λ_{SB} is the center of the stopband, Δn the refractive index difference of the layers and n_{eff} the effective refractive index defined by

$$n_{\text{eff}} = 2\left[\frac{1}{n_{\text{low}}}+\frac{1}{n_{\text{high}}}\right]^{-1} \tag{2.3}$$

From these equations it can be seen that the reflection is higher for a high refractive index difference or an increased number of layers. In practice the number of layers is minimized due to technological constrains (e.g. to minimize the growth time and ensure stable molecular fluxes during epitaxy). Another reason to limit the number of DBR pairs in SDL applications is the thermal management of the laser; a thicker DBR is less heat conducting and will cause heating of the component. However, this is mainly a limitation for flip-chip approach where the substrate is removed and the heat is extracted via the DBR and not from the top of the device [17, 29].

Ultimately, the DBR's reflectivity depends on the material choice, as can be seen from Table 2.1. Compared to DBR mirrors fabricated for other wavelength regions, the GaSb-based mirrors can achieve very broad stopband and high reflectance with the lowest number of mirror pairs. As mentioned before, the mirrors can be grown entirely lattice-matched to a GaSb substrate.

When considering a bulk material as active region, it would have a thickness of several hundred nanometers and its density of states would be a continuous parabola in k-space. By reducing the thickness to less than 20 nanometers, energy levels will quantize in the direction of thickness, density of states is reduced to a step-function and the structure forms a quantum well (QW) [60]. Since the quantization is limited to only one dimension, the energy levels can be calculated by simplifying to the particle in a box model [60]. For an electron in a two dimensional well, the Schrödinger equation's

Table 2.1: DBR characteristics for mostly used semiconductor materials [56–59].

DBR materials	Substr.	$n_{\text{high}}/n_{\text{low}}$	Δn	N	λ_{B} (nm)	$R(\lambda_{\text{B}})$ (%)	$\Delta\lambda_{99\%}$ (nm)
GaAs/AlAs	GaAs	3.49/2.99	0.50	60	1060	>99.9	99
GaSb/AlAsSb	GaSb	3.89/3.22	0.67	36	2020	>99.8	203
InP/AlGaInAs	InP	3.17/3.51	0.34	81	1550	>99.9	91
InP/InGaAsP	InP	3.17/3.44	0.27	81	1550	>99.8	64

solutions will be entirely discrete energy states instead of continuous states. This feature makes semiconductor QW lasers interesting and easy to comprehend; the carriers are confined in the QW and recombination occurs efficiently in direct band gap materials from the lowest states of the conduction band, to the highest states of the valence band. The energy levels and their energy difference are temperature dependent, and thus they are slightly affected by heating caused for example by optical pumping of the QW.

One thing that makes the GaSb material system interesting and somehow challenging from the QW design point of view is that both so called type I and type II band alignments can be achieved. This concept is schematically present in Figure 2.7 and also seen in Figure 2.2. In lasers the most favourable type of alignment is type I, since in this case both electrons and holes are well confined in the QW and recombination is efficient. Therefore, the selection of the barrier materials is crucial [24]. In a type II QW the recombination is not direct as can be seen from the figure 2.7, however, for certain applications and wavelengths the use of type II QWs can be beneficial [61, 62].

For operation at 2 μm wavelength, quite standard materials such as GaSb, Ga_x-$In_{1-x}Sb_{1-y}$, and $AlAs_ySb_{1-y}$ compounds with known growth parameters can be utilized by avoiding the miscibility gap and choosing nearly lattice-matched binary and ternary compounds. To reach longer wavelengths, one would either need to broaden the QWs or increase the In-fraction in the QWs to narrow the band gap, thus increasing the operation wavelength. The width of the QWs is limited by the critical thickness, which

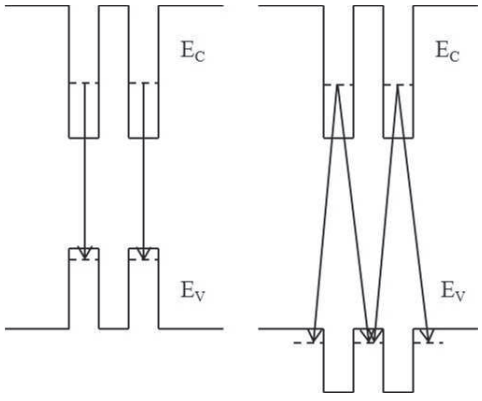

Figure 2.7: Type I and II (also referred as W) band alignment schematics.

is the maximum thickness a layer can elastically accommodate for the strain caused by lattice mismatch. Adding In to the QWs will increase the lattice mismatch and decrease the critical thickness. Thus both techniques can lead to plastic relaxation in the layer, causing defects and poor crystal quality.

Excess strain can be avoided by choosing quaternary $Ga_xIn_{1-x}As_ySb_{1-y}$ in such a way that the QWs still remain compressively strained. In this case the QW confinement of the holes will slightly decrease unless the barrier material is also changed to an $Al_xGa_{1-x}As_ySb_{1-y}$ compound. The change of barrier material ensures a significantly better carrier confinement and while moving to even longer wavelengths in order to remain clearly in type I band alignment, quaternary compounds for QWs and cavity are a necessity (Figure 2.2). For $Ga_xIn_{1-x}As_ySb_{1-y}$ there are many possible choices of compositions for certain bandgaps as indicated in Figure 2.8 by dashed lines, which correspond to constant bandgap compositions labeled in the figure. However, the choice is limited by the strain, miscibility and other growth-related issues. In $Ga_xIn_{1-x}As_ySb_{1-y}$, the miscibility gap is present only for lattice-matched and slightly tensile compounds and in the case of QWs, compressive strain is preferred.

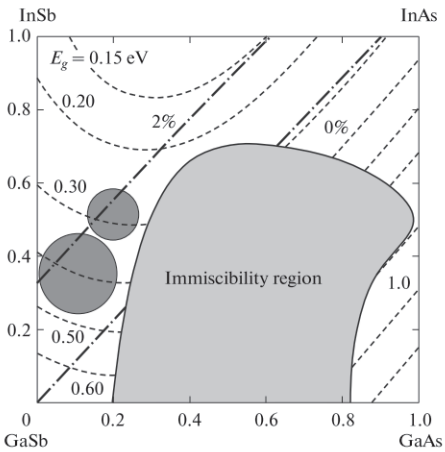

Figure 2.8: Schematic diagram of parameters of an $Ga_xIn_{1-x}As_ySb_{1-y}$ alloy. The alloy composition corresponding to the constant band gap is represented by the dashed lines. The dash-and-dot lines correspond to the alloys lattice-matched to GaSb and also 2% compressively strained. The miscibility gap is also shown. Reprinted with permission from [63]. Copyright 2010, Springer.

Besides the choice of QWs and DBR properties, another feature that should be taken into account when designing gain-mirrors for the SDLs, is the thickness of the layers surrounding the QWs. The surrounding layers define the available pump volume and the amount of electron-hole pairs supplied to the QWs. Moreover, due to Fresnel reflection at the semiconductor-air interface, a FP microcavity is formed between the top surface and the DBR. In general, to maximize the interaction between optical field and the QWs, the optical length of this FP microcavity is designed to be resonant at the emission wavelength of the QWs. To satisfy this, the cavity length L is defined as

$$L = \begin{cases} m\dfrac{\lambda}{2}, & \text{for resonant operation,} \\ (2m+1)\dfrac{\lambda}{4}, & \text{for antiresonant operation.} \end{cases} \tag{2.4}$$

Here λ is the operating wavelength and m an integer. In a microcavity shown in Figure 2.9, to maximize the gain, the QWs or a group of QWs are placed at the antinodes of the standing wave optical field [64]. This will cause a resonant phenomenon that will increase the effective light-matter interaction by recirculating the light inside the microcavity. The design is commonly known as the resonant periodic gain (RPG) [65].

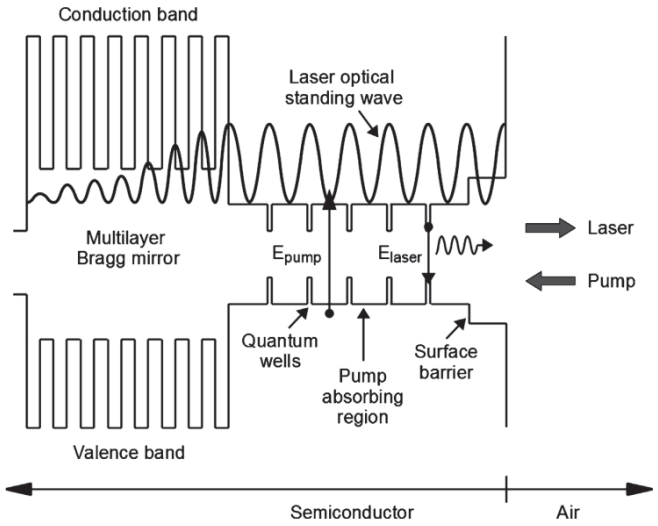

Figure 2.9: SDL microcavity schematic. Reprinted with permission from [64]. Copyright 2010, John Wiley and Sons.

The resonance wavelength of the cavity is also temperature dependent due to different thermal expansion coefficients and the thermal dependence of refractive index. Due to the thermal load of optical pumping, the temperature of FP cavity is increased during the operation decreasing SDL performance and output power. Eventually this will lead to thermal roll-over, i.e. the gain spectrum is not matched with cavity resonance, since the gain provided by QWs shifts faster with temperature than resonance. Usually this is considered already in structure design by choosing QWs emission wavelength and cavity resonance wavelength to be slightly shorter than the operation wavelength.

2.3.2 SDL processing

For SDL operation, a very important aspect is the thermal management of the chip. Optical pumping of the gain material using a laser with higher photon energy than the energy gap of the absorbing layer (i.e. the quantum defect) [66] will create phonons into the material. Heating up the gain material changes the refractive indexes [66] and can cause deterioration in the output power. Thermal roll-over may also occur as the lasing threshold is increased exponentially [66]. In the worst case the operation at the targeted wavelength is prevented or the gain chip might be destroyed because of the thermal load. There are two commonly known ways for thermal management: extracting heat through the DBR by etching off the substrate (flip-chip) [17, 29] and attaching gain mirror onto a heatsink, or the one used for the GaSb-based structures in this thesis, intracavity heatspreader approach [67], which is shown in Figure 2.10.

For GaSb-based materials, the thermal resistivity of DBR materials is reported to be an order of magnitude larger compared to GaAs or InP based materials, therefore removing the generated heat directly from gain region by intracavity heat spreader is preferred for GaSb-SDLs [68]. In addition, the flip-chip process requires a lattice-matched etch stop layer enabling removal of the substrate by selective etching. The etch stop layer should either not absorb at the operation wavelength or be easily removable. Even though some studies about development of such layer have been reported [69–71], a proper candidate which would meet all the requirements has not been found.

The intracavity heatspreader approach exploits a transparent conductor placed on top of the gain chip. The material selection is very limited due to the fact that the heat-

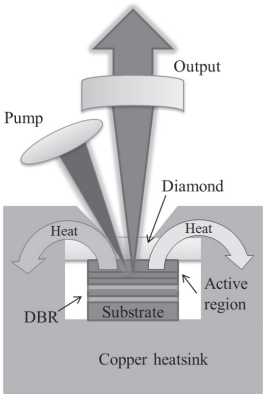

Figure 2.10: Intracavity heatspreader schematic

spreader is placed inside the laser cavity. Materials such as natural or artificial diamond, sapphire or silicon carbide are used. The heatspreader surface must be very flat, even, and clean, since it is bonded to the semiconductor surface with capillary waterbonding. The heatspreader and gain chip are bonded and attached into a watercooled heatsink with In-foil. The greatest advantage of the intracavity heatspreader approach is the simplified growth and processing compared to the flip-chip method. However, the intracavity approach is not entirely non-problematic. The heatspreader causes disturbance to the output spectrum and makes mode-locking more difficult to achieve since it is acting as a FP-etalon.

2.4 Semiconductor saturable absorber mirrors

Semiconductor saturable absorber mirrors are nonlinear semiconductor mirrors, in which the optical losses of the incoming light are reduced at high intensities, owing to bleaching of absorption [19, 72]. Consequently, when used as a cavity mirror in a laser setup, a SESAM triggers formation of high intensity pulses and leads to operation in mode-locking or Q-switching regimes. A typical SESAM structure is rather similar to an SDL gain mirror structure; it consists of a highly reflective bottom mirror, such as a DBR, and an active region that incorporates QWs or QDs. The main difference compared to

SDL gain mirror is that the active region of a SESAM operates as an absorber instead of providing the gain. A FP-microcavity is also formed between the bottom reflector and the semiconductor-air interface, and the microcavity effects can be used to tailor the SESAM properties.

The main effect governing the operation of SESAMs is the interband absorption. This requires that the band-gap of the semiconductor used in the absorbing region is smaller than the energy of incoming photons. For high enough light intensities, the valence band states are depleted and excited states are full, and the absorption is said to be bleached or saturated. Ideally the absorption in the active region could be completely bleached by the incoming light. However, this is not the case in reality due to other loss mechanisms presents in semiconductors, such as scattering losses, that give rise to the so called unbleachable/unsaturated absorption.

The nonlinear reflectivity response of SESAMs is characterized by a set of parameters, depicted in Fig. 2.11. These are the nonsaturable losses α_0, the modulation depth ΔR, the saturation fluence F_{sat} , and the recovery time of the saturable absorption τ_{rec} (addressed separately in this section). As it can be seen in Figure 2.11, at low intensities of light, the reflection from SESAM is lowest due to unbleached absorption. After a certain fluence of incoming light the SESAM starts to saturate and finally reaches the value of maximum reflectivity, when the saturable absorption is fully bleached. The intensity dependence of the reflectivity can be expressed as

$$R(F) = R_{\text{s}} - [1 - exp\,(-F/F_{\text{sat}})]\,\frac{\Delta R}{F/F_{\text{sat}}}, \tag{2.5}$$

where F is the incident signal fluence and R_s the reflectance maximum at saturation. α_0 includes the scattering losses in the DBR and other interfaces and is indeed linked to the maximum reflectivity provided by the DBR.

The nonlinear reflectivity of SESAM can be tailored by the cavity design and material composition of the absorber region or by adjusting the reflectivity of the top most surface. The cavity can be designed to be resonant or antiresonant the same way as a laser microcavity at the operating wavelength. In a resonant structure, the effective interaction length of light in the absorber material is enhanced at the operation wave-

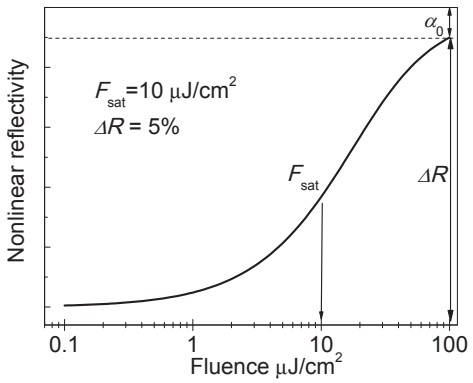

Figure 2.11: Nonlinear reflectivity calculated from the Equation 2.5 with an example values shown. Nonlinear parameters are shown.

length, which strongly enhances the modulation depth of the nonlinear reflectivity but at the same time enhances the nonsaturable losses. Typical nonlinearities for antiresonant SESAMs are between 0.3–3% [19] while resonant SESAMs can achieve nonlinearities as high as 80% [20].

In a low single-pass gain laser, such as the SDL involving high-Q cavities, antiresonant SESAM design is favourable as the resonant design would provide too much initial losses, preventing lasing. Anti-resonance is achieved normally by selecting the cavity length according to Equation 2.4 by reducing or increasing the thickness of the cavity layer on top of the QWs. This way the positioning of the QWs remains in the required positions relative to the DBR, as shown in Figure 2.9. More details concerning the design of SESAMs for mode-locking of SDLs can be found in the review by Keller and Tropper [45].

Besides the static response of the nonlinear reflectivity, another very important parameter governing the operation of SESAMs as mode-lockers is the recovery time of the absorption τ_{rec}, i.e. the time required for the photo-excited carriers to recombine and relocate to the valance-band. Typically τ_{rec} consists of two components, fast and slow. The slow component arises from radiative and non-radiative electron-hole recombination and trapping of the carriers, while the fast component is due to carrier thermalization. For passive mode-locking, τ_{rec} should attain a value in the range of picoseconds or hundreds of femtoseconds (similar to the pulse duration of the mode-locked pulse train).

Table 2.2: Techniques for SESAM absorption recovery time control

Method	**Materials where can be used**	**Features**	**References**
Low temperature growth	GaAs, InP	Simplicity Defects non-uniform	[73–75]
Ion irradiation	GaAs, InP, GaSb	Control of defect density Dedicated equipment	[76, 77]
Surface QW	GaAs, GaSb	Simplicity Limited amount of QWs	[78]
Metamorphic growth	GaAs/InP	Simplicity Defect control difficult	[79–81]
Doping of active region	GaAs, InP, GaSb	Simplicity Material quality degradation	[74, 75, 82]

In the most common GaAs and InP based QW SESAMs, the naturally occurring absorption recovery time is typically in nanoseconds range, much longer than is required for the production of ultra-short optical pulses. Therefore, special post-processing and growth techniques, such as low-temperature growth [73–75], ion irradiation/implantation [76, 77], or use of surface quantum wells [78], have been developed for controlling the absorption recovery time of these SESAMs. However, most of these methods increase the defect density and thus optical losses of the SESAM. They can also have constraints in the design possibilities, as is the case of surface QWs, where only the top QW would see the surface proximity effect. A summary of the typical methods to control τ_{rec} is listed in Table 2.2.

The reason which makes GaSb-based SESAMs especially interesting is that in narrow band gap materials, such as GaSb and related materials, the Auger-recombination process is known to be more dominant. In fact, in GaSb the Auger recombination coefficients are an order of magnitude larger than in GaAs and InP based materials [83, 84]. Strong Auger recombination provides a significant increase of the fast non-radiative

losses leading to carrier lifetimes that are several orders of magnitude smaller than those of conventional GaAs and InP heterostructures. Another interesting feature of Auger processes in $Ga_xIn_{1-x}As_ySb_{1-y}$ material is that the dominating process is the CHCC-process, which includes exciton recombination and an excitation of a conduction band electron [85]. This is the only Auger process that includes excitation of a conduction band electron, and it is dominant because of the favorable energy band structure; the spin split-off gap is bigger than the energy gap [85].

The fast dynamics of GaSb-SESAMs have been reported for the first time in [P2] and then studied thoroughly in [P4–P5], representing one of the main novelty aspects of this work. Contrary to other material systems, our studies have also shown that low temperature growth has very little influence on the absorption recovery time of GaSb-based SESAMs.

2.5 Basic characterization of heterostructures developed

While in principle it is possible to grow any materials with moderate lattice mismatch as a heterostructure, also growth-related issues and temperature gradients need to be considered. For example, in addition to growth layer quality, a too high growth temperature can cause annealing, undesired diffusion, and broadening of the interfaces or even the destruction of the already grown layers in the sample. To avoid material quality problems, careful optimization and characterization is essential in every fabrication step by using non-destructive methods such as X-ray diffraction (XRD), photoluminescence (PL) and reflectance measurement. These methods were used to characterize heterostructures presented in this thesis.

High resolution XRD measurement is a characterization method that gives information about the lattice strain, layer composition and thickness and it is used to study the fine structure of single crystal materials. In material with organized lattice structure the X-rays can only diffract to the directions defined by Bragg's law:

$$2d\sin\theta_{\mathrm{B}} = m\lambda \tag{2.6}$$

where d is the distance between atomic layers, θ_B is the angle between the incoming X-ray and surface normal, λ is the X-ray wavelength and m an integer.

The X-ray diffraction pattern i.e. the XRD rocking curve measured by fixing the angle between the detector and incoming beam, will give information of the layer thicknesses by variations of intensity and strain by variation of the diffraction angle [86]. Normally the substrate peak is clearly recognisable due to high intensity and narrow peak. Broadening of the peak is typically caused by dislocation or other imperfections in crystal lattice. Since the substrate and the overlaying strained structure diffract to different angles, their relative strain and interface quality can be evaluated. Fringes forming between the peaks in rocking-curve are typical for samples with good interface, and missing of this fringe pattern is the main evidence of defects in the interface [86]. The intensity of the peaks relates to the scattering matter and the volume sampled, and the oscillation period to the thickness of the layer [86]. With simulation programs the rocking curve can be simulated and compared to the measured one, which gives information about the material parameters.

PL-measurement is a non-destructive method to study the emission wavelength of the sample and to estimate the crystalline quality based on the intensity of the emission peak. The sample is illuminated with a laser, which has more energetic photons than the assumed bandgap of the absorbing material. The laser will thus excite electrons from valence band to the conduction band after which they will spontaneously recombine with the holes. The photons emitted in this process are focused to a monochromator for wavelength selection and the intensity is analyzed with a detector. The spontaneously emitted photons will have a certain spectral distribution which can be also used as an indication of the material quality.

Another useful way of analyzing the PL is its temperature dependence. At lower temperatures more peaks are visible; at room temperature they exhibit peak broadening due to exciton-phonon interaction. By measuring the temperature dependent PL, information about the carrier escape dynamics can be obtained. At low temperatures carriers are frozen in the QWs, but at higher temperatures they have enough energy to escape in non radiative ways. By fitting the $1/T$ temperature dependent PL intensity to an Arrhenius dependence, one can derive the carrier escape activation energies for nonradiative

channels. The temperature dependence of PL intensity as a function on $1/T$ is can be written as

$$I(T) = \frac{I_0}{1 + C_1 e^{-E_{\text{act1}}/kT} + C_2 e^{-E_{\text{act2}}/kT}} \tag{2.7}$$

for two carrier escape channels. It has a double exponential decay characteristics, where I is the PL intensity, I_0 maximum intensity, C_i and E_acti the weight factor and the activation energy corresponding to channel i, k Boltzmann's constant, and T temperature. This model is used in [P4] and [P5] to determine carrier escape dynamics connection to absorption recovery time in SESAMs.

The SESAMs were also characterized by using *reflectance and pump probe measurements*. For the reflectance characterization the samples are illuminated with a broad spectrum lamp and the reflected light is directed to a monochromator which selects one wavelength at a time to be measured by a detector. For the absolute value of reflectance a nearly perfect high reflectance reflector such as Au or Ag mirror can be used. The important characteristics obtained from the reflectance spectrum are the reflectance band width and its center wavelength, and also the placement and depth of a possible resonance dip.

The pump probe measurement is used to study ultra-fast phenomena, and concerning this thesis, the absorption recovery time. In this method, the sample is excited with an ultra-fast laser producing a pulse train, which is divided into two beams: the sample is excited by one pulse train (pump) and the changes it induces in the sample are probed by the second pulse train (probe), which is suitably delayed with respect to the pump. The time dependent behaviour of reflectance related to the probe is then monitored to investigate the changes produced by the pump in the sample. This gives information about the relaxation time and the manner of relaxation of the excited states in the sample. The absorption recovery times of the SESAMs in [P2, P4–P5] were determined with a pump-probe system available at Max Born Institut, Berlin, Germany.

Chapter 3

High-power and broadly-tunable lasers emitting at 2.0–2.5 μm

This chapter summarizes the development of GaSb-based SDLs emitting at 2–2.5 μm wavelength region in *cw* mode. First the design of the gain mirrors are discussed and then the use of the gain mirror in SDL is demonstrated. The section corresponds to results presented in [P1] and [P3] but includes also some unpublished data.

3.1 Gain mirrors for high power operation

The gain mirrors were grown by MBE on *n*-doped (100)-oriented GaSb substrates. First a GaSb buffer layer was grown to smooth the surface. The buffer was followed by a lattice-matched $AlAs_{0.08}Sb_{0.92}$/GaSb DBR with either 18.5 or 21.5 layer pairs. The QWs' composition and detailed structures for different wavelengths are given in Table 3.1.

The 2 μm SDL's active region consists of five groups of $In_{0.2}Ga_{0.8}Sb$ QWs embedded in GaSb, each group containing three QWs with a width of 8 nm. For the 2.35 μm SDL the structure consists of three groups of three 10 nm quantum wells of $In_{0.35}Ga_{0.65}As_xSb_y$ embedded in $Al_{0.3}Ga_{0.7}As_xSb_y$ barrier cavity. The third gain mirror designed for 2.5 μm has a bit more complex structure consisting of five groups of three 9.5 nm $In_{0.35}Ga_{0.65}As_{0.09}Sb_{0.91}$ quantum-wells (QWs) surrounded by 20 nm thick

Table 3.1: Laser structures, λ_{OP} is the target operation wavelength.

SDL	λ_{OP}	In%	As%	N:o QWs	QW thickness	Barrier	Waveguide
T1204	2	20	0	5x3	8	GaSb	GaSb
T1542	2.35	47	18	3x3	10	Al0.3	Al0.3
T1615	2.5	35	9	5x3	9.5	Al0.35	Al0.5

$Al_{0.35}Ga_{0.65}As_{0.035}Sb_{0.965}$ barriers to increase the pump volume. These were embedded in $Al_{0.5}Ga_{0.5}As_{0.04}Sb_{0.96}$ waveguide for better confinement. For each gain mirror the active region was closed with a window layer of $Al_xGa_{1-x}As_ySb_{1-y}$ with high aluminium content to ensure sufficient carrier confinement, followed by a thin GaSb cap layer to prevent oxidation of the aluminium-containing layer.

The structures of the gain mirrors for 2 and 2.5 μm are shown in Figure 3.1 and for 2.35 μm in Figure 3.2. All the micro-cavities were designed to be resonant with layer thicknesses selected to form a $n\lambda$ microcavity between the DBR and the semiconductor-

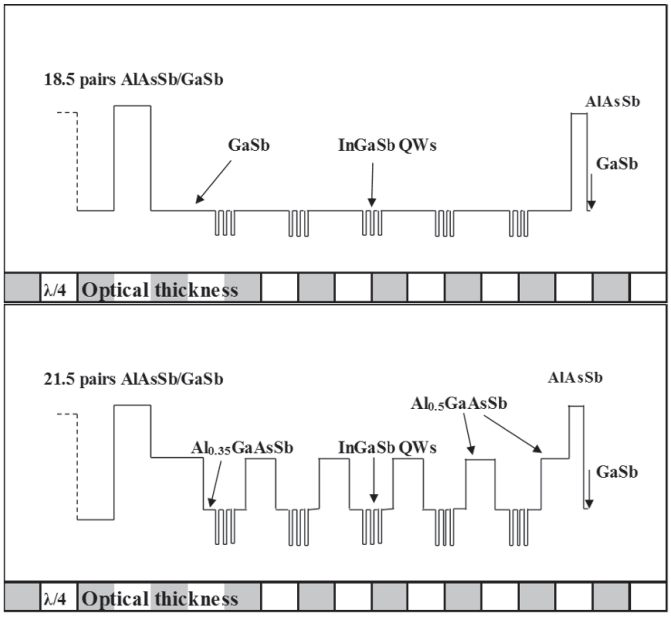

Figure 3.1: The structures of the 2 and 2.5 μm gain mirrors.

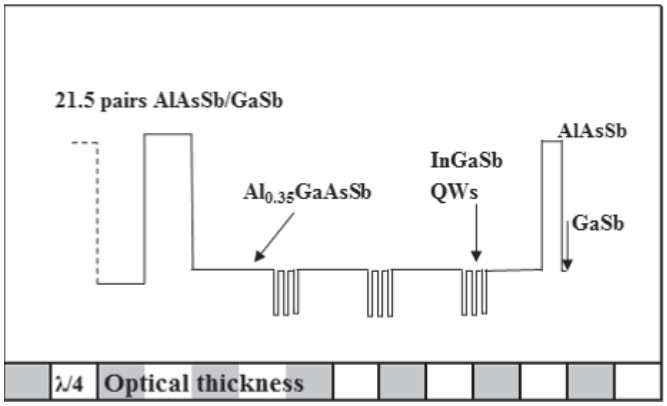

Figure 3.2: The structure of the 2.35 μm gain mirror.

air boundary. The QW groups were located at the antinodes of the standing-wave optical field in the microcavity. The refractive indexes for optical cavity design were evaluated based on the values and calculations obtained from literature [87, 88].

Before the final gain mirror was fabricated, several calibration structures were grown. This included $Al_xGa_{1-x}As_ySb_{1-y}$-bulk-samples in order to determine the lattice-matching condition of growth parameters and the growth parameters for desired group V composition. These samples had a GaSb-buffer layer of 50–100 nm, a 300–500 nm layer of $Al_xGa_{1-x}As_ySb_{1-y}$ with the desired Al% and a GaSb-cap layer to prevent oxidation. The composition was analysed by XRD and an example of a clearly visible and good quality AlAsSb-peak is shown in Figure 3.3 together with the simulated XRD rocking curve for the specific composition and thickness.

PL calibration samples, incorporating QWs similar to the actual SDL design, were used to set the operation wavelength and optimize the material quality of the QWs by optical microscope, PL-measurement and XRD. Examples of the optimization of PL intensity are shown in Figure 3.4. The measured PL intensities from the optimized PL-samples grown prior the gain mirror structures are shown in Figures 3.5(a) and 3.5(b) for 2 and 2.5 μm SDLs. Also the reflectance measured from the actual gain mirrors are included, together with the simulated reflectance for the design. Reflectance measurement systems used were not optimum, and caused some artefact to the spectra. This can be seen for example as a drop of intensity at wavelengths longer than 2.05 μm in Figure

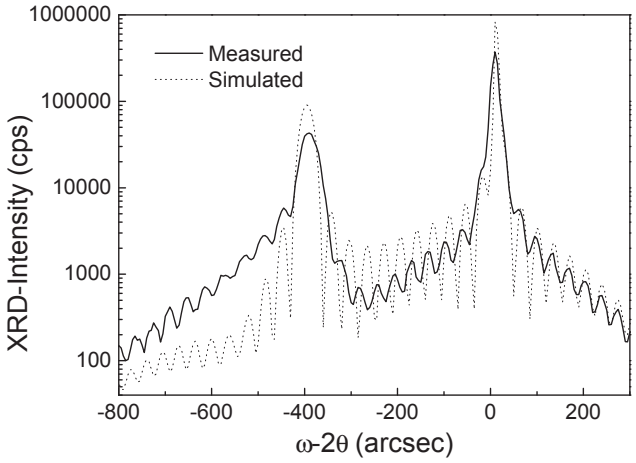

Figure 3.3: Measured and simulated XRD rocking curves of nearly GaSb lattice-matched good quality AlAsSb

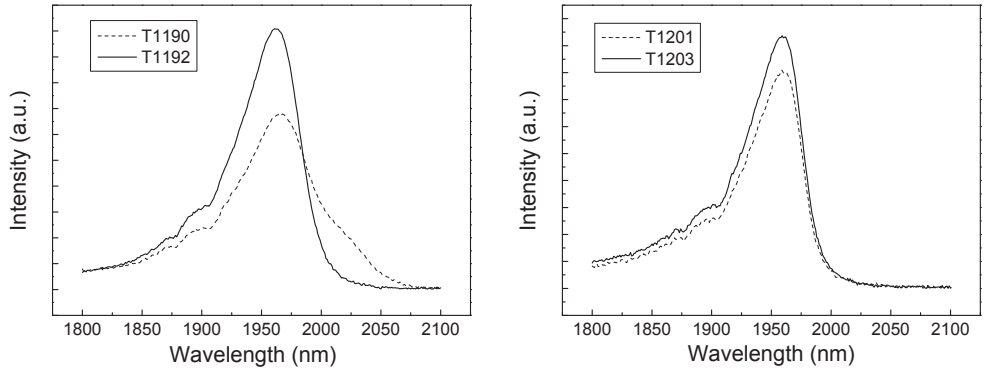

(a) (b)

Figure 3.4: PL intensities of PL samples in which the intensity has been improved by a) narrowing QW width and lowering the QW growth temperature and b) by improving the material quality of the layers surrounding the QW with As composition adjustment and growth temperature optimization.

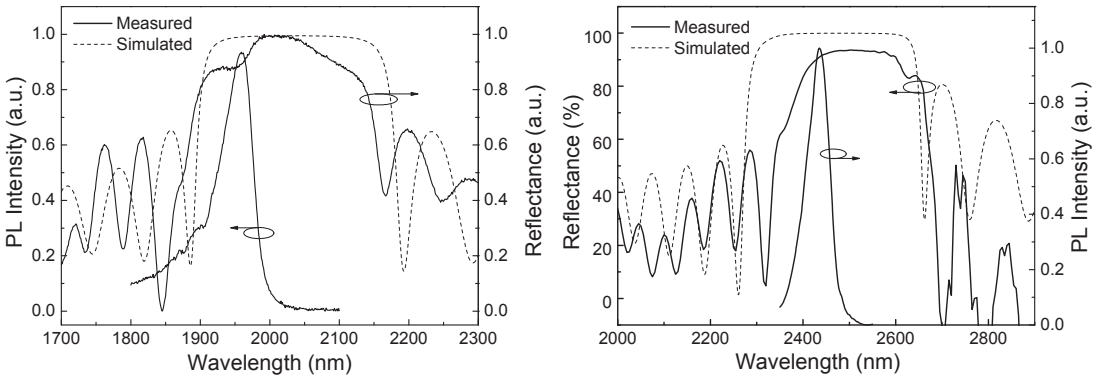

(a) (b)

Figure 3.5: PL intensities measured from PL-sample corresponding to 2 and 2.5 μm SDL gain mirrors, reflectance measured from the actual gain mirrors and reflectance simulated for the designs.

3.5(a) caused by rudimentary measurement system set up on an optical table. The reason for the artefact remains unresolved since the purchase of a new measurement system made it no longer necessary. However as it can be seen from Figure 3.5(b); also the new system has its limitations due to a drastic decrease of signal level at wavelengths longer than 2.7 μm.

3.1.1 Laser cavity

After the growth the gain mirror chips with a size of 2.5×2.5 mm^2 were capillary bonded with water to a diamond heat spreader (see section 2.3.2 concerning details on thermal management). The bonded chips were mounted to a water cooled copper heat sink that was integrated in the laser cavity. The outer surface of the diamond can also be anti-reflection coated to reduce the signal and pump reflection if desired.

SDLs were characterized using a V-shaped cavity configuration shown in Figure 3.6. The cavity incorporated also a highly reflecting spherical mirror and a partially reflecting output coupler (OC) mirror. The pump laser was focused to a small spot on the sample at an angle, the exact values depending on the specific measurement. Additional features of the SDLs developed are shown in Table 3.2. To study tunability a birefringent filter (BF)

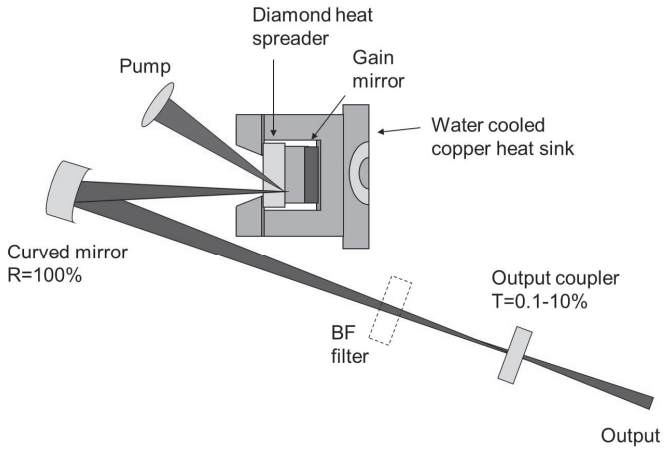

Figure 3.6: Laser setup

Table 3.2: Processing and measurement details

λ_{OP} (μm)	Diamond type	Diamond thickness (μm)	OC (%)	Pump source	Spot size (μm)/ angle ($^\circ$)
2	IIa	300	98–99	980 nm	290/22
2.35	IIIa	300	97–99	808 nm	180 /37
2.5	IIa	300	99	980 nm	180/30

was added to the measurement setup, shown in Figure 3.6 with dashed line. A BF-filter is an optical filter that is used to adjust the dominant resonant wavelength by changing the wavelength which has minimum transmission losses. The operation wavelength can be adjusted by rotating or by changing the angle. The filter causes also losses in the cavity, decreasing the laser operating power, even though it is placed on a Brewster angle to minimise the reflection.

3.1.2 Output characteristics

For the SDL optimized for high power operation at 2 μm, the output power was measured in a temperature range of 10–50 °C and exhibited excellent temperature behaviour.

The output power was over 4 W at 15 °C, and still 3.6 W at room temperature at a wavelength of 1970 nm. Lasing was observed up to a temperature as high as 50 °C. The lasing characteristics are shown in Figure 3.7. The pumping threshold increased exponentially with temperature and was close to 2 W near room temperature. The emission wavelength could be tuned by about 75 nm, from 1925 to 2002 nm. The typical output spectrum and beam profile are presented in Figure 3.7(b). The peaks in the spectrum correspond to the FP-etalon effect induced by the intra-cavity diamond. The beam profile is symmetric as is expected for a surface emitting structure.

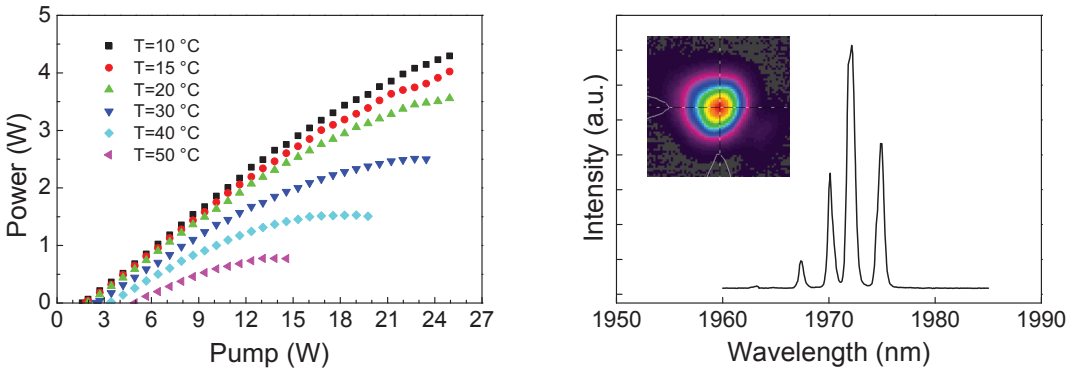

(a) (b)

Figure 3.7: a) The output power vs. pump power at different temperatures for 2 um SDL, incorporating a 2% transmissive output coupler. b) Beam profile and a typical wavelength spectrum of 2 μm SDL

The M^2 value that is used generally to describe the quality of the beam requires a special measurement system and is described by ISO-11146 standard. It states that M^2 value is defined by the ratio of beam parameter product and diffraction limited Gaussian beam parameter product. Beam parametric outcome is the product of beam waist radius and beam divergence. The smallest value theoretically possible is 1 and generally values close to one are considered sign of excellent quality beam. M^2 values larger than one can limit focusing and effect to brightness.

In practice an M^2 measurement is performed with pyrocamera for beam diameter measurement in waist and several other points. The M^2 value for this SDL was de-

termined later at different measurement to be 1.94 horizontal and 2.04 vertical. The obtained values are reasonable, but better results would have been possible with better optimization of the cavity as was in the first measurement. However, at that time the measurement was not possible due to lack of instruments.

Our aim to reach longer wavelengths was realised first with a 2.35 μm SDL. For this wavelength we discovered a decrease in output power but still remaining in high-power range with a maximum output power of nearly 1 W. The cavity was designed for a 300 μm pump spot diameter, while the actual size was 180 μm. Thus the achievable power may have been significantly higher than the power obtained in these measurements. Temperature behavior remained good as well as the beam quality, as can be seen from Figure 3.8. One should also notice that the quantum defect is 65.6%, so improved efficiency could be expected with 1550 nm pumping. The large quantum defect (i.e. pump wavelength is much smaller than lasing wavelength) is likely to be one of the main sources of the high thermal load to the gain element, and this combined with inefficient heat removal due to the GaSb material system's poor thermal conductivity leads to decreased output power. M^2 measurement has not been performed for this laser.

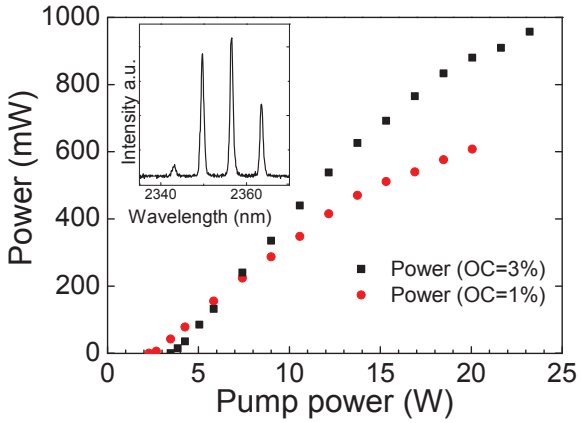

Figure 3.8: Output power vs. pump for 2.3 μm SDL, emission spectrum as an inset.

While aiming for even longer wavelengths, the SDL targeted at 2.5 μm was fabricated and output power of $\sim$600 mW has been achieved at heatsink temperature of 5 °C, as seen from Figure 3.9. M^2 was measured to be below 1.6 for the highest output power

of 0.6 W. Wavelength tuning of 75 nm was achieved and it has been reported in more detail in [P3].

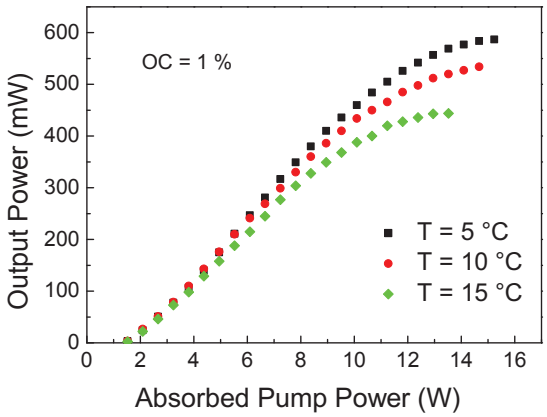

Figure 3.9: Output power vs. pump for 2.5 μm SDL

3.2 Gain mirror for broad wavelength tunability

A standard SDL design has only limited wavelength tunability because of the constraint imposed by the gain bandwidth ensured by a certain QW composition and homogeneous broadening in QW-based semiconductor lasers. Since GaSb-based DBRs have an extremely broad stopband, laser operation in a broader wavelength range would be possible if the gain bandwidth was increased. To expand the wavelength tunability a special design supporting multiple operation wavelengths was introduced [P1]. The structure of the broadly tunable laser is similar to the 2 μm gain mirror, except for its active region. It contains three groups of $In_{0.2}Ga_{0.8}Sb$ QWs with thicknesses of 6.5 nm, 9.5 nm and 16 nm and having also GaSb barriers with different thicknesses (See Figure 3.10 for details on the active region design). A thin $AlAs_{0.08}Sb_{0.92}$ layer was grown between each QW group to prevent carrier diffusion between the QW groups and to promote more equalized carrier injection in QWs groups. Each type of QW was calibrated independently with separate PL-samples. Before the growth of the actual SDL structure, a PL

calibration sample containing the three different QWs was also grown; the corresponding PL signal is displayed in Figure 3.11.

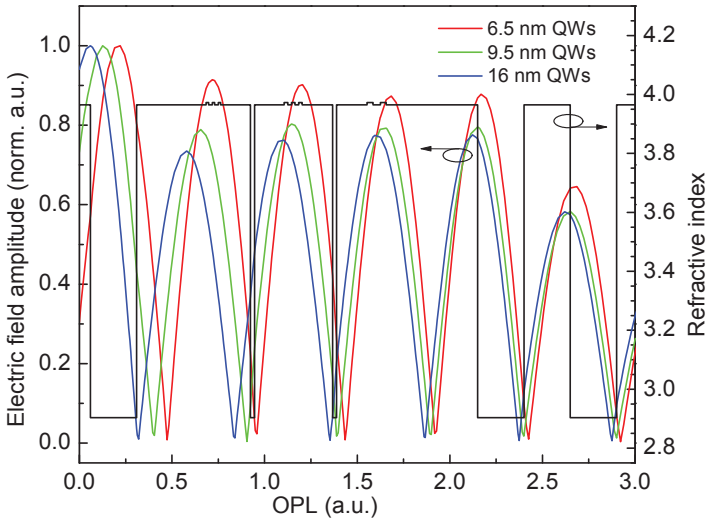

Figure 3.10: The structure of broadly tunable gain mirror.

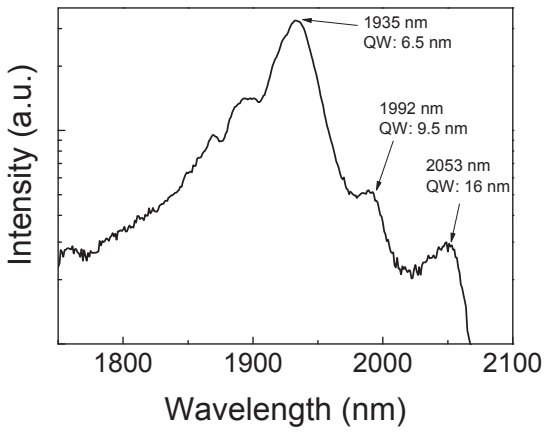

Figure 3.11: PL-intensity measured from sample with three different QWs, peak emission from each QW group is indicated.

For the SDL designed for broad tunability, an exceptionally broad tuning range was measured. The output coupler used for the broadly tunable 2 μm SDL had a transmit-

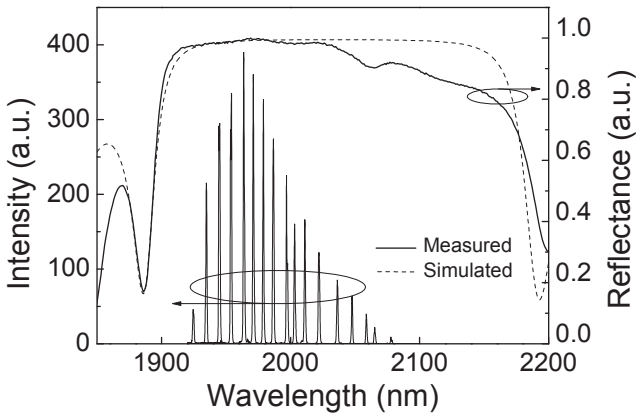

Figure 3.12: Selected tuning spectra with intensity normalized to emitted power, shown together with simulated DBR-reflectance and measured reflectance. Each peak in the graph represents a separate narrowband spectrum selected by the birefringent filter at a time.

tivity of about 1%. Owing to the modified gain region incorporating asymmetric QWs, we achieved a tuning range of 156 nm (1924–2080 nm) at operation temperatures of 10–15 °C. The tuning characteristics are shown in Figure 3.12. Compared to the high power SDL, the use of asymmetric quantum wells led to a 100% increase of the tuning range. As shown in Figure 3.12 the broad DBR stop-band would support laser operation far beyond 2080 nm. Therefore it is reasonable to assume that by further optimization of the gain region the tuning range could be extended beyond 150 nm.

3.3 Summary

To summarize, when increasing the operation wavelength, a clear trend towards lower output powers is obvious. While this is typically seen also for LDs [15] other differences in designs may contribute to this trend. A systematic approach was not made to study the limits of the wavelengths possible to achieve with GaSb cavity and GaInSb QWs. Another useful study that has not been made would be to thoroughly investigate the effect of growth parameters such as group V pressure or growth temperature on GaSb growths. Such time consuming tests may be required to optimize the structure design

Table 3.3: Summary on laser results

λ (μm)	λ_{OP} (μm)	P_{out} (W)	Tunability (nm)	Publication
2	1.97	5	75	[P1]
2	1.92–2.08	0.4	156	[P1]
2.35	2.36	1	–	–
2.5	2.5	0.6	50	[P3]

and quality in order to improve the laser operation at longer wavelengths. A summary of results we obtained is presented in Table 3.3.

Chapter 4

Techniques to control the absorption recovery-time of GaSb-based SESAMs

This chapter describes the design and fabrication of GaSb-based SESAMs aimed for mode-locking a GaSb-based SDL operating at around 2 μm. An important part of the work was focused on investigating several techniques to control the absorption recovery time in such SESAMs. Mode-locking experiment will be explained in more detail in Chapter 5.

4.1 SESAM structure

Here we describe the generic structure of GaSb-based SESAMs. All SESAMs were grown on an (100) n-GaSb substrate with 18.5 pairs of a lattice-matched $AlAs_ySb_{1-y}$/-GaSb DBR (as in SDL structures). The absorber region was designed to be anti-resonant at the operating wavelength and it consists of $Ga_xIn_{1-x}As_ySb_{1-y}$ quantum wells embedded in GaSb. While the total length of the optical cavity was selected to be anti-resonant, the QW-group or single QW, depending on the sample, was placed at the antinode of the optical field respect to the DBR-cavity interface. SESAMs were grown with the growth conditions (temperature, fluxes) as described in section 2.2. if not otherwise stated. The generic structure of SESAMs is presented in Figure 4.1(a) and the reflectance which is identical to all the SESAMs is presented in Figure 4.1(b).

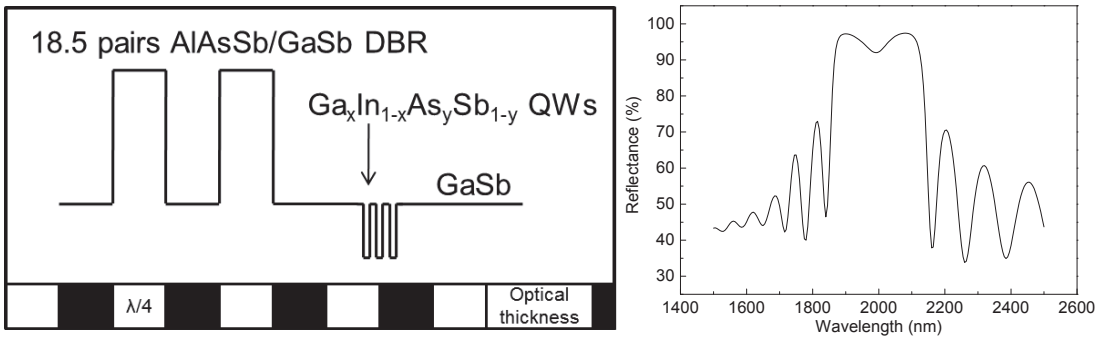

(a) (b)

Figure 4.1: a) Basic structure of SESAM and b) measured reflectance of SESAM, which is identical to all the SESAMs presented.

4.2 Influence of low temperature growth on absorption recovery time

One of the most common techniques to reduce the recovery time of SESAMs is the introduction of lattice defects via low-temperature growth of the QWs. As this technique can selectively limit the defects to the QWs in the structure, it has developed into a quasi-standard for fabricating commercial GaAs SESAMs. Therefore, low-temperature growth acts a natural starting point for a study of GaSb-based SESAMs.

A set of SESAMs was fabricated with GaSb-cavity including three 8.5 nm thick $Ga_{0.73}In_{0.27}Sb$ QWs with GaSb barriers grown at temperatures ranging from 350 to

Table 4.1: Information and results on SESAMs grown at different temperatures

SESAM	T_{QW} (°C)	N:o of QWs	QW thick. (nm)	In%	λ_{PL} nm
T1986	350	3	8.85	27.4	2061
T1984	450	3	8.96	26.9	2057
T2010	530	3	8.82	26.7	2049

530 °C; highest being the same as used for gain mirrors. While other parameters besides the QW growth temperature were fixed, some variations were observed for the room temperature (RT) PL wavelength (Table 4.1). This finding is explained by a variation of the In-composition and QW thickness occurring due to temperature dependent sticking coefficients. Simulations for high resolution X-ray diffraction rocking curves (see Figure 4.2) indicate varying In-composition in QWs and results are shown in Table 4.1.

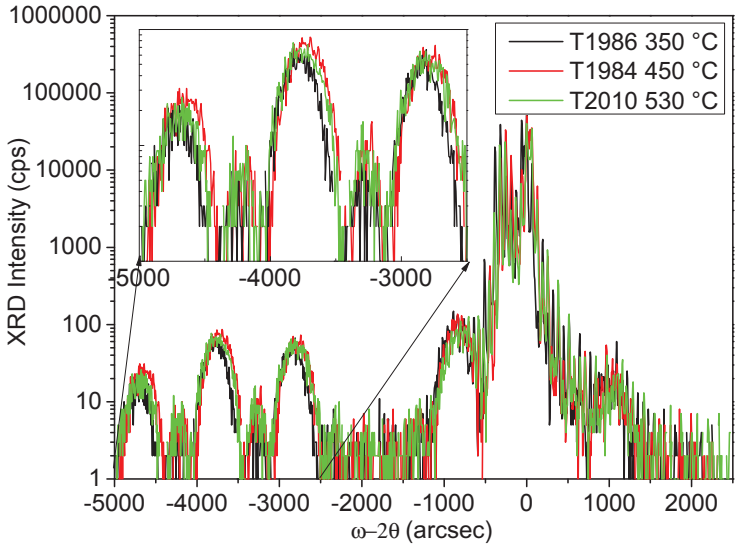

Figure 4.2: XRD rocking curves for SESAMs grown with different QW temperatures indicating small variations in QW-composition.

To investigate the absorption recovery dynamics and carrier escape via non-radiative channels, we performed pump-probe measurements and recorded the temperature dependent PL. The pump-probe absorption recovery traces for different growth temperatures are plotted in Figure 4.3(a). Quite remarkably, these traces reveal only minor differences between the fast components (between 0.25–0.27 ps) and slow components (between 5.5–6.8 ps). In fact, only the sample grown at 350 °C seems to exhibit a slight acceleration of the interband recombination times.

The temperature dependent PL was recorded for a temperature range from 10 K to 300 K. The measured PL intensities for all SESAMs are shown in Figure 4.3(b). Sev-

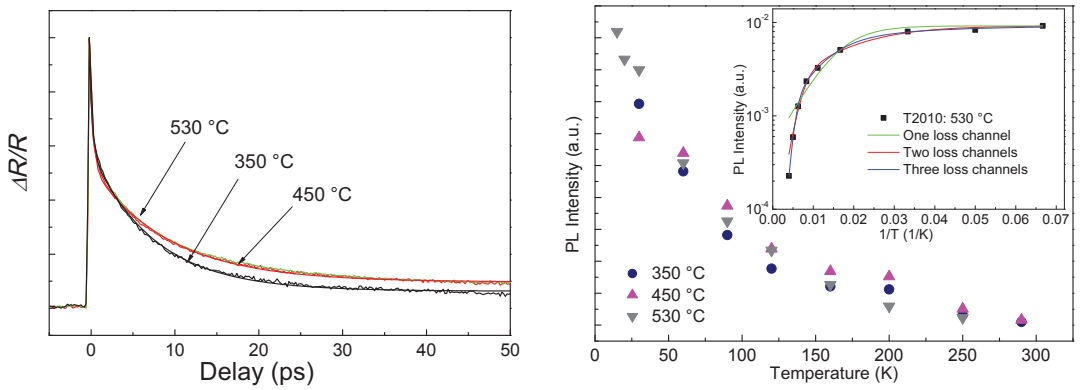

(a) (b)

Figure 4.3: a) Pump probe traces for SESAMs with varying QW growth temperature. b) Temperature dependent PL intensity of SESAMs. Inset: PL intensity for T2010 as a function of $1/T$ is shown with an Arrhenius plot for one, two and three loss channels.

eral fits of Equation 2.7 are shown as an inset in Figure 4.3(b) for T2010. Figure 4.3(b) clearly shows that the decay is not explained only by one channel, but the fits with two or three channels are quite similar. The results are compiled in Table 4.2. The activation energy E_{act2} and the corresponding weight factor C_2 are widely similar for all samples, indicating that the PL intensity is mainly affected by carrier thermalization at room temperature, as expected. However, the activation energy E_{act1} and the corresponding constant C_1 for the low temperature grown samples (T1986 and T1984) differ radically from the reference sample T2010 grown at 530 °C. The magnitude of the activation energy

Table 4.2: Information and results on SESAMs grown at different QW temperatures

SESAM	T_{QW} (°C)	C_1	E_{act1} (meV)	C_2	E_{act2} (meV)
T1986	350	5.8×10^9	430	18	19
T1984	450	5.2×10^8	396	15	25
T2010	530	249	55	4	8

E_{act1} ∼400 meV appears to be related to deep levels found in GaSb [89, 90]. This observation corroborates that low-temperature growth also generates deep levels in GaSb barrier material, as previously observed in other semiconductor materials. In contrast, the sample T2010 grown in typical temperature does not show any clear indications for such deep levels.

Thus the data suggests that low-temperature growth increases the number of growth related defects also in GaSb based SESAMs, but the absorber dynamics are only marginally affected by the growth related defects. This indicates that there is another dominant recombination process in the GaSb-based SESAMs. A possible candidate for this process is Auger recombination.

4.3 Effect of QW strain on absorption recovery time

To study the effect of material composition, we grew a set of three samples with different In and As composition in QWs, resulting in different strain, yet with otherwise similar optical design. All the QWs and barrier layers were grown at 530 °C. The In and As content were changed in a way to ensure the same operation wavelength and to simultaneously decrease the structure strain. The QW strain was verified by performing XRD measurement and by using peak-split software to define strain and lattice-mismatch based on separation of the XRD peaks. XRD rocking curves measured of these SESAMs are shown in Figure 4.4, QW parameters obtained are included.

The conductance band energy states for these three SESAMs are presented in Figure 4.5(b). In Figure 4.5(a) the conductance and valence bands are presented for the SESAM T1816 with typical strain. As it can be seen, T1816 has two states at the valence band with relatively low confinement. Reducing strain and remaining at the same wavelength results in even poorer carrier confinement for holes; valence band becomes nearly a flat-band, thus reducing the probability of radiative recombination processes. This is expected to cause an increase in the slow recovery time component τ_2.

The pump-probe and temperature dependent PL measurements were also performed for this sample set and the results are summarized in Table 4.3, where the calculated energy level offsets E_C and E_V relative to GaSb band edges are also included.

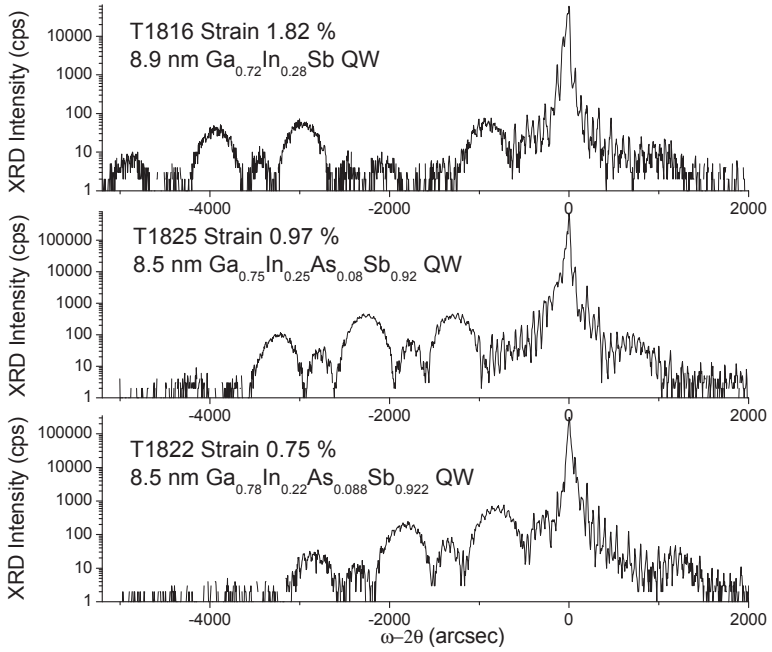

Figure 4.4: XRD rocking curves for SESAMs grown with different QW composition and strain. QW compositions, thicknesses and strain obtained are shown.

As expected, samples T1825 and T18122 with the poor hole confinement also exhibit the longest slow time component τ_2. The activation energies of the SESAMs T1822 and T1825 correspond to the energy levels at conduction band E_C and are associated to the escape of the electrons. On the other hand, the activation energy E_{act1} is significantly smaller than E_C for T1816, but comparable to E_V, which suggests that the carrier escape mechanism in this type of SESAM is most likely thermal escape of the holes. The electrons in sample T1816 are more likely to escape via excited conduction band (CHCC) Auger process consisting of recombination of an electron and a heavy-hole as well as a simultaneous electron excitement in the conduction band [85]. Additionally, the electron hole pair recombination is also more likely due to better confinement of holes. This process will also contribute to the fast absorption recovery. The CHCC Auger process is known to dominate in this type of those narrow band gap materials that display an energy gap smaller or comparable to the spin split-off gap [85]. Based on the data shown in Table 4.3, we can conclude that there is a notable correlation between the slow recov-

ery time component and the composition in the quantum well. The slow recovery time τ_2 was observed to vary in the range 9–18 ps. To investigate only the effect of strain on the recombination dynamics, another set of samples should be studied employing $Al_xGa_{1-x}As_ySb_{1-y}$-barriers instead of GaSb. This would allow to maintain the carrier confinement similar in each sample.

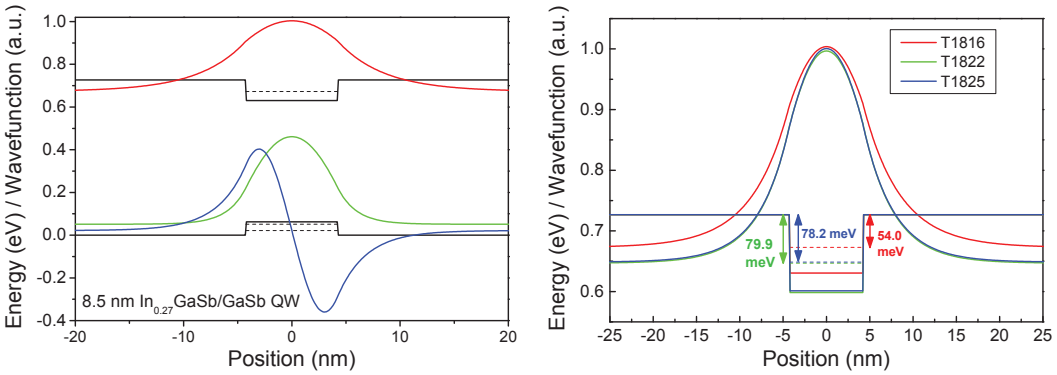

(a) (b)

Figure 4.5: Energy band diagrams for a) SESAM with normal strain and no As in QW, displaying both conductance band with one state and valence band with two states and b) for SESAMs with varying composition and strain showing only conductance band since valence band offset is close to 0 eV.

Table 4.3: Information and results on SESAMs with different QW strain

SESAM	Strain (%)	τ_1 (ps)	τ_2 (ps)	C_1	E_{act1} (meV)	C_2	E_{act2} (meV)	E_C (meV)	E_V (meV)
T1816	1.82	0.44	9.24	30	33	1	5	54.0	21.6 51.3
T1825	0.97	0.53	14.10	409	62	1	5	78.2	0.0
T1822	0.75	0.35	18.50	852	72	5	9	79.9	0.0

4.4 Effect of surface proximity on absorption recovery time

Yet another method for achieving fast absorption recovery time is the placement of the QW in close proximity to the semiconductor surface, exploiting fast surface recombination effects [45]. The QW is typically separated from the surface by a cap layer of only a few nanometers. For our studies we used four samples with nearly identical QW composition, but with different placement and number of QWs in the optical microcavity.

The first sample had a single $Ga_{0.73}In_{0.27}Sb$ QW separated from the surface with a GaSb cap having a thickness of 5 nm (T2015). The second sample (T2013) included two QWs near the surface; the cap thickness was 5 nm cap and the QWs were separated by 10 nm GaSb barrier. The third sample (T2012) had two QWs with 10 nm barrier placed 50 nm below the surface. Finally, the last sample (T2010) had design of typical SESAM with QWs buried into the cavity, with three QWs placed 300 nm deep. Thicker QWs were used near surface for a compensation of the PL shift due to band bending near surface. The cavity schematics of the SESAMs are illustrated in Figure 4.6, indicating the refractive index profile and the optical field in the cavity.

Additionally, a piece of each material was coated with a dielectric 2-layer AR coating for further comparative studies. As dielectric coatings are often exploited for surface passivation of semiconductor samples we need to point out that we mostly aimed at increasing the overall absorption and to increase the mode-locking force in the laser experiments. The AR-coating consisted of a 233 nm TiO_2 layer with 62 nm of SiO_2 on top, both deposited by e-beam evaporation at a sample temperature of 90 °C. Detailed structures and the characterization results of the near surface QWs are shown in Table 4.4.

The pump probe measurements were performed on as-grown and AR-coated SESAMs. For the as-grown near-surface SESAM, the slow component of τ_{rec} appears slightly smaller compared to typical cavities incorporating thick capping. This reduction is readily explained by fast recombination via surface states. In SESAM T2013 employing two QWs, the reduction of τ_2 due to surface recombination is not as pronounced as for T2015, since the second QW is already farther away from the surface.

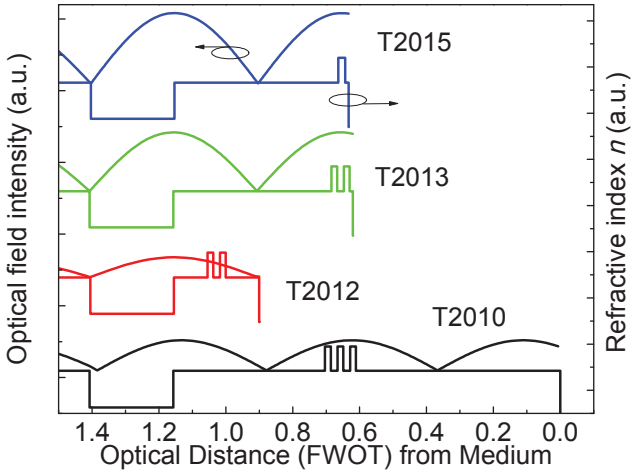

Figure 4.6: Optical cavity schematics for SESAMs with near surface QWs (T2013 and T2015), for SESAM with QWs misplaced in optical field (T2012) and a typical SESAM with thick capping (T2010). Cavities are placed in graph such that DBRs are in line with each other. The refractive index of QWs is not on scale; it is intended to make the graph more informative, guide the eye and make the QWs clearly visible.

Table 4.4: Information and results on SESAMs with different microcavity designs

SESAM	QWs (nm)	QW In %	Cap (nm)	λ_{PL} (nm)	τ_1 (ps)	τ_2 (ps)	AR effect on τ_2
T2010	3x8.5	26.7	300	2049	0.31	8.67	
AR					0.29	9.68	+12
T2012	2x8.5	27	50	2060	0.24	20.85	
AR					0.29	20.89	0 %
T2013	2x8.5	27	5	2040	0.35	8.36	
AR					0.27	4.12	-51 %
T2015	1x10	27	5	2000	0.50	5.24	
AR					0.47	1.69	-68 %

A very intriguing observation is that the AR coating significantly reduced the slow recovery component for the surface quantum well samples while a similar effect was

not observed for samples having QWs buried deeper in the structure. Out of the two near-surface QW samples the effect of the AR is most pronounced in T2015, which had the slow recovery component further reduced from 5.24 ps to 1.69 ps after coating. For sample T2013 the effect of the dielectric coating is significant, but as expected, due to the deeper buried second QW the recovery time is longer than for the single quantum well samples (τ_2=4.12 ps with AR-coating). We attribute the decrease of the recovery time to increased Auger recombination owing to enhancement of the interaction between the optical field and the surface QW; to recall, the Auger recombination is proportional to the cube of the carrier density: $I_{Auger} \sim n^3$ [91]. Another factor is the surface passivation provided by the dielectric and the change in surface recombination sites, which has been suspected in the case of GaAs-based SESAMs [92]. Besides the mode-locking of SDLs, described in the next chapter and [P2], the ability of these SESAMs to mode-lock was verified in a Tm:YAG laser [22].

4.5 Summary of novel studies concerning dynamics of GaSb SESAMs

We have investigated the effect of growth temperature on the dynamics of GaSb-SESAMs. Our studies provide evidence of deep levels in GaSb and yet show negligible effect of growth temperature on τ_{rec} on absorption recovery time. The slow component of τ_{rec} in GaSb-SESAM can be tailored to some limited extend by changing the material composition of QWs. This is due to modified hole confinement. Yet further optimization with different barrier material is proposed to investigate the effect of different strain to GaSb-SESAM dynamics.

Near-surface placement of the QWs and the use of AR coatings offer rather unique possibilities for tailoring τ_{rec} by adjusting the interaction of the optical field with the absorbing region. Extremely low τ_{rec} (τ_1 ~0.5 ps and τ_2 ~1.7 ps) was found for AR-coated samples incorporating one QW placed 5 nm from the surface. This particular SESAM was also successfully used for mode-locking a Tm:YAG laser. [22] The techniques and the observed effects are listed in Table 4.5.

Table 4.5: Summary of techniques to control absorption recovery time in GaSb-based SESAMs

Method	Range studied	Effect on τ_{rec}	Observations
T_{QW}	530–350 °C	negligible	Deep levels in GaSb
Strain/band gap	1.9–0.8 %	modest	Effects slow component
Surface proximity	5–300 nm	modest	AR-coating enhances the effect

Chapter 5

Ultrashort pulse generation using GaSb-based SESAMs

Typical laser output is composed of multiple longitudinal modes that oscillate with spacing $\Delta\nu = c/2L$, where c is the speed of light in vacuum and L is the optical length of the cavity. The average output intensity of *cw* laser tends to fluctuate due to the random phases of light of individual modes at certain time. In a mode-locked laser the phases of modes are fixed to be separated by a constant phase of ϕ. This will result a constructive interference and thus a train of pulses. A more detailed theory of mode-locking can be found in literature [60, 93].

SESAMs are widely used for mode-locking lasers, since their behaviour is passive, self-starting and they enable production of high-quality pulse trains with high power and ultrashort pulse length. More details of designing issues of SESAM utilized in mode-locking can be found from [19, 45]. Here we present the mode locking experiment with fast GaSb-based SESAM using a GaSb-based SDL and a Tm:Ho-YAG lasers.

5.1 Passively mode-locked GaSb-based SDL at 2 μm

The semiconductor gain mirror used for mode-locking experiment has been introduced in Chapter 3, as high power gain mirror for 2 μm wavelength. The design and fabrication of the SESAM was the same as for T1816 and T2010 presented in Chapter 4,

although the SESAM itself was grown at different time. To verify the fast dynamics of the SESAM, pump probe measurements were performed and they confirmed fast absorption recovery similar to that we already presented in Chapter 4.

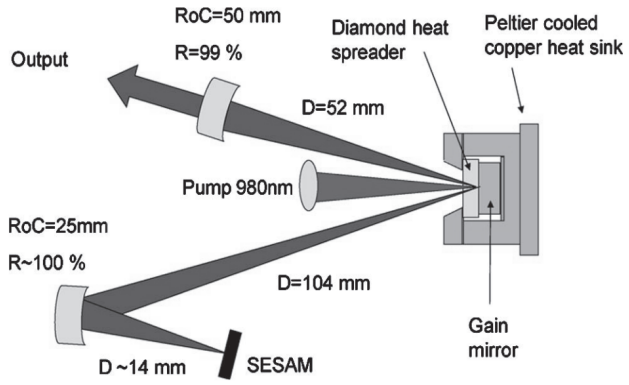

Figure 5.1: The z-type cavity used for mode-lock experiment.

Figure 5.1 shows the z-shaped SDL cavity employed, with the gain chip and the SESAM serving as folding mirror and cavity end mirror, respectively. A $\sim$230 μm diameter spot on the gain mirror was pumped optically with a fiber-coupled 980 nm diode laser. The laser mode size was matched to the pumped area on the gain. The simulated mode diameter on the SESAM was $\sim$25 μm.

The output of the laser was coupled into a single-mode optical fiber and further analyzed by a 2.5 GHz photo diode, a spectrum analyzer, and an autocorrelator. The output power characteristics were measured with a thermal power meter and exhibited a hysteresis typical for many mode-locked lasers. Mode-locking was initiated at 8 W of pump power. Once initiated, the pump power could be reduced to $\sim$6.8 W with stable mode-locking. The radio frequency (RF) spectrum in Figure 5.2 reveals clean mode-locking at the fundamental cavity repetition rate of 881.2 MHz with a pedestal-like substructure at below -50 dBc at a 1 kHz resolution bandwidth. The absence of pronounced frequency components indicates the practical absence of Q-switched mode-locking. Lasing was observed near the 1950 nm wavelength. The pulse width of the laser was measured using an interferometric autocorrelation method with 1.9 ps width (FWHM). The procedure for extracting the intensity autocorrelation retrieves a pulse duration of 1.1 ps, which is a factor of 1.8 above the bandwidth limit.

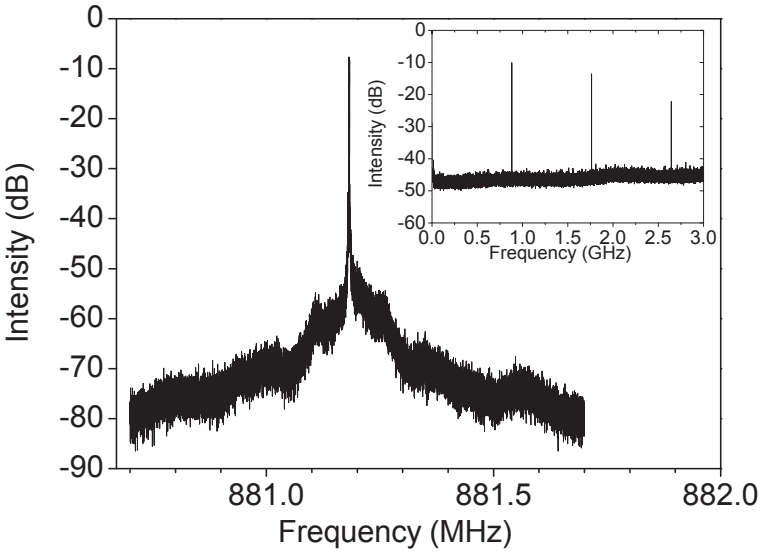

Figure 5.2: RF-spectrum of the output pulse train with 881:2 MHz repetition frequency. Resolution bandwidth 1 kHz. Measured with a 2:5 GHz photodiode. Inset, wide-scan RF-spectrum

Modulations in the spectrum were observed to originate from the double-sided polished gain and SESAM wafers acting as etalons in the laser cavity. To prevent such undesirable reflections, the secondary surfaces of the SESAM and gain mirror chips were mechanically roughened to scatter any incident light. With the improved setup the measured autocorrelation indicates a pulse width of 384 fs, which is within only 2% of the bandwidth limit calculated from the spectrum [23]. To the best of our knowledge, these are the shortest pulses ever obtained from a GaSb disk laser. Quite surprisingly, they also show that dispersion management at these wavelengths appears to be much less of a problem than previously reported in the near-infrared spectral region.

5.2 Passively mode-locked Tm,Ho:YAG laser at 2 μm

An intresting experiment to compare our GaSb-based SESAM (the same as used for mode-locking a GaSb-based SDL) with a commercial GaInAs-based SESAM (Batop Inc.) was done by K. Yang et al. [21] by passive mode-locking of Tm,Ho:YAG lasers with the mentioned SESAMs.

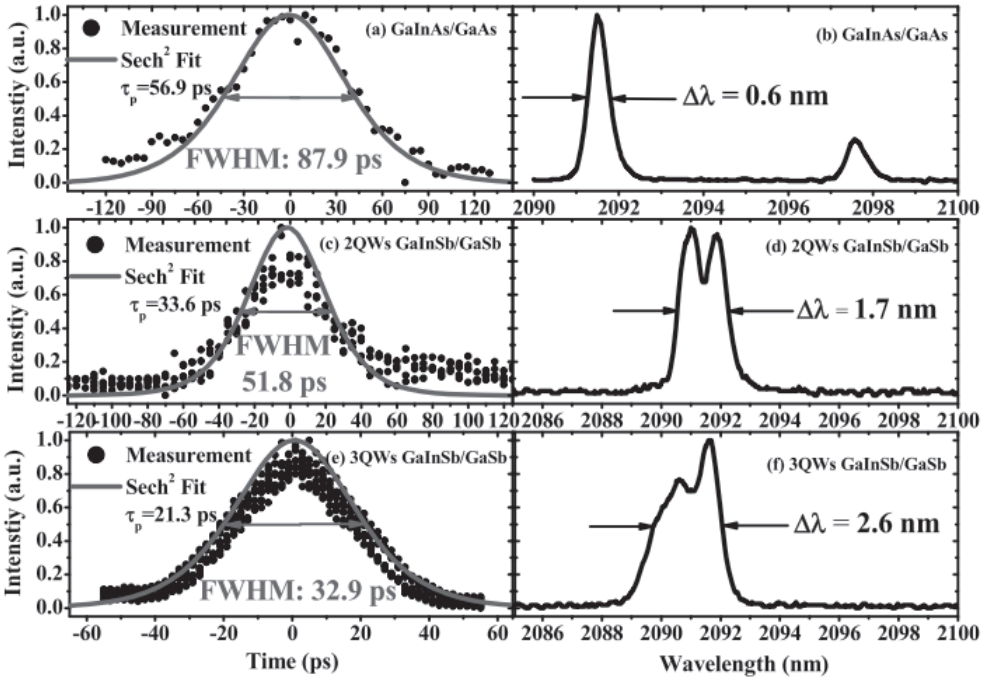

Figure 5.3: Autocorrelation signal and spectra from mode-locked Tm,Ho:YAG laser. Reprinted with permission from [21], Copyright 2013, OSA.

When using a SESAM comprising three GaInSb/GaSb QWs, pulses as short as 21.3 ps were demonstrated. The pulses were two times shorter than for the case of GaInAs SESAM and the results are shown in Figure 5.3. Compared to GaAs SESAMs, the GaInSb-based QWs also exhibit sub-ps recovery time for as-grown and high quality structures and they are nearly lattice-matched to the substrates for the 2 μm wavelength range. This brings more flexibility for designing the optical properties of the SESAM. Further optimization of the GaSb-based SESAM and compensation of the intracavity dispersions are expected to lead to the generation of even shorter pulses.

Chapter 6

Conclusions

This thesis concerned the design and characterization of GaSb-based materials and vertical cavity heterostructures for high-power, broadly tunable and ultra-short pulse lasers. The primary focus was on developing materials for the 2–2.5 μm wavelength range. The main achievements of this thesis are as follows:

We demonstrated GaSb-based SDLs emitting high output power and exhibiting a broad tuning range at 2–2.5 μm [P1, P3]. A SDL emitted a *cw* output power of over 4 W at 1970 nm wavelength operating near room temperature. The structure exhibited a tuning range of 75 nm, and by using a modified structure with asymmetric QW design we achieved a spectral tuning of about 156 nm [P1].

The first passively mode-locked GaSb disk laser at 2 μm was demonstrated. A three quantum well InGaSb SESAM was deployed in the laser that produced pulses with a duration of about 1.1 ps [P2]. By improving the measurement setup and sample preparation, 384 fs optical pulses at 1960 nm wavelength were demonstrated [23]. To the best of our knowledge, these are the shortest pulses ever obtained from a semiconductor lasers operating at wavelength longer than 1.8 μm.

The dependence of absorption recovery dynamics on growth temperature, QW strain, and QW location in optical cavity in GaSb-based SESAMs was studied.

A negligible effect of growth temperature on τ_{rec} was observed even though our studies reveal the presence of deep levels for the case of low temperature growth on GaSb. A decreasing confinement of the holes is considered to cause the observed effect of strain and band alignment on absorption recovery time. By placing QWs near surface and by employing AR coating τ_{rec} can be reduced further; recovery times as fast as τ_1 ~0.5 ps and τ_2 ~1.7 ps are reported. This particular SESAM was also successfully used for mode-locking a Tm:YAG laser. [22] The study reporting absorption recovery dynamics in GaSb SESAMs is the first of its kind.

Additional results, not included in the thesis concerned the development of GaSb SESAMs for Q-switching of fiber lasers [20] and use of GaSb SESAMs for mode-locking the first ceramic Tm:YAG solid-state laser [22].

There are indeed other aspects to this work that can be considered in the future. Despite that the results are showing an excellent performance at 2–2.5 μm wavelength range with high power and also ultra-short pulse operation at 2 μm, there are several development steps that are required for applications. Concerning these SDLs, for example decreasing quantum defect would likely improve the output power characteristics. The greatest challenges for SDLs and SESAMs presented in this work are however the need for external pump and the optical cavity interference caused by the intra-cavity heatspreader diamond. There are at least two approaches that could provide solutions for these.

First one is the development of the GaSb-based flip-chip devices. This approach could improve the functionality of the SDL and gain access to high volume production. The absence of intra-cavity diamond would remove FP-etalon effects and be beneficial for ultra-short pulse production and wavelength tuning. The challenges arise from the fact that processing for this material group is not yet very well developed. Some effective etch stop layers for substrate removal have been published [69–71], but the full process still needs more attention. On the other hand even with perfect processing for removing the substrate, the thermal resistance of GaSb-based DBR may still become a problem with the thermal management in flip-chip approach.

Another interesting technology lies in electrically pumped GaSb SDLs. These would be very compact laser sources, since there is no need for external optical pumping. The attainable output power levels are a challenge as well as the doping scheme of the mirrors. On the other hand high doping levels lower the electrical resistance, but at the same time increase the absorption. First demonstration of electrically pumped GaSb SDL has already been made [94], but the development has barely begun and many issues related to thermal management and current spreading need to be addressed.

Considering GaSb-based SESAMs, we have barely scratched the surface. Some techniques to tailor non-linear properties have been explored, but there is much room for improvement. Since we have focused only on quite simple materials at 2 μm, one has to ask, what lies beyond? Moving to longer wavelengths will provide challenges, and the use of quaternary QW materials with ternary barriers will offer interesting new material systems to study. One of the main goals in devices will be mode-locking of GaSb SDL, operating at longer wavelengths, with GaSb SESAM, and in materials research point of view, to continue the study of SESAM dynamics at 2 μm and longer wavelengths.

Bibliography

[1] T. H. Maiman, "Stimulated Optical Radiation in Ruby," *Nature*, vol. 187, no. 4736, pp. 493–494, 1960.

[2] R. N. Hall, G. E. Fenner, J. D. Kingsley, T. J. Soltys, and R. O. Carlson, "Coherent Light Emission From GaAs Junctions," *Physics Review Letters*, vol. 9, pp. 366–368, 1962.

[3] I. Hayashi, M. Panish, and P. Foy, "A low-threshold room-temperature injection laser," *IEEE Journal of Quantum Electronics*, vol. 5, no. 4, pp. 211–212, 1969.

[4] R. F. Curl and F. K. Tittel, "Tunable infrared laser spectroscopy," *Annual Reports on the Progress of Chemistry Section C*, vol. 98, pp. 219–272, 2002.

[5] L. Rothman, D. Jacquemart, A. Barbe, D. Benner, M. Birk, L. Brown, M. Carleer, C. Chackerian, K. Chance, L. Coudert, V. Dana, V. Devi, J. Flaud, R. Gamache, A. Goldman, J. Hartmann, K. Jucks, A. Maki, J. Mandin, S. Massie, J. Orphal, A. Perrin, C. Rinsland, M. Smith, J. Tennyson, R. Tolchenov, R. Toth, J. Vander Auwera, P. Varanasi, and G. Wagner, "The HITRAN 2004 molecular spectroscopic database," *Journal of Quantitative Spectroscopy Radiative Transfer*, vol. 96, pp. 139–204, 2005.

[6] A. L. McKenzie, "Physics of thermal processes in laser-tissue interaction," *Physics in Medicine and Biology*, vol. 35, pp. 1175–1209, 1990.

[7] I. Vurgaftman, J. R. Meyer, and L. R. Ram-Mohan, "Band parameters for III–V compound semiconductors and their alloys," *Journal of Applied Physics*, vol. 89, no. 11, pp. 5815–5875, 2001.

[8] A. Härkönen, M. Guina, O. Okhotnikov, K. Rößner, M. Hümmer, T. Lehnhardt, M. Müller, A. Forchel, and M. Fischer, "1-W antimonide-based vertical external cavity surface emitting laser operating at 2-μm," *Optics Express*, vol. 14, no. 14, pp. 6479–6484, 2006.

[9] J.-M. Hopkins, N. Hempler, B. Rösener, N. Schulz, M. Rattunde, C. Manz, K. Köhler, J. Wagner, and D. Burns, "High-power, (AlGaIn)(AsSb) semiconductor disk laser at 2.0 μm," *Optics Letters*, vol. 33, no. 2, pp. 201–203, 2008.

[10] J.-M. Hopkins, A. J. Maclean, E. Riis, N. Schulz, M. Rattunde, C. Manz, K. Köhler, J. Wagner, and D. Burns, "Tunable, single-frequency, diode-pumped 2.3 μm VECSEL," *Optics Express*, vol. 15, no. 13, pp. 8212–8217, 2007.

[11] D. Barat, J. Angellier, A. Vicet, Y. Rouillard, L. L. Gratiet, S. Guilet, A. Martinez, and A. Ramdan, "Antimonide-based DFB lasers emitting above 2.6 μm," *Electronics Letters*, vol. 43, no. 23, pp. 1281–1282, 2007.

[12] K. Rößner, M. Hümmer, T. Lehnhardt, M. Müller, A. Forchel, M. Fischer, and J. Koeth, "Continuous-Wave Operation of GaInAsSb-GaSb Type-II Ridge Waveguide Lasers Emitting at 2.8 μm," *IEEE Photonics Technology Letters*, vol. 18, no. 13, pp. 1424–1426, 2006.

[13] T. Hosoda, G. Belenky, L. Shterengas, G. Kipshidge, and M. V. Visin, "Continuous-wave room temperature operated 3.0 μm type I GaSb-based lasers with quinternary AlInGaAsSb barriers," *Applied Physics Letters*, vol. 92, pp. 091 106–091 109, 2008.

[14] K. Haring, J. Viheriälä, M.-R. Viljanen, J. Paajaste, R. Koskinen, S. Suomalainen, A. Laakso, K. Leinonen, T. Niemi, and M. Guina, "Laterally-coupled distributed feedback InGaSb/GaSb diode lasers fabricated by nanoimprint lithography," *Electronics Letters*, vol. 46, no. 16, pp. 1146–1147, 2010.

[15] L. Shterengas, G. L. Belenky, J. G. Kim, and R. U. Martinelli, "Design of high-power room-temperature continuous-wave GaSb-based type-I quantum-well lasers

with $\lambda > 2.5$ μm," *Semiconductor Science and Technology*, vol. 19, no. 5, p. 655, 2004.

[16] J. G. Kim, L. Shterengas, R. U. Martinelli, and G. L. Belenky, "High-power room-temperature continuous wave operation of 2.7 and 2.8 μm In(Al)GaAsSb/GaSb diode lasers," *Applied Physics Letters*, vol. 83, no. 10, pp. 1926–1928, 2003.

[17] M. Kuznetsov, F. Hakimi, R. Sprague, and A. Mooradian, "Design and characteristics of high-power (>0.5-W CW) diode-pumped vertical-external-cavity surface-emitting semiconductor lasers with circular TEM00 beams," *IEEE Journal of Selected Topics in Quantum Electronics*, vol. 5, no. 3, pp. 561–573, 1999.

[18] L. Fan, M. Fallahi, J. T. Murray, R. Bedford, Y. Kaneda, A. R. Zakharian, J. Hader, J. V. Moloney, W. Stolz, and S. W. Koch, "Tunable high-power high-brightness linearly polarized vertical-external-cavity surface-emitting lasers," *Applied Physics Letters*, vol. 88, no. 2, pp. 021 105–021 108, 2006.

[19] U. Keller, K. Weingarten, F. Kartner, D. Kopf, B. Braun, I. Jung, R. Fluck, C. Honninger, N. Matuschek, and J. Aus der Au, "Semiconductor saturable absorber mirrors (SESAM's) for femtosecond to nanosecond pulse generation in solid-state lasers," *IEEE Journal of Selected Topics in Quantum Electronics*, vol. 2, no. 3, pp. 435–453, 1996.

[20] S. Kivistö, R. Koskinen, J. Paajaste, S. D. Jackson, M. Guina, and O. G. Okhotnikov, "Passively Q-switched Tm3+, Ho3+-doped silica fiber laser using a highly nonlinear saturable absorber and dynamic gain pulse compression," *Optics Express*, vol. 16, no. 26, pp. 22 058–22 063, 2008.

[21] K. Yang, D. Heinecke, J. Paajaste, C. Kölbl, T. Dekorsy, S. Suomalainen, and M. Guina, "Mode-locking of 2 μm Tm,Ho:YAG laser with GaInAs and GaSb-based SESAMs," *Optics Express*, vol. 21, no. 4, pp. 4311–4318, 2013.

[22] A. Gluth, X.Mateos, J. Paajaste, S. Suomalainen, A. Härkönen, M. Guina, G. Steinmeyer, S. Veronesi, M. Tonelli, J. Li, Y. Pan, J. Guo, V. Petrov, and U. Griebner,

"Passively Mode-Locked Tm:YAG Ceramic Laser at 2 μm." Paris, France: Advanced Solid State Lasers (ASSL) Congress, 2013.

[23] A. Härkönen, C. Grebing, J. Paajaste, R. Koskinen, J. P. Alanko, S. Suomalainen, G. Steinmeyer, and M. Guina, "Modelocked GaSb disk laser producing 384 fs pulses at 2 μm wavelength," *Electronics Letters*, vol. 47, no. 7, pp. 454–456, 2011.

[24] M. Rattunde, J. Schmitz, C. Mermelstain, R. Kiefer, and J. Wagner, *III-Sb-based Type-I QW Diode Lasers, Chapter 3: Mid-Infrared Semiconductor Optoelectronics*. 233 Springstreet, NY 10013, US.: Springer Science+Business Media, Inc., 2006.

[25] J. Lazzari, J. Leclercq, P. Grunberg, A. Joullie, B. Lambert, D. Barbusse, and R. Fourcade, "Liquid phase epitaxial growth of AlGaAsSb on GaSb," *Journal of Crystal Growth*, vol. 123, no. 3–4, pp. 465–478, 1992.

[26] M. A. Herman, *Molecular Beam Epitaxy: Fundamentals and Current Status*, 2nd ed. Berlin Heidelberg, New York: Springer-Verlag, 1996.

[27] M. Henini, *Molecular Beam Epitaxy: From Research to Mass Production*, 1st ed. Elsevier Science and Technology, 2012.

[28] H. Ibach and H. Lüth, *Semiconductors*. Springer Berlin Heidelberg, 2009, pp. 419–515.

[29] M. Kuznetsov, F. Hakimi, R. Sprague, and A. Mooradian, "High-power (>0.5-W CW) diode-pumped vertical-external-cavity surface-emitting semiconductor lasers with circular TEM_{00} beams," *Photonics Technology Letters*, vol. 9, no. 8, pp. 1063–1065, 1997.

[30] B. Heinen, T.-L. Wang, M. Sparenberg, A. Weber, B. Kunert, J. Hader, S. Koch, J. Moloney, M. Koch, and W. Stolz, "106 W continuous-wave output power from vertical-external-cavity surface-emitting laser," *Electronics Letters*, vol. 48, pp. 516–517, 2012.

[31] Y. Kaneda, J. M. Yarborough, L. Li, N. Peyghambarian, L. Fan, C. Hessenius, M. Fallahi, J. Hader, J. V. Moloney, Y. Honda, M. Nishioka, Y. Shimizu, K. Miyazono, H. Shimatani, M. Yoshimura, Y. Mori, Y. Kitaoka, and T. Sasaki, "Continuous-wave all-solid-state 244 nm deep-ultraviolet laser source by fourth-harmonic generation of an optically pumped semiconductor laser using $CsLiB_6O_{10}$ in an external resonator," *Optics Letters*, vol. 33, no. 15, pp. 1705–1707, 2008.

[32] M. Rahim, F. Felder, M. Fill, and H. Zogg, "Optically pumped 5 μm IV-VI VECSEL with Al-heat spreader," *Optics Letters*, vol. 33, no. 24, pp. 3010–3012, 2008.

[33] T. Kurita, K. Sueda, K. Tsubakimoto, and N. Miyanaga, "Experimental demonstration of spatially coherent beam combining using optical parametric amplification," *Optics Express*, vol. 18, no. 14, pp. 14 541–14 546, 2010.

[34] N. Schulz, M. Rattunde, C. Ritzenthaler, B. Rösener, C. Manz, K. Köhler, J. Wagner, and U. Brauch, "Resonant optical in-well pumping of an (AlGaIn)(AsSb)-based vertical-external-cavity surface-emitting laser emitting at 2.35 μm," *Applied Physics Letters*, vol. 91, no. 9, pp. 091 113–091 116, 2007.

[35] A. Maclean, A. Kemp, S. Calvez, J.-Y. Kim, T. Kim, M. Dawson, and D. Burns, "Continuous Tuning and Efficient Intracavity Second-Harmonic Generation in a Semiconductor Disk Laser With an Intracavity Diamond Heatspreader," *IEEE Journal of Quantum Electronics*, vol. 44, no. 3, pp. 216–225, 2008.

[36] B. Rudin, A. Rutz, M. Hoffmann, D. J. H. C. Maas, A.-R. Bellancourt, E. Gini, T. Südmeyer, and U. Keller, "Highly efficient optically pumped vertical-emitting semiconductor laser with more than 20 W average output power in a fundamental transverse mode," *Optics Letters*, vol. 33, no. 22, pp. 2719–2721, 2008.

[37] A. Khadour, S. Bouchoule, G. Aubin, J.-C. Harmand, J. Decobert, and J.-L. Oudar, "Ultrashort pulse generation from 1.56 μm mode-locked VECSEL at room temperature," *Optics Express*, vol. 18, no. 19, pp. 19 902–19 913, 2010.

[38] S. Hilbich, W. Seelert, V. Ostroumov, C. Kannengiesser, R. Elm, J. Mueller, E. Weiss, H. Zhou, and J. Chilla, "New wavelengths in the yellow-orange range

between 545 nm and 580 nm generated by an intracavity frequency-doubled optically pumped semiconductor laser," *Proceedings of SPIE*, vol. 6451, pp. 64 510C–7, 2007.

[39] B. Rösener, M. Rattunde, R. Moser, S. Kaspar, T. Töpper, C. Manz, K. Köhler, and J. Wagner, "Continuous-wave room-temperature operation of a 2.8 μm GaSb-based semiconductor disk laser," *Optics Letters*, vol. 36, no. 3, pp. 319–321, 2011.

[40] T. Leinonen, J. Puustinen, V.-M. Korpijarvi, A. Harkonen, M. Guina, and R. Epstein, "Generation of high power (>7W) yellow-orange radiation by frequency doubling of GaInNAs-based semiconductor disk laser," in *Lasers and Electro-Optics Europe (CLEO EUROPE/EQEC)*, 2011, pp. 1–1.

[41] A. Rantamäki, A. Sirbu, A. Mereuta, E. Kapon, and O. G. Okhotnikov, "3 W of 650 nm red emission by frequency doubling of wafer-fused semiconductor disk laser," *Optics Express*, vol. 18, no. 21, pp. 21 645–21 650, 2010.

[42] J. Lyytikäinen, J. Rautiainen, A. Sirbu, V. Iakovlev, A. Laakso, S. Ranta, M. Tavast, E. Kapon, and O. Okhotnikov, "High-Power 1.48-μm Wafer-Fused Optically Pumped Semiconductor Disk Laser," *IEEE Photonics Technology Letters*, vol. 23, no. 13, pp. 917–919, 2011.

[43] J. Rautiainen, J. Lyytikäinen, A. Sirbu, A. Mereuta, A. Caliman, E. Kapon, and O. G. Okhotnikov, "2.6 W optically-pumped semiconductor disk laser operating at 1.57-μm using wafer fusion," *Optics Express*, vol. 16, no. 26, pp. 21 881–21 886, 2008.

[44] A. Aschwanden, D. Lorenser, H. J. Unold, R. Paschotta, E. Gini, and U. Keller, "2.1-W picosecond passively mode-locked external-cavity semiconductorlaser," *Optics Letters*, vol. 30, no. 3, pp. 272–274, 2005.

[45] U. Keller and A. C. Tropper, "Passively modelocked surface-emitting semiconductor lasers," *Physics Reports*, vol. 429, no. 2, pp. 67–120, 2006.

[46] W. Zhang, A. McDonald, T. Ackemann, E. Riis, and G. McConnell, "Femtosecond synchronously in-well pumped vertical-external-cavity surface-emitting laser," *Optics Express*, vol. 18, no. 1, pp. 187–192, 2010.

[47] H. Lindberg, M. Sadeghi, M. Westlund, S. Wang, A. Larsson, M. Strassner, and S. Marcinkevicius, "Mode locking a 1550 nm semiconductor disk laser by using a GaInNAs saturable absorber," *Optics Letters*, vol. 30, no. 20, pp. 2793–2795, 2005.

[48] A. Rutz, V. Liverini, D. J. H. C. Maas, B. Rudin, A. R. Bellancourt, S. Schon, and U. Keller, "Passively modelocked GaInNAs VECSEL at centre wavelength around 1.3 μm," *Electronics Letters*, vol. 42, no. 16, pp. 926–927, 2006.

[49] J. Rautiainen, A. Härkönen, V.-M. Korpijärvi, J. Puustinen, L. Orsila, M. Guina, and O. Okhotnikov, "Red and UV Generation Using Frequency-Converted GaInNAs-Based Semiconductor Disk Laser," in *Conference on Lasers and Electro-Optics/International Quantum Electronics Conference*. Optical Society of America, 2009.

[50] J.-M. Hopkins, N. Hempler, B. RÃűsener, N. Schulz, M. Rattunde, C. Manz, K. KÃűhler, J. Wagner, and D. Burns, "5W Mid-IR optically-pumped semiconductor disk laser," 2008.

[51] J. Chilla, S. Butterworth, A. Zeitschel, J. Charles, A. C. M. Reed, and L. Spinelli, "High-power optically pumped semiconductor lasers," *Proceecings of SPIE*, vol. 5332, pp. 143–150, 2004.

[52] J. Rautiainen, V.-M. Korpijärvi, J. Puustinen, M. Guina, and O. Okhotnikov, "Passively mode-locked GaInNAs disk laser operating at 1220 nm," *Optics Express*, vol. 16, no. 20, pp. 15 964–15 969, 2008.

[53] D. A. Ackerman, P. A. Morton, G. E. Shtengel, M. S. Hybertsen, R. F. Kazarinov, T. Tanbun-Ek, and R. A. Logan, "Analysis of T_0 in 1.3 μm multi-quantum-well and bulk active lasers," *Applied Physics Letters*, vol. 66, no. 20, pp. 2613–2615, 1995.

[54] T. Schwarzback, R. Bek, F. Hargart, C. A. Kessler, H. Kahle, E. Koroknay, M. Jetter, and P. Michler, "High-power InP quantum dot based semiconductor disk laser exceeding 1.3 W," *Applied Physics Letters*, vol. 102, no. 9, p. 092101, 2013.

[55] E. F. Schubert and N. E. J. Hunt, *Enhancement of Spontaneous Emission in Microcavities, Chapter 3: Vertical-Cavity Surface-Emitting Lasers*. UK: Cambridge University Press, 1999.

[56] E. D. Palik, *Handbook of Optical Constants of Solids*. San Diego CA: Academic Press, 1985.

[57] M. Redd, T. Asano, R. Koda, D. Buell, and L. Coldren, "Molecular beam epitaxy grown AlGaInAs/InP distributed Bragg reflectors for 1.55 μm VCSELs," *IET Electronics Letters*, vol. 38, no. 20, pp. 1181–1182, 2002.

[58] M. M. Uribe, C. E. M. de Oliveira, J. H. Clerice, R. S. Miranda, M. B. Zakia, M. M. G. de Carvakho, and N. B. Patel, "Measurement of refractive index of GaSb (1.8 to 2.56 μm) using prism," *IET Electronics Letters*, vol. 32, no. 3, pp. 262–264, 1996.

[59] R. E. Fern and A. Onton, "Refractive index of AlAs," *Journal of Applied Physics*, vol. 42, no. 9, pp. 3499–3500, 1971.

[60] O. Svelto, *Principles of Lasers*, 4th ed. 233 Springstreet, NY 10013, US.: Springer Science+Business Media, Inc., 1998.

[61] M. Motyka, G. Sek, K. Ryczko, J. Misiewicz, T. Lehnhardt, S. Hofling, and A. Forchel, "Optical properties of GaSb-based type II quantum wells as the active region of midinfrared interband cascade lasers for gas sensing applications," *Applied Physics Letters*, vol. 94, no. 25, p. 251901, 2009.

[62] Y. Chen, H. Li, and K. Wang, "Study of stark effect in alsb/gasb/inas/alsb quantum well," *Superlattices and Microstructures*, vol. 14, no. 2–3, p. 137, 1993.

[63] D. Firsov, L. Shterengas, G. Kipshidze, V. Zerova, T. Hosoda, P. Thumrongsilapa, L. Vorobjev, and G. Belenky, "Dynamics of photoluminescence and recombination

processes in Sb-containing laser nanostructures," *Semiconductors*, vol. 44, no. 1, pp. 50–58, 2010.

[64] M. Kuznetsov, *VECSEL Semiconductor Lasers: A Path to High-Power, Quality Beam and UV to IR Wavelength by Design*. Wiley-VCH Verlag GmbH and Co. KGaA, 2010, pp. 1–71.

[65] M. Y. A. Raja, S. Brueck, M. Osinski, C. Schaus, J. McInerney, T. Brennan, and B. Hammons, "Resonant periodic gain surface-emitting semiconductor lasers," *IEEE Journal of Quantum Electronics*, vol. 25, no. 6, pp. 1500–1512, 1989.

[66] A. Giesen and J. Speiser, "Fifteen Years of Work on Thin-Disk Lasers: Results and Scaling Laws," *IEEE Journal of Selected Topics in Quantum Electronics*, vol. 13, no. 3, pp. 598–609, 2007.

[67] W. J. Alford, T. D. Raymond, and A. A. Allerman, "High power and good beam quality at 980 nm from a vertical external-cavity surface-emitting laser," *Journal of Optical Society America B*, vol. 19, no. 4, pp. 663–666, 2002.

[68] A. Kemp, G. Valentine, J. M. Hopkins, J. Hastie, S. Smith, S. Calvez, M. Dawson, and D. Burns, "Thermal management in vertical-external-cavity surface-emitting lasers: finite-element analysis of a heatspreader approach," *IEEE Journal of Quantum Electronics*, vol. 41, no. 2, pp. 148–155, 2005.

[69] J.-P. Perez, A. Laurain, L. Cerutti, I. Sagnes, and A. Garnache, "Technologies for thermal management of mid-IR Sb-based surface emitting lasers," *Semiconductor Science and Technology*, vol. 25, no. 4, p. 045021, 2010.

[70] J. Lindfors, J. Paajaste, R. Koskinen, A. Härkönen, S. Suomalainen, and M. Guina, "Highly Selective Etch Stop Layer for GaSb Substrate Removal." Stockholm, Sweden: 16th Semiconducting and Insulating Materials Conference SIMC XVI, 2011.

[71] B. Klein, J. Montoya, N. Gautam, and S. Krishna, "Selective InAs/GaSb strained layer superlattice etch stop layers for GaSb substrate removal," *Applied Physics A*, vol. 111, no. 2, pp. 671–674, 2013.

[72] U. Keller, D. A. B. Miller, G. D. Boyd, T. H. Chiu, J. F. Ferguson, and M. T. Asom, "Solid-state low-loss intracavity saturable absorber for Nd:YLF lasers: an antiresonant semiconductor Fabry–Perot saturable absorber," *Optics Letters*, vol. 17, no. 7, pp. 505–507, 1992.

[73] S. Gupta, J. Whitaker, and G. Mourou, "Ultrafast carrier dynamics in III-V semiconductors grown by molecular-beam epitaxy at very low substrate temperatures," *IEEE Journal of Quantum Electronics*, vol. 28, no. 10, pp. 2464–2472, 1992.

[74] R. Takahashi, Y. Kawamura, and H. Iwamura, "Ultrafast 1.55 μm all-optical switching using low-temperature-grown multiple quantum wells," *Applied Physics Letters*, vol. 68, no. 2, pp. 153–155, 1996.

[75] M. Haiml, U. Siegner, F. Morier-Genoud, U. Keller, M. Luysberg, P. Specht, and E. R. Weber, "Femtosecond response times and high optical nonlinearity in beryllium-doped low-temperature grown GaAs," *Applied Physics Letters*, vol. 74, no. 9, pp. 1269–1271, 1999.

[76] M. Lederer, B. Luther-Davies, H. H. Tan, and C. Jagadish, "GaAs based antiresonant Fabry –Perot saturable absorber fabricated by metal organic vapor phase epitaxy and ion implantation," *Applied Physics Letters*, vol. 70, no. 25, pp. 3428–3430, 1997.

[77] E. L. Delpon, J. L. Oudar, N. Bouche, R. Raj, A. Shen, N. Stelmakh, and J. M. Lourtioz, "Ultrafast excitonic saturable absorption in ion-implanted InGaAs/InAlAs multiple quantum wells," *Applied Physics Letters*, vol. 72, no. 7, pp. 759–761, 1998.

[78] O. Ostinelli, W. Bachtold, H. Haiml, R. Grange, U. Keller, E. Gini, and G. Almuneau, "Carrier lifetime reduction in 1.5 μm AlGaAsSb saturable absorbers with air and AlAsSb barriers," *Applied Physics Letters*, vol. 89, no. 7, pp. 071 114–6, 2006.

[79] S. Suomalainen, A. Vainionpää, O. Tengvall, T. Hakulinen, S. Karirinne, M. Guina, O. G. Okhotnikov, T. G. Euser, and W. L. Vos, "Long-wavelength fast semicon-

ductor saturable absorber mirrors using metamorphic growth on GaAs substrates," *Applied Physics Letters*, vol. 87, no. 12, p. 121106, 2005.

[80] S. Suomalainen, A. Vainionpää, O. Tengvall, T. Hakulinen, R. Herda, S. Karirinne, M. Guina, and O. G. Okhotnikov, "Long-wavelength semiconductor saturable absorber mirrors using metamorphic InP grown on GaAs by molecular beam epitaxy," *Journal of Vacuum Science and Technology B*, vol. 24, no. 3, pp. 1496–1499, 2006.

[81] S. Suomalainen, M. Guina, T. Hakulinen, O. G. Okhotnikov, T. G. Euser, and S. Marcinkevicius, "1 μm saturable absorber with recovery time reduced by lattice mismatch," *Applied Physics Letters*, vol. 89, no. 7, p. 071112, 2006.

[82] A. Marceaux, S. Loualiche, O. Dehaese, and B. Lambert, "High-speed 1.55 μm Fe-doped multiple-quantum-well saturable absorber on InP," *Applied Physics Letters*, vol. 78, no. 26, pp. 4065–4067, 2001.

[83] S. Anikeev, D. Donetsky, G. Belenky, S. Luryi, C. A. Wang, J. M. Borrego, and G. Nichols, "Measurement of the Auger recombination rate in p-type 0.54 eV GaInAsSb by time-resolved photoluminescence," *Applied Physics Letters*, vol. 83, no. 16, pp. 3317–3319, 2003.

[84] G. Benz and R. Conradt, "Auger recombination in GaAs and GaSb," *Physics Review B*, vol. 16, pp. 843–855, 1977.

[85] A. Sugimura, "Band-to-band auger effect in long wavelength multinary III-V alloy semiconductor lasers," *IEEE Journal of Quantum Electronics*, vol. 18, no. 3, pp. 352–363, 1982.

[86] D. K. Bowen and B. K.Tanner, *High Resolution X-ray Diffractometry and Topography*. 1 Gunpowder Square, London: Taylor and Francis Ltd, 1998.

[87] S. Adachi, "Band gaps and refractive indices of AlGaAsSb, GaInAsSb, and InPAsSb: Key properties for a variety of the 2–4-μm optoelectronic device applications," *Journal of Applied Physics*, vol. 61, no. 10, pp. 4869–4876, 1987.

[88] C. Alibert, M. Skouri, A. Joullie, M. Benouna, and S. Sadiq, "Refractive indices of AlSb and GaSb-lattice-matched $Al_xGa_{1-x}As_ySb_{1-y}$in the transparent wavelength region," *Journal of Applied Physics*, vol. 69, no. 5, pp. 3208–3211, 1991.

[89] E. Kuramochi, N. Kondo, Y. Takanashi, and M. Fujimoto, "Observation of deep levels in undoped GaSb grown by molecular beam epitaxy," *Applied Physics Letters*, vol. 63, no. 19, pp. 2664–2666, 1993.

[90] P. S. Dutta, K. S. R. K. Rao, K. S. Sangunni, H. L. Bhat, and V. Kumar, "Donor-related deep level in bulk GaSb," *Applied Physics Letters*, vol. 65, no. 11, pp. 1412–1414, 1994.

[91] K. S. Gadedjisso-Tossou, S. Belahsene, M. A. Mohou, E. Tournie, and Y. Rouillard, "Recombination channels in 2.4–3.2 μm GaInAsSb quantum-well lasers," *Semiconductor Science and Technology*, vol. 28, no. 1, p. 015015, 2013.

[92] A. Jasik, J. Muszalski, K. Hejduk, and M. Kosmala, "The reduced temporal parameters of passivated semiconductor saturable absorber mirror," *Thin Solid Films*, vol. 518, no. 1, pp. 171–173, 2009.

[93] H. Haus, "Mode-locking of lasers," *IEEE Journal of Selected Topics in Quantum Electronics*, vol. 6, no. 6, pp. 1173–1185, 2000.

[94] A. Härkönen, A. Bachmann, S. Arafin, K. Haring, J. Viheriälä, M. Guina, and M.-C. Amann, "2.34–μm electrically pumped VECSEL with buried tunnel junction," *Proceedings SPIE*, vol. 7720, p. 772015, 2010.

Appendix A

Publication 1

High-power and broadly tunable GaSb-based optically-pumped VECSELs emitting near 2 μm

Jonna Paajaste*, Soile Suomalainen, Riku Koskinen, Antti Härkönen, Mircea Guina, and Markus Pessa

Optoelectronics Research Centre, Tampere University of Technology, P.O. Box 692, FIN-33101 Tampere, Finland

*jonna.paajaste@tut.fi

Abstract:

We demonstrate GaSb-based vertical-external-cavity surface-emitting lasers (VECSELs) emitting multi-Watt output power and exhibiting a broad tuning range. A VECSEL gain structure comprising 15 $In_{0.2}Ga_{0.8}Sb$ quantum wells grown on (100) *n*-doped GaSb substrate emitted continuous wave output power of over 4 W at 1970 nm wavelength operating near room temperature. Lasing was detected even at 50 °C. Optimized for high power operation, the structure exhibited a tuning range of 75 nm. Using a modified VECSEL gain structure, comprising three different kinds of quantum wells, we achieved a spectral tuning of about 156 nm.

PACS: 42.55.Xi, 73.61.Ey, 42.72.Ai

Keywords: A3. Molecular beam epitaxy, B1. Antimonides, B2. Semiconducting III-V materials, B3. Infrared devices

1. Introduction

Single-mode lasers operating in the 2–3 μm wavelength range are attractive for various sensing and laser spectroscopy applications, and in particular for the detection of atmospheric pollutants [1]. High-power, edge-emitting diode lasers based on the (AlGaIn)(AsSb) material system can cover the 2.0–2.7 μm band, but they have a poor-quality elliptical output beam [2].

Optically-pumped vertical-external-cavity surface-emitting lasers (OP-VECSELs), also known as optically-pumped semiconductor disk lasers (OP-SDLs), provide a good quality, nearly diffraction limited beam and output power much higher than a single-mode laser diode (LD). Moreover, the external cavity configuration enables the use of intra-cavity filters for wavelength tuning [3, 4]. When compared with LDs, OP-VECSELs are more advantageous also in terms of fabrication complexity; there is no need for doping associated with electrical injection [5].

The GaSb material system enables the use of lattice matched distributed Bragg reflectors (DBRs) comprised of layers with a high refractive index contrast, namely $AlAs_{0.08}Sb_{0.92}$ and GaSb. Such DBRs have an exceptionally broad stopband (~300 nm [3]) and require a relatively small number of layer pairs to achieve high reflectance. The broad stopband makes GaSb-based vertical-cavity lasers highly interesting for

spectroscopic applications requiring a wide tuning range. In this study we demonstrate both high power VECSELs as well as VECSELs with a broad wavelength tuning range.

2. Growth details and structural design

The semiconductor structures were grown using a conventional solid source molecular beam epitaxy (MBE) reactor. Elemental indium, aluminum and gallium together with As_4 and Sb_4 were used as group-III and -V sources respectively. The group-V constituents were cracked into As_2 and Sb_2 using high temperature cracking tubes.

The laser gain mirror structures consist of a distributed Bragg reflector and a gain region with multiple quantum wells (QWs). First a GaSb buffer layer was grown on an *n*-doped (100)-oriented GaSb substrate to smoothen the surface. The buffer was followed by 18.5 pairs of lattice matched $AlAs_{0.08}Sb_{0.92}$/GaSb layers forming the DBR and the QW active region. The active region for the high-power VECSEL (VECSEL-1) consists of five groups of $In_{0.2}Ga_{0.8}Sb$ QWs, each group containing three quantum wells having a width of 8 nm. The QWs were embedded in GaSb and the structure was closed with a lattice matched $AlAs_{0.08}Sb_{0.92}$ window layer to ensure good carrier confinement. The window was followed by a thin GaSb cap layer to prevent oxidation. The QW groups were located at the antinodes of the standing wave optical field in the 3-λ micro-cavity formed by the DBR and the semiconductor-air interface. The VECSEL structure is shown in Fig. 1a. The room-temperature photoluminescence (PL) and reflectivity curves for VECSEL-1 are shown in Fig. 2.

The broadly tunable structure (VECSEL-2) is similar to VECSEL-1, except for its active region. It contains three groups of non-identical $In_{0.2}Ga_{0.8}Sb$ QWs: 3 × 6.5 nm, 3 ×

9.5 nm and 2 × 16 nm with GaSb barriers of different thickness. A thin $AlAs_{0.08}Sb_{0.92}$ layer was grown between each QW group to prevent carrier diffusion between different QW groups and to promote more equalized pumping of different QWs. The thicknesses of pump absorbing GaSb layers between the QW groups were calculated in such a way that each QW group would be placed at an antinode of the standing wave optical field formed within the gain microcavity. The VECSEL-2 structure is shown in Fig. 1b. Each type of QW was calibrated independently using PL-samples. Before the growth of the actual VECSEL-2 structure, a PL calibration sample containing the three different QWs was also grown; the corresponding PL signal is displayed in Fig. 3.

Both VECSELs were processed into 2.5 × 2.5 mm^2 gain chips that were capillary bonded with water to a type IIa natural diamond or to an artificial diamond heat spreader of 300–500 μm thickness. The diamond allows efficient heat removal from the gain region and avoids the need to conduct thermal energy through a heat resistant DBR [6]. The bonded chips were mounted to a water cooled copper heat sink that was integrated in the VECSEL cavity. The outer surface of the diamond on VECSEL-1 was also antireflection coated to reduce the signal and pump reflection.

3. Experimental results and discussion

The gain chips were measured using a V-type cavity configuration consisting of the mounted gain chip, a high reflective folding mirror with a radius of curvature of 200 mm, and a partially reflective planar output coupler (OC). The pump source used was a

980 nm fiber coupled diode laser. The pump beam was focused onto the sample to a spot of about 290 μm in diameter. The laser schematic is presented in Fig. 4.

VECSEL-1, optimized for high power operation, was operated with a 2 % transmissive output coupler. It exhibited excellent temperature behavior. The output power was over 4 W at 15 °C, and still 3.6 W at room temperature at a wavelength of 1970 nm. Lasing was observed up to a temperature as high as 50 °C. The lasing characteristics (output powers and a typical optical spectrum) are shown in Fig. 5. The pumping threshold was close to 2 W near room temperature.

To achieve wavelength tuning and narrow emission we placed a birefringent filter inside the laser cavity at the Brewster angle. The emission wavelength of the VECSEL-1 could be tuned about 75 nm, from 1925 to 2002 nm, by rotating the birefringent filter.

The output coupler used for VECSEL-2 had a transmission of about 1 %. Owing to the modified gain region incorporating asymmetric QWs, we achieved a tuning range of 156 nm (1924–2080 nm) at an operation temperature of 10–15 °C. The tuning characteristics are shown in Figs. 6 and 7. Compared to structure VECSEL-1, the use of asymmetric quantum wells in VECSEL-2 led to a 100% increase of the tuning range. As shown in Fig. 6 the broad DBR stop-band would support laser operation far beyond 2080 nm. Therefore, it is reasonable to assume that by further optimization of the gain region the tuning range could be extended beyond the current state-of-the-art of ~150 nm [7]. Fig. 7 shows the output power for different wavelengths. The maximum output power was 390 mW. We should note that a significant part of the laser radiation is lost as parasitic reflection from the birefringent filter. This effect is attributed to the

birefringency of the intra-cavity diamond, which introduces a certain amount of retardation to the polarization during each round trip [8].

4. Conclusions

We have studied the lasing characteristics of GaSb-based VECSELs exploiting two different designs for the gain mirrors. Using a gain mirror comprised of $In_{0.2}Ga_{0.8}Sb$/GaSb QWs with identical thickness we attained multi-watt high power room temperature operation. The tuning range for this structure was about 75 nm. Using a modified gain mirror design, which consisted of $In_{0.2}Ga_{0.8}Sb$/GaSb QWs having different thicknesses, we doubled the tuning range to about 150 nm while preserving an output power level suitable for practical spectroscopic applications. Further studies will focus on the demonstration of passive mode-locking operation and development of VECSELs with emission at wavelengths beyond 2 μm [9].

Acknowledgements

Authors wish to acknowledge financial support of Finnish Funding Agency for Technology and Innovation within project Nanophotonics (161147-2) and the State Provincial Office of Western Finland (EAKR-funding). The authors thank Lasse Orsila for the VECSEL antireflection coating and J. Nikkinen and J. Rautiainen for their work concerning the VECSEL characterization.

References:

[1] T. Bleuel, M. Müller, A. Forchel, IEEE Photon. Technol. Lett. **13** (2001) 553

[2] H. K. Choi, J. N. Walpole, G. W. Turner, M. K. Connors, L. J. Missaggia, M. J. Manfra, IEEE Photon. Technol. Lett. **10** (1998) 938

[3] A. Härkönen, M. Guina, O. Okhotnikov, K. Röβner, M. Hümmer, T. Lehnhardt, M. Müller, A. Forchel, M. Fischer, Opt. Express **14** (2006) 6479

[4] L. Fan, M. Fallahi, J.T. Murray, R. Bedford, Y. Kaneda, A.R. Zakharian, J. Hader, J.V. Moloney, W. Stolz, S.W. Koch, Appl. Phys. Lett. **88** (2006) 021105

[5] J.-M. Hopkins, N. Hempler, B. Rösener, N. Schulz, M. Rattunde, C. Manz, K. Köhler, J. Wagner, D. Burns, Opt. Lett. **33** (2008) 201

[6] A. J. Kemp, G. J. Valentine, J.-M. Hopkins, J. E. Hastie, S. A. Smith, S. Calvez, M. D. Dawson, D. Burns, IEEE J. Quantum Electron. **41** (2005) 148

[7] J.-M. Hopkins, N. Hempler, B. Rösener, N. Schulz, M. Rattunde, C. Manz, K. Köhler, J. Wagner, D. Burns, *CLEO/QELS 2008*, (2008)

[8] F. van Loon, A. J. Kemp, A. J. Maclean, S. Calvez, J.-M. Hopkins, J. E. Hastie, M. D. Dawson and D. Burns, Opt. Express, **14** (2006) 9250

[9] B. Rösener, N. Schulz, M. Rattunde, C. Manz, K. Kuhler, J. Wagner, IEEE Photon. Technol. Lett., **20** (2008) 502

Figure captions:

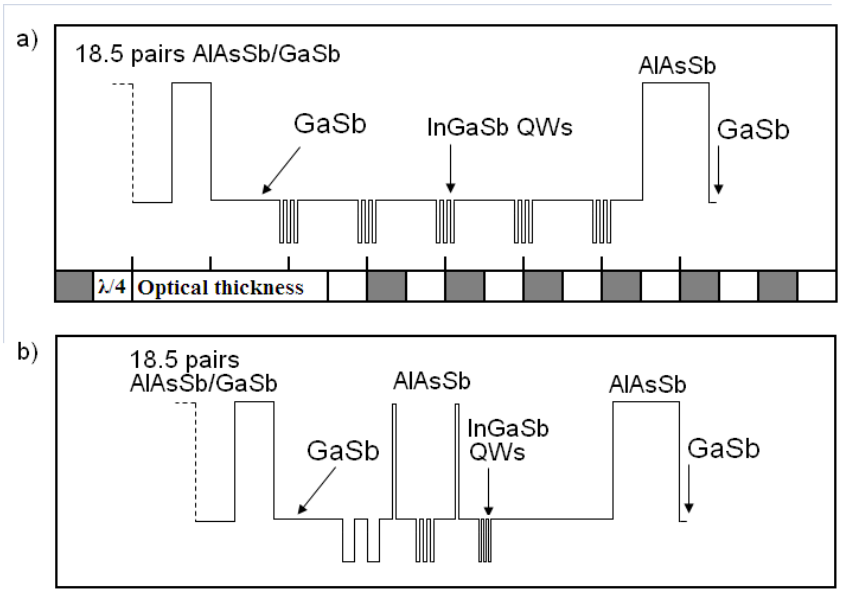

Figure 1. VECSEL structures for a) High-power VECSEL-1 and b) Broadly tunable VECSEL-2

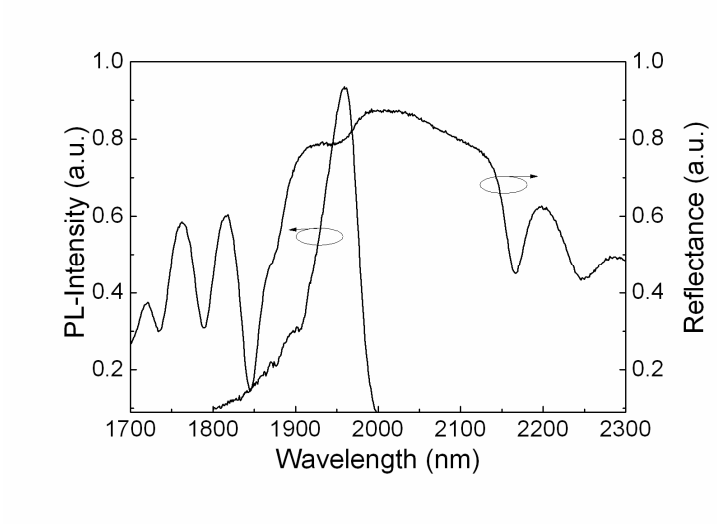

Figure 2. Room temperature PL and reflectance from VECSEL-1

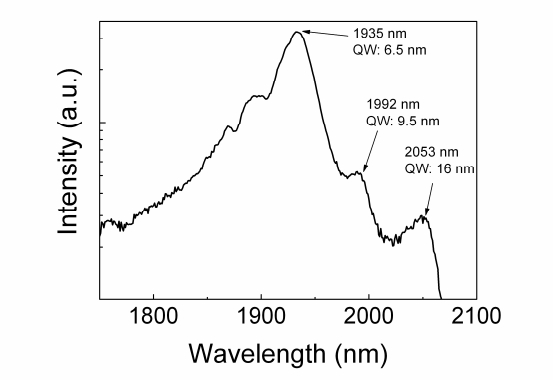

Figure 3. Room temperature PL from VECSEL-2 PL-sample

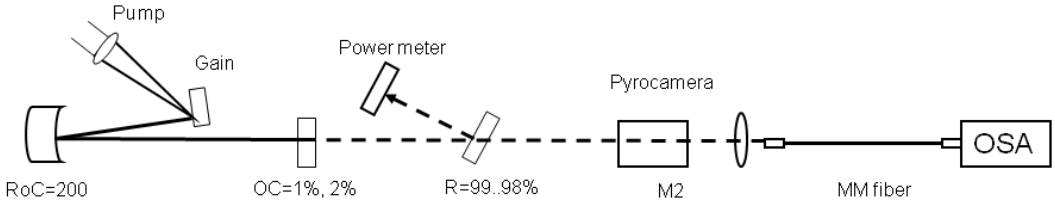

Figure 4. Measurement setup for VECSELs (OSA=optical spectrum analyzer, RoC=radius of curvature, MM=multimode)

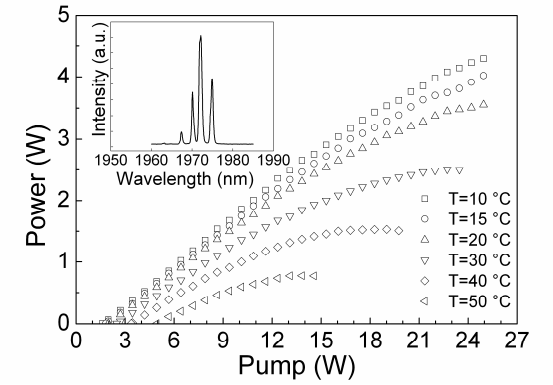

Figure 5. Light output characteristics of VECSEL-1 at different mount temperatures, given as a function of incident 980 nm pump power. About 12 % of the pump was reflected from the sample. The reflected power is not taken into account in this graph. Inset: typical laser spectrum.

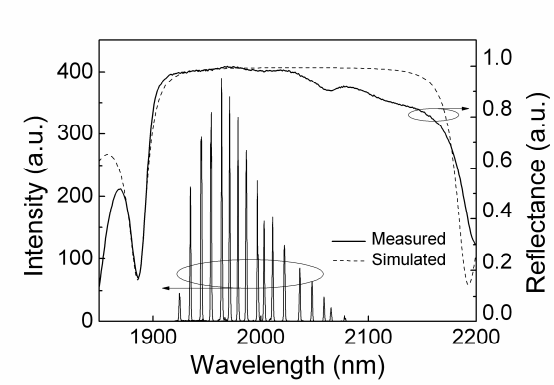

Figure 6. Example of spectra obtained by filtering (the intensity is normalized to maximum emitted power). Each lasing peak in the graph represents a narrowband spectrum selected by the birefringent filter and consists of multiple longitudinal modes. The simulated DBR-reflectance and the reflectance corresponding to VECSEL-2 are also presented.

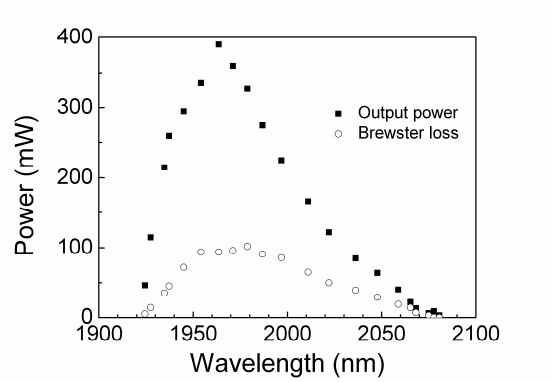

Figure 7. Output power of VECSEL-2 at different wavelengths. Brewster losses refer to reflection losses from the birefringent filter.

Appendix B

Publication 2

Picosecond passively mode-locked GaSb-based semiconductor disk laser operating at 2 μm

Antti Härkönen,[1,*] Jonna Paajaste,[1] Soile Suomalainen,[1] Jukka-Pekka Alanko,[1] Christian Grebing,[1] Riku Koskinen,[1] Günter Steinmeyer,[2,1] and Mircea Guina[1]

[1]*Optoelectronics Research Centre, Tampere University of Technology, Korkeakoulunkatu 3, 33720 Tampere, Finland*

[2]*Max Born Institute for Nonlinear Optics and Short Pulse Spectroscopy, Max-Born-Straße 2 A, 12489 Berlin, Germany*

**Corresponding author: antti.harkonen@tut.fi*

Received September 29, 2010; revised November 8, 2010; accepted November 8, 2010; posted November 10, 2010 (Doc. ID 135844); published December 1, 2010

We report on a passively mode-locked optically pumped GaSb-based semiconductor disk laser producing stable picosecond optical pulses at a 1.95 μm wavelength. The gain mirror was comprised of a 15 quantum well InGaSb/GaSb structure. A fast semiconductor saturable absorber mirror with three InGaSb/GaSb quantum wells was used to attain self-starting mode-locked operation at a fundamental repetition rate of 881.2 MHz. The laser produced pulses with 30 pJ energy and a duration of 1.1 ps within a factor of 2 of the Fourier limit. © 2010 Optical Society of America

OCIS codes: 140.3070, 140.4050, 140.5960, 140.7270.

The gallium-antimonide (GaSb) material system enables fabrication of semiconductor lasers operating in the 2–4 μm wavelength range. This eye-safe wavelength region is particularly important for spectroscopic, sensing, medical, and military applications [1–3]. Present edge-emitting diode lasers based on the (AlGaIn)(AsSb) material system can cover the 2.0–2.7 μm spectral band but exhibit poor-quality elliptical output beams or relatively low output powers. Their tuning range is also typically below 10 nm. On the other hand, semiconductor disk lasers (also called VECSELs [4]) generally offer good beam quality, wavelength versatility, and narrow linewidth emission [5], as well as a large tuning range (~150 nm) and multiple watts of output power [6,7]. Recently, electrically pumped devices and active mode-locking have also been demonstrated [8,9]. However, the demonstration of ultrashort pulse operation based on passive mode-locking has remained elusive so far, partially due to a lack of technological developments for the key components, such as semiconductor saturable absorber mirrors (SESAMs). In contrast, passively mode-locked GaAs-based ~1 μm semiconductor disk lasers have been developed intensively for a number of years, owing to the wide availability of the semiconductor gain material and mature fabrication technology. These developments have led to notable achievements in terms of high average power and ultrashort pulse operation [10,11]. The laser architecture allows also for high pulse repetition rates using short cavity lengths, and for the use of integrated gain-absorber-mirror structures [12]. There is a strong motivation to transfer the favorable qualities of mode-locked semiconductor disk lasers also to the 2–3 μm wavelength region, where short pulse lasers could find applications in time-resolved molecular spectroscopy as pump sources for synchronously pumped optical parametric oscillators (OPOs) operating in the mid-IR above 5 μm, or as seeders for optical amplifiers and mid-IR supercontinuum lasers [13].

In this Letter, we report the development of an ultrashort pulse 2 μm semiconductor disk laser based on the use of gain and saturable absorber mirrors comprising InGaAs/GaSb quantum wells (QWs). To our knowledge, this is the first report on a passively mode-locked antimonide disk laser.

The semiconductor gain and absorber mirrors used in this study were grown using a conventional solid source molecular beam epitaxy reactor. The gain mirror included a distributed Bragg reflector (DBR) and a resonant periodic gain region with 15 quantum wells. First, a GaSb buffer layer was grown on an n-doped (100)-oriented GaSb substrate, which was followed by 18.5 pairs of lattice matched AlAsSb/GaSb $\lambda/4$ layers forming the bottom DBR with 99.9% theoretical reflectivity. The active region included five equally spaced groups of $In_{0.2}Ga_{0.8}Sb$ QWs, each group containing three quantum wells with 8 nm thickness embedded in GaSb. The structure was concluded with a lattice matched $AlA_{0.08}Sb_{0.92}$ window layer and a thin GaSb cap layer. The microcavity between the DBR and the window layer had an optical thickness of 3 λ. The window and cap layer were, in total, $\lambda/4$ thick. A 2.5 mm × 2.5 mm piece of as-grown gain material was capillary bonded to a wedged diamond heat spreader with 3 mm × 3 mm × 0.2–0.3 mm size. The heat spreader ensures excellent heat extraction from the pumped spot and was later antireflection coated to avoid surface reflections. The component was clamped to a large copper heat sink that was kept at 15 °C with a Peltier element.

The SESAM had an antiresonant design [14] comprising three $In_{0.29}Ga_{0.71}Sb$ QWs embedded within GaSb layers. The modulation depth of the SESAM was estimated to be in the range of 1.5%–2%. The absorption recovery time was determined with a pump–probe system where the source was an idler wave of a Spectra Physics Opal OPO tuned to 2.0 μm. The average power from the source was about 150 mW with a 80 MHz repetition rate, a 150 fs pulse duration, and about 2 nJ pulse energy.

0146-9592/10/244090-03$15.00/0

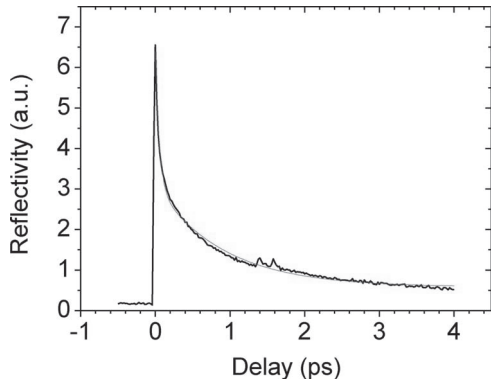

Fig. 1. (Color online) Pump–probe recovery trace measured from a six quantum well test sample. Double exponential fitting has a fast time component of 0.53 ps and a slow time component of 9 ps. The two small peaks at about 1.5 ps delay appear due to insufficiently suppressed spurious reflections in the pump–probe setup.

Estimated pulse fluence was less than 60 μJ/cm^2. Because of the low measurement sensitivity of the 2 μm pump–probe system used to characterize the absorption recovery time, we were not able to obtain reliable characterization data for the SESAM incorporating only three QWs. Instead, for recovery time measurements, we have used mirrors incorporating six and ten QWs, and, hence, having higher modulation depth, with otherwise similar composition as the SESAM used in the mode-locking experiments. The pump–probe absorption recovery trace is shown in Fig. 1, revealing double exponential decay characteristics with a fast time component of 0.53 fs and a slow component of 9 ps. The measurement should give a fair estimate of the SESAM properties and indicates that it is very fast.

Figure 2 shows the z-shaped laser cavity employed, with the gain chip and the SESAM serving as folding mirror and cavity end mirror, respectively. A ~230 μm diameter spot on the gain mirror was pumped optically with a fiber-coupled 980 nm diode laser. The laser mode size was matched to the pumped area on the gain. The simulated mode diameter on the SESAM was ~25 μm. The output of the laser was coupled into a single-mode optical fiber and further analyzed by a 2.5 GHz photodiode, spectrum analyzer, and an autocorrelator.

The output power characteristics shown in Fig. 3 were measured with a thermal power meter and exhibited a hysteresis typical for many mode-locked lasers. Mode

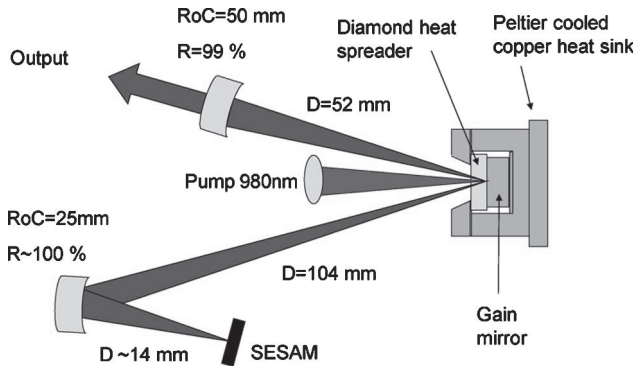

Fig. 2. (Color online) Schematics of the laser cavity. RoC, radius of curvature; R, reflectivity.

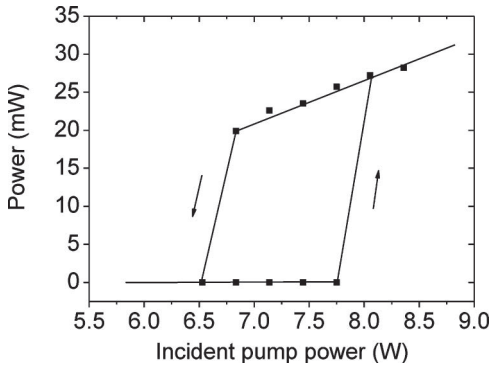

Fig. 3. Laser output with bi-stable characteristics.

locking was initiated at 8 W of pump power. Once initiated, the pump power could be reduced to ~6.8 W with stable mode locking. The slope efficiency estimated from the graph was about 0.6%.

The rf spectrum shown in Fig. 4 was measured from the output pulse train using a commercial 2.5 GHz photodiode. The rf spectrum reveals clean mode locking at the fundamental cavity repetition rate of 881.2 MHz with a pedestal-like substructure at below –50 dBc at a 1 kHz resolution bandwidth. The absence of pronounced frequency components indicates the practical absence of Q-switched mode-locking.

Lasing was observed near the 1950 nm wavelength, as shown in Fig. 5(a). Modulations in the spectrum were observed to originate from the double-sided polished gain and SESAM wafers acting as etalons in the laser cavity. The central operation wavelength could vary up to 10 nm with the alignment of the laser. The pulse width of the laser was measured using an interferometric autocorrelation method. We obtained an autocorrelation trace with 1.9 ps width (FWHM), as shown in Fig. 5(b). For diagnostic purposes, we extracted the intensity autocorrelation from this trace and fitted a polynomial spectral phase to the amplitude data from Fig. 5(a) to obtain the best possible agreement with the measured autocorrelation; see Fig. 5(c). The reconstructed pulse shape is shown in Fig. 5(d). Our procedure retrieves a pulse duration of 1.1 ps, which is a factor of 1.8 above the bandwidth limit. Assumption of a sech^2 pulse shape results in a slightly longer pulse duration of 1.2 ps. Our analysis indicates a dominant contribution from second-order dispersion with an estimated absolute value of ~0.29 ps^2. The dispersion

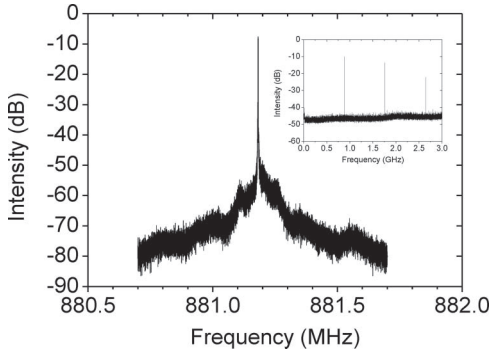

Fig. 4. Radio-frequency spectrum of the output pulse train with 881.2 MHz repetition frequency. Resolution bandwidth 1 kHz. Measured with a 2.5 GHz photodiode. Inset, wide-scan rf spectrum.

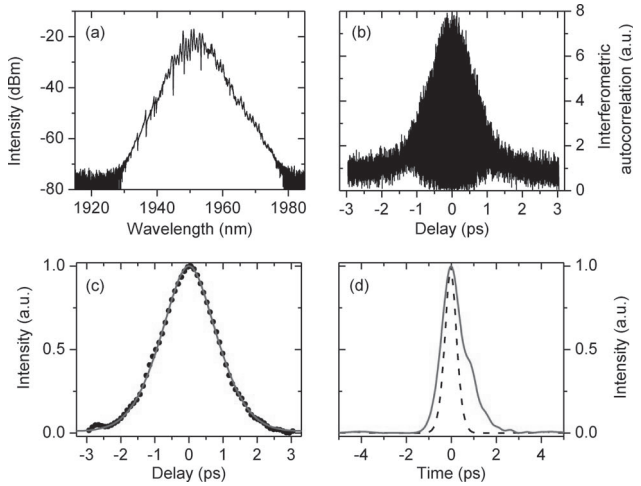

Fig. 5. (Color online) (a) Optical spectrum at 1950 nm. (b) Measured interferometric two-photon absorption autocorrelation trace. (c) Intensity autocorrelation traces extracted from the measured interferometric signal (black dots) and calculated from the reconstructed pulse shape (red solid curve). (d) Reconstructed temporal pulse shape (red solid curve) and transform-limited pulse (black dashed curve) calculated from the laser spectrum. Measurement carried out with 8.4 W of pump power.

is likely to originate from the fiber patch cord used to couple light to the autocorrelator.

In conclusion, we have demonstrated a short pulse passively mode-locked GaSb disk laser that was operated at a 881.2 MHz repetition rate at the wavelength of 1950 nm. A three quantum well InGaSb saturable absorber mirror was deployed in the laser that produced pulses with a duration of about 1.1 ps. The combination of high repetition rate and near-picosecond pulse duration, together with 25 mW output power, opens a new perspective for the otherwise difficult-to-access wavelength regime above 2 μm.

The authors thank Jari Nikkinen for coating the diamond and Lasse Orsila for valuable technical help with the measurement equipment. This work was financially supported by the United States Office of Naval Research (ONR) Global under the grant number N62909-10-1-7030.

References

1. R. Targ, B. C. Steakley, J. G. Hawley, L. L. Ames, P. Forney, D. Swanson, R. Stone, R. G. Otto, V. Zarifis, P. Brockman, R. S. Calloway, S. H. Klein, and P. Robinson, Appl. Opt. **35**, 7117 (1996).
2. D. Theisen, V. Ott, H. W. Bernd, V. Danicke, R. Keller, and R. Brinkmann, Proc. SPIE **5142**, 96 (2003).
3. F. K. Tittel, D. Richter, and A. Fried, in *Solid-State Mid-Infrared Laser Sources*, I. T. Sorokina and K. L. Vodopyanov, eds., Vol. 89 of Topics in Applied Physics (2003), pp. 445–516.
4. M. Kuznetsov, F. Hakimi, R. Sprague, and A. Mooradian, IEEE Photon. Technol. Lett. **9**, 1063 (1997).
5. M. Rattunde, B. Rösener, S. Kaspar, R. Moser, C. Manz, K. Köhler, and J. Wagner, "GaSb-based semiconductor disk lasers for the 2–3 μm wavelength range: versatile lasers for high-power and narrow linewidth emission," presented at Conference on Lasers and Electro-Optics/Quantum Electronics and Laser Science, May 16–21, 2010, San Jose, Calif., paper CWE3.
6. J.-M. Hopkins, N. Hempler, B. Rösener, N. Schulz, M. Rattunde, C. Manz, K. Köhler, J. Wagner, and D. Burns, Opt. Lett. **33**, 201 (2008).
7. J. Paajaste, S. Suomalainen, R. Koskinen, A. Härkönen, M. Guina, and M. Pessa, J. Cryst. Growth **311**, 1917 (2009).
8. A. Härkönen, A. Bachmann, S. Arafin, K. Haring, J. Viheriälä, M. Guina, and M.-C. Amann, Proc. SPIE **7720**, 772015 (2010).
9. A. Härkönen, J. Rautiainen, L. Orsila, M. Guina, K. Rössner, M. Hümmer, T. Lehnhardt, M. Müller, A. Forchel, M. Fischer, J. Koeth, and O. G. Okhotnikov, IEEE Photon. Technol. Lett. **20**, 1332 (2008).
10. A. Aschwanden, D. Lorenser, H. J. Unold, R. Paschotta, E. Gini, and U. Keller, Opt. Lett. **30**, 272 (2005).
11. K. G. Wilcox, Z. Mihoubi, G. J. Daniell, S. Elsmere, A. Quarterman, I. Farrer, D. A. Ritchie, and A. Tropper, Opt. Lett. **33**, 2797 (2008).
12. A.-R. Bellancourt, Y. Barbarin, D. J. H. C. Maas, M. Shafiei, M. Hoffmann, M. Golling, T. Südmeyer, and U. Keller, Opt. Express **17**, 9704 (2009).
13. J. H. V. Price, T. M. Monro, H. Ebendorff-Heidepriem, F. Poletti, P. Horak, V. Finazzi, J. Y. Y. Leong, P. Petropoulos, J. C. Flanagan, G. Brambilla, X. Feng, and D. J.Richardson, IEEE J. Sel. Top. Quantum Electron. **13**, 738 (2007).
14. U. Keller, K. J. Weingarten, F. X. Kärtner, D. Kopf, B. Braun, I. D. Jung, R. Fluck, C. Hönninger, N. Matuschek, and J. Aus der Au, IEEE J. Sel. Top. Quantum Electron. **2**, 435 (1996).

Appendix C

Publication 3

Power scalable 2.5 μm (AlGaIn)(AsSb) semiconductor disk laser grown by molecular beam epitaxy

J. Paajaste*, R. Koskinen, J. Nikkinen, S. Suomalainen and O. G. Okhotnikov

Optoelectronics Research Centre, Tampere University of Technology, P.O. Box 692, FIN-33101 Tampere, Finland

*jonna.paajaste@tut.fi

Abstract:

We demonstrate first GaSb-based semiconductor disk laser (SDL) emitting 0.6 W of output power at 2.5 μm. A gain structure comprising 15 strained $In_{0.35}Ga_{0.65}As_{0.09}Sb_{0.91}$ quantum wells sandwiched between $Al_{0.35}Ga_{0.65}As_{0.035}Sb_{0.965}$ barriers was grown by molecular beam epitaxy on (100) n-doped GaSb substrate and demonstrates promising potential for power scaling and wavelength tuning.

Keywords: A3. Molecular beam epitaxy, B1. Antimonides, B2. Semiconducting III-V materials, B3. Infrared devices

1. Introduction

The nearly lattice-matched III–V semiconductor material system (AlGaIn)(AsSb) establishes a firm platform for optoelectronic devices operating in the mid-infrared spectral range. Lattice-matched or strain-compensated structures employing InGaAsSb as the active material and

AlGaAsSb for barrier and cladding layers grown on GaSb substrates are demonstrated to be the best choice for long-wavelength lasers and photodetectors. Their applications include chemical sensing, biomedicine and thermal imaging [1–3].

The primary advantage of semiconductor disk laser (SDL) concept compared with in-plane diode lasers is an improved mode control which enables high output power with diffraction-limited beam quality [4-7]. The GaSb system is particularly suitable for lasers with vertical-cavity configuration since this material system enables the use of lattice matched distributed Bragg reflectors (DBRs) comprised of layers with a high refractive-index contrast, namely $AlAs_{0.08}Sb$ and GaSb. Such DBRs have an exceptionally broad stop-band and require a relatively small number of layer pairs to achieve high reflectance. The broad stopband makes GaSb-based vertical-cavity lasers highly promising for spectroscopic application requiring a wide tuning range.

In this study we focus on MBE growth of an optically-pumped semiconductor disk lasers emitting at 2.5 μm and study their potential for power scalability.

2. Growth details and structural design

The semiconductor structures used in this work were grown using a conventional solid source molecular beam epitaxy reactor (ten-port V80H). Elemental indium, aluminum and gallium together with As_4 and Sb_4 were used as group III and V sources respectively. The group V constituents were cracked into As_2 and Sb_2 using high temperature cracking tubes. SDL structure was grown on an n-GaSb wafer (100). The structure consists of 21.5 pairs of lattice matched $GaSb/AlAs_{0.085}Sb_{0.915}$ distributed Bragg reflector (DBR) and a gain region with 15 strained $In_{0.35}Ga_{0.65}As_{0.09}Sb_{0.91}$ quantum-wells (QWs) surrounded by 20 nm thick $Al_{0.35}Ga_{0.65}As_{0.035}Sb_{0.965}$ barriers.

The type I QWs were 9.5 nm thick and embedded in groups of three in $Al_{0.5}Ga_{0.5}As_{0.04}Sb_{0.96}$ waveguide which provides dominant pump absorption. The gain structure was closed with a $AlAs_{0.085}Sb_{0.915}$ window layer to ensure good carrier confinement, and a thin GaSb cap layer was grown on top to prevent oxidation. The GaSb layers were grown at 500 °C with V/III ratio 4 where as aluminium containing layers were grown at higher temperature (520 °C) and also with higher V/III ratios (DBR with V/III ratio 18 and barriers with 6). The QWs were grown at 450 °C with V/III ratio 5. Layer thicknesses were selected to form a 3λ micro-cavity between the DBR and the semiconductor-air boundary; QW groups were located at the antinodes of the standing-wave optical field in the micro-cavity. The photoluminescense (PL) and reflectance measured from the structure are shown in Fig.1 together with the SDL cavity conductance band energy schematic.

The structure was processed using an intra-cavity diamond heat spreader technique [8]. A 2.5×2.5 mm^2-size gain chip was capillary bonded with water to a type IIa natural diamond heat spreader to enable efficient heat removal from the active region. The bonded chip was finally pressed between two copper plates, with a small hole in the top plate allowing the passage of pump and signal. The mounted sample was attached to a water cooled copper heat sink.

3. Experimental results

The laser cavity, shown in Fig. 2, has a V-type configuration comprised of mounted gain chip, a high reflective folding mirror with radius of curvature of 100 mm and a 1 % plane output coupler. The pump beam from 980 nm fiber coupled diode laser is focused on the gain mirror to a spot of 180 μm in diameter at an angle of 30° to the surface normal. The cavity was simulated numerically to ensure that the mode size at the gain mirror matches the pump spot. The output power of ~600 mW

has been achieved at heatsink temperature of 5 °C, as seen from Fig. 3, with the typical spectrum shown as an inset. The beam quality factor increases with pump power, as shown in Fig. 4. M^2 value was determined by measuring 50 times $1/e^2$ width around the waist with pyrocamera and by fitting data to Gaussian beam equation. M^2 was measured to be below 1.6 for the highest output power of 0.6 W. It can be seen that the power scaling is limited by thermal rollover indicating an excessive heating of the gain medium. Laser operation has been achieved for the heatsink temperatures up to 40 °C. The wavelength tuning from 2.45 µm beyond 2.5 µm has been observed by changing the pump power (Fig. 5). The fringes in the spectrum are due to the Fabry-Pèrot etalon effect induced by the uncoated intracavity diamond heat spreader. The large quantum defect (i.e. pump wavelength is much smaller than lasing wavelength) is likely to be one of the main sources of the high thermal load to the gain element and together with inefficient heat removal due to GaSb material system's poor thermal conductivity, it degreases the output power achieved. Further improvement in power scaling is expected therefore with implementation of long-wavelength pumping.

4. Conclusions

This study presents the fabrication and characterization of a GaSb-based semiconductor disk laser emitting around 2.5 µm. With an intra-cavity diamond heat spreader for thermal management, 600 mW of output power has been achieved with good beam quality. The results show that the advantages of high-power disk laser technology can be extended to 2.5 µm and beyond utilizing (AlGaIn)(AsSb) semiconductor compounds. Future development includes 1.6–2 µm low quantum defect pumping to prevent thermal rollover and beam degradation due to thermal lens which would allow achieving multi-Watt operation.

5. Acknowledgements

This work was supported by the Academy of Finland and the Ministry of Education of Finland (NanoPhotonics Extencion project) and the National Graduate School of Material Physics.

References:

[1] P.Werle, A review of recent advances in semiconductor laser based gas monitors Spectrochem. Acta A, Mol. Bimol. Spectrosc 54, 2 (1998) 197–236

[2] R. F. Curl and F. K. Tittel, Tunable infrared laser spectroscopy, Annu. Rep. Prog. Chem., Sect. C 98 (2002) 219–272

[3] A. L. McKenzie, Physics of thermal processes in laser-tissue interaction, Phys. Med. Biol. 35 (1990) 1175-1209

[4] H. K. Choi, J. N. Walpole, G. W. Turner, M. K. Connors, L. J. Missaggia, and M. J. Manfra, GaInAsSb–AlGaAsSb Tapered Lasers Emitting at 2.05 m with 0.6-W Diffraction-Limited Power, IEEE Photon. Technol. Lett., 10, 7 (1998)

[5] A. Härkönen, M. Guina, and O. Okhotnikov, K. Röβner, M. Hümmer, T. Lehnhardt, M. Müller, and A. Forchel, M. Fischer, 1-W antimonide-based vertical external cavity surface emitting laser operating at 2-μm, Opt. Expr. 14, 14 (2006)

[6] L. Fan, M. Fallahi, J.T. Murray, R. Bedford, Y. Kaneda, A.R. Zakharian, J. Hader, J.V. Moloney, W. Stolz and S.W. Koch, Tunable high-power high-brightness linearly polarized vertical-external-cavity surface-emitting lasers, Appl. Phys. Lett. 88 (2006)

[7] J.-M. Hopkins, N. Hempler, B. Rösener, N. Schulz, M. Rattunde, C. Manz, K. Köhler, J. Wagner, and D. Burns: High-power, (AlGaIn)(AsSb) semiconductor disk laser at 2.0 µm, Opt. Lett. 33, 2 (2008)

[8] A. J. Kemp, G. J. Valentine, J.-M. Hopkins, J. E. Hastie, S. A. Smith, S. Calvez, M. D. Dawson, and D. Burns: Thermal Management in Vertical-External-Cavity Surface-Emitting Lasers: Finite-Element Analysis of a Heatspreader Approach, IEEE J. Quantum Electr. 41, 2, (2005)

Figure captions:

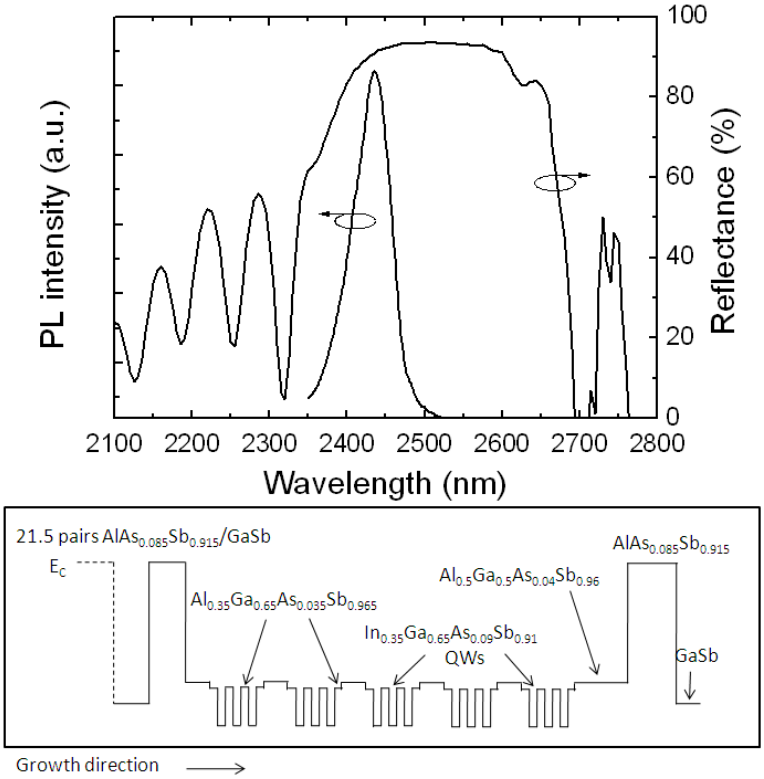

Figure 1. PL and reflectance measured from the structure are shown together with the SDL cavity conductance band energy (E_C) schematic.

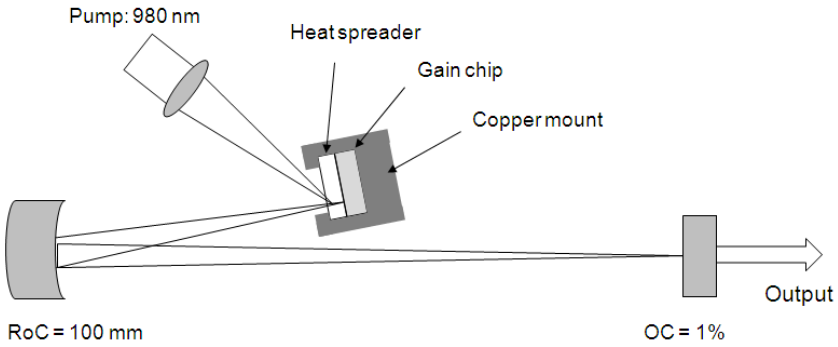

Figure 2. V-type cavity of the laser. RoC=radius of curvature, OC=output coupler, curved mirror reflectance is 100%.

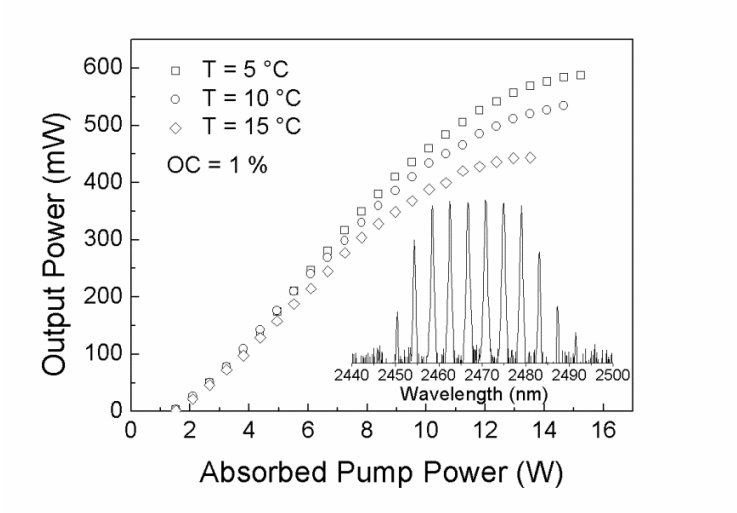

Figure 3. Output power versus 980 nm absorbed pump power. Inset: typical optical spectrum.

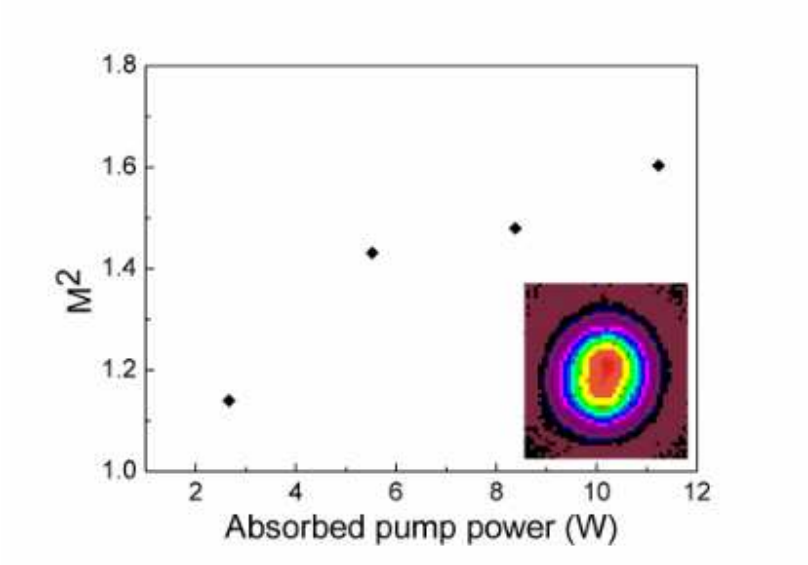

Figure 4. M^2 as a function of absorbed pump power, T = 5 °C. Inset: typical beam profile. Absorbed pump power is 11.2 W.

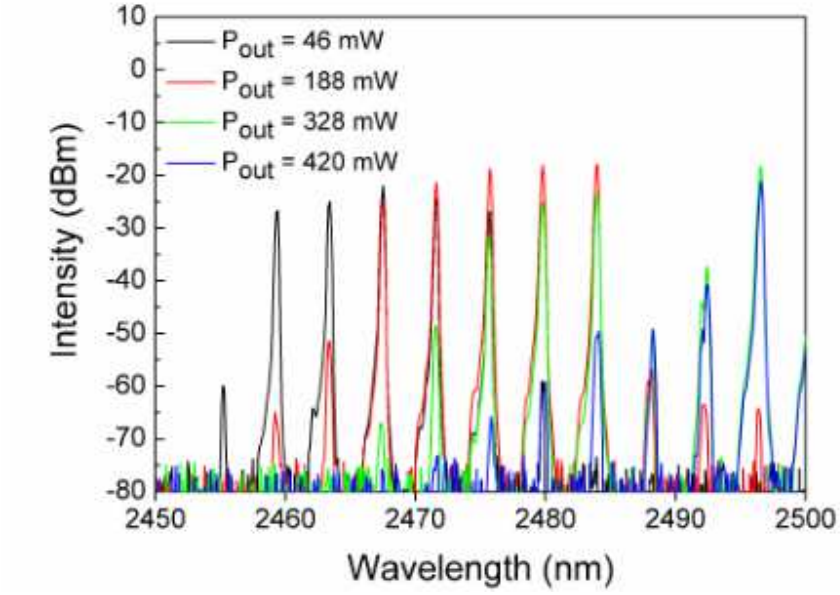

Figure 5. Laser spectra measured for different pump powers, T = 15 °C.

Appendix D

Publication 4

Phys. Status Solidi C 9, No. 2, 294–297 (2012) / DOI 10.1002/pssc.201100299

physica status solidi c
www.pss-c.com
current topics in solid state physics

GaSb-based semiconductor saturable absorber mirrors for mode-locking 2 μm semiconductor disk lasers

Jonna Paajaste[*,1], Soile Suomalainen[,1], Riku Koskinen[1], Antti Härkönen[1], Günter Steinmeyer[1,2], and Mircea Guina[1]**

[1] Optoelectronics Research Centre, Tampere University of Technology, P.O. Box 692, 33101 Tampere, Finland
[2] Max Born Institute for Nonlinear Optics and Short Pulse Spectroscopy, Max-Born-Straße 2 A, 12489 Berlin, Germany

Received 1 July 2011, revised 8 August 2011, accepted 15 August 2011
Published online 9 November 2011

Keywords GaSb, molecular beam epitaxy, SESAM, mode-locking

* Corresponding author: e-mail jonna.paajaste@tut.fi, Phone: +358 (0)40 198 1053
** e-mail soile.suomalainen@tut.fi, Phone: +358 (0)40 198 1067

GaAs- and InP-based Semiconductor saturable absorber mirrors (SESAMs) operating at around 1 μm and 1.55 μm wavelength domains are well understood reliable components used in a large variety of ultrafast lasers. Recently, we demonstrated the first 2 μm GaSb based saturable absorber mirrors used for pico- and femtosecond pulse generation in a mode-locked semiconductor disk laser. Here we report on the fabrication and characterization of similar type of GaSb-based SESAMs with an in-depth focus on the growth parameters and their impact on the dynamic properties of the SESAMs. In particular the effects of quantum well growth temperature and strain on absorption recovery time were investigated by pump probe measurements. The results reveal fast absorption recovery times for SESAMs grown under typical growth conditions used to fabricate high quality quantum-well laser structures. The absorption recovery exhibited a double exponential decay characteristic with a fast component having a characteristic time of about 0.5 ps and a slow component of about 10 ps.

1 Introduction Semiconductor saturable absorber mirrors (SESAMs) have had a strong impact on the development of practical ultrafast lasers [1]. More recently, SESAMs have been used for mode-locking of semiconductor disk lasers (SDLs) [2], also known as vertical external cavity surface emitting lasers [3]. It has been shown that integration of a gain mirror and a SESAM serves to provide a highly compact laser design, capable of producing multiple watts of output power [4]. The compactness, together with the wavelength versatility and mature semiconductor fabrication technology, makes this laser concept very interesting also from a commercial point of view.

Passively mode-locked SDLs have been developed for a number of years using gain structures grown on GaAs and InP substrates. Lasers based on these two material systems typically emit light at 630–1600 nm, although in some cases the InP laser can be engineered to emit at longer wavelengths. Lately, the advances in the development of GaSb-based semiconductor disk lasers operating at spectral range between 1.95 and 2.8 μm [5, 6] have created an interest to extend the mode-locked SDL concept for coverage of 2–3 μm, as well.

Recently, we reported the first SESAM mode-locked semiconductor disk lasers at 2 μm based on the gallium-antimonide (GaSb) material system [7, 8]. In this paper we report the first investigation of ultrafast nonlinear processes in GaSb-based SESAMs used for mode-locking of 2-μm SDLs. The GaSb SESAMs operating at wavelengths around 2 μm and above would have a significant impact on the development of practical ultrafast lasers required for important applications in medicine [9], time-resolved molecular spectroscopy, or as seeders for optical amplifiers and mid-IR supercontinuum lasers [10].

2 SESAM characteristics and fabrication

SESAMs are nonlinear mirrors, in which the optical losses are reduced at high intensities of incoming light. Consequently, when used as a cavity mirror in a laser, the SESAM supports formation of high intensity pulses. A typical structure consists of a highly reflective semiconductor bottom mirror (distributed Bragg reflector – DBR)

and an absorber region that may be either semiconductor bulk material or, more typically, incorporate quantum wells (QWs) or quantum dots. A Fabry–Pérot microcavity is formed between the bottom reflector and the semiconductor–air interface that may sometimes be coated to have a particular value of reflectivity. The cavity can be designed to be resonant or anti-resonant at the operating wavelength, the former implying that the optical length of the microcavity is a multiple of the operating wavelength. In such a resonant structure, the effective interaction length of light in the absorber material is enhanced at the operation wavelength, which strongly enhances the modulation depth on the nonlinear reflectivity. In a low gain laser such as the semiconductor disk laser, antiresonant SESAM design is usually favourable. The nonlinear reflectivity of SESAMs can be also tailored by the design and material composition of the absorber region and by adjusting the reflectivity of the top most surface.

The nonlinear behaviour of SESAMs is characterized by a set of parameters such as nonsaturable losses α_0, modulation depth ΔR, saturation fluence F_{sat}, and the recovery time of the saturable absorption τ_{rec}. A schematic of the nonlinear characteristic of a SESAM, pointing out the main device parameters, is shown in Fig. 1. Typically the recovery time of the absorption is composed of fast and slow time components. The fast response is due to carrier thermalization and the slow one is governed by radiative or non-radiative electron-hole recombination and trapping of carriers. Both, fast and slow response, contribute to passive mode-locking.

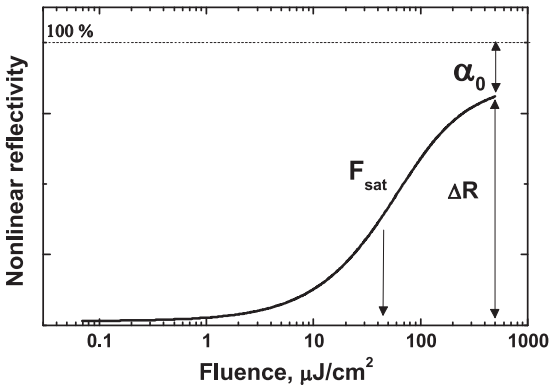

Figure 1 An example of the nonlinear characteristics of a SESAM.

Traditional InP- and GaAs-based SESAM materials have been studied thoroughly for the past decade. Within these materials, the recovery of saturable absorption in as-grown QW structures usually occurs on a nanosecond time scale. However, in many applications such as mode-locking, τ_{rec} is preferably in the range of picoseconds or hundreds of femtoseconds [11]. Therefore, appropriate growth and post-processing methods have been developed for these materials, in order to obtain SESAMs suitable for mode-locking. Techniques, such as low-temperature growth [12], doping of the active region [13], and heavy-ion-implantation, have been exploited for this purpose. All these methods have also disadvantages, such as critical control of growth parameters and/or the degradation of the optical quality of the material.

The GaSb based SESAM structures were grown using a conventional molecular beam epitaxy system. Elemental In, Ga, and Al were used, and Sb_2 and As_2 were cracked from Sb_4 and As_4. First, a GaSb-buffer was grown on a (100) n-GaSb substrate followed by 18.5 pairs of lattice-matched AlAsSb/GaSb distributed Bragg reflector structure. The absorber region was designed to be antiresonant at the operating wavelength, and it consisted of three 8.5 nm $In_xGa_{1-x}As_ySb_{1-y}$ quantum wells embedded in GaSb (a schematic of the design is shown in Fig. 2).

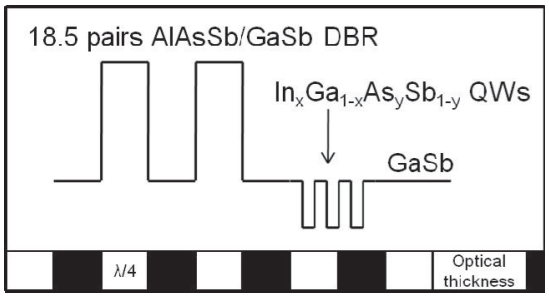

Figure 2 The basic layer structure of the studied GaSb SESAMs .

In order to analyze the impact of growth condition on the absorption recovery time of GaSb-based absorbers, we fabricated two sets of samples using different growth temperature and QWs designs. Samples T1816, T1817, and T1818, comprised $In_{0.29}Ga_{0.71}Sb$ QWs grown at 530 °C, 480 °C, and 430 °C respectively. In another series, the strain of the QWs was varied; the strain values for samples T1816, T1822 and T1825 were 1.82 %, 0.75 % and 0.97 %, respectively. The corresponding QW compositions were $In_{0.29}Ga_{0.71}Sb$, $In_{0.22}Ga_{0.78}As_{8.8}Sb_{91.2}$ and $In_{0.25}Ga_{0.75}As_{8.1}Sb_{91.9}$ for samples T1816, T1822 and T1825, respectively. The composition was changed in such a way that the peak of the photoluminescence remained at 2030–2050 nm, as shown in Fig. 3.

The reflectance spectra of all SESAMs were very similar since the DBRs were identical in all the samples. An example of the reflectance is shown in Fig. 3.The QW strain was determined from XRD measurements.

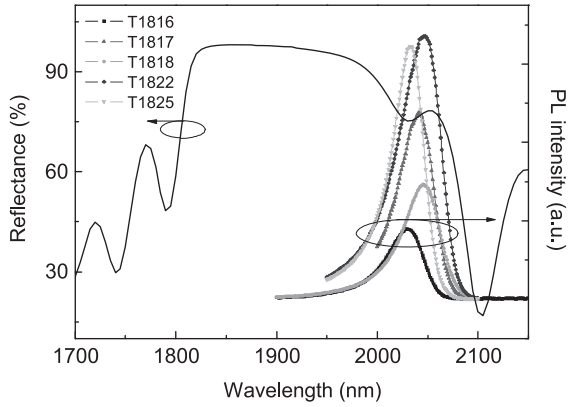

Figure 3 Photoluminescence of all SESAMs and an example graph of the reflectance.

3 Results

The absorption recovery times of the SESAMs were determined with a pump–probe system, where the source was an idler wave of a Spectra Physics Opal OPO tuned to 1.99 μm. The average power from the source was about 150 mW with an 80 MHz repetition rate, 150 fs pulse duration, and about 2 nJ pulse energy. The estimated pulse fluence was less than 60 μJ/cm^2.

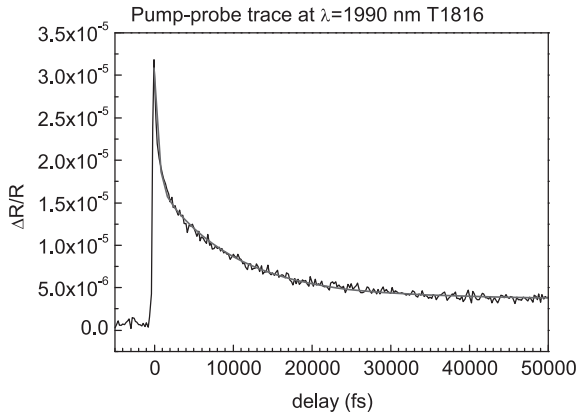

Figure 4 A pump-probe trace with double exponential fitting.

The pump-probe absorption recovery trace for sample T1816 is shown as an example in Fig. 4, revealing double-exponential decay characteristics with a fast time component of 0.44 ps and a slow component of 9.24 ps. The characterization results of all SESAMs are compiled in Table 1.

The measurements give a fair estimate of the SESAMs properties and indicate that SESAMs grown under normal laser growth conditions are already very fast. From Table 1 it can be seen that the effect of decreasing QW growth temperature on absorption recovery time is negligible in the tested temperature range. Moreover, when QW composition is tailored to reduce the strain in QWs, only a slight increase in recovery time is observed. This behavior is rather peculiar when compared to GaAs and InP material systems. It is interesting to note that the as-grown QW structures exhibit such a small value of the absorption recovery time, while at the same time showing excellent optical quality. For comparison, the absorption recovery time of as-grown high-quality InP-based SESAMs is in the range of 1 ns. The reason for different properties of GaSb-based SESAMs is very interesting and raises many questions. The increase of recovery time with lower strain values can be explained partially by reduced confinement of valence band holes. Considering the general recombination properties of GaSb-based materials compared to GaAs and InP-based materials, we consider Auger recombination a likely explanation for the faster response. It is known that the Auger recombination coefficients are larger in GaSb by an order of magnitude than in GaAs and InP based materials [14–16].

Table 1 Pump probe measurement results.

Sample	QW temp. (°C)	Strain (%)	τ_1 (ps)	τ_2 (ps)
T1818	430	1.82	0.56	9.44
T1817	480	1.82	0.44	9.38
T1816	530	1.82	0.44	9.24
T1825	530	0.97	0.53	14.10
T1822	530	0.75	0.35	18.50

4 Conclusions

We report on the first investigation of absorption recovery dynamics in GaSb-based SESAMs operating at around 2 μm. In particular we investigated the dependence between the growth temperature of InGaAsSb QWs and the absorption recovery time of SESAM incorporating such QWs. Results indicate that the recovery time is almost constant for the investigated variation of QW temperature and strain. Compared with traditional GaAs and InP-based SESAMs, the growth temperature used typically for fabrication of high quality QWs results in SESAMs with fast recovery time. The recovery time is within ps range, a value suitable for mode-locking of a large variety of lasers. SESAMs which do not require special growth techniques or post-growth treatments to induce structural defects for achieving fast recovery time, would exhibit more stable parameters for prolonged use in high power ultrafast lasers. A high Auger recombination coefficient typical for low-bandgap materials could explain the ultrafast absorption recovery time. Nevertheless additional material investigations are needed to fully understand the mechanism of absorption recovery for the future development of GaSb based SESAMs.

Acknowledgements The authors would like to thank The National Graduate School of Material Physics, Finnish Foundation for Technology Promotion and US Office of Naval Research Global (NICOP program) for the financial support.

References

[1] U. Keller, K.J. Weingarten, F.X. Kärtner, D. Kopf, B. Braun, I.D. Jung, R. Fluck, C. Hönninger, N. Matuschek, and J. Aus der Au, IEEE J. Sel. Top. Quantum Electron. **2**, 435–453 (1996).

[2] U. Keller and A. C. Tropper, Phys. Rep. 429, 67-120 (2006).

[3] M. Kuznetsov, F. Hakimi, R. Sprague, and A. Mooradian, IEEE Photon. Technol. Lett. **9**, 1063–1065 (1997).

[4] B. Rudin, V.J. Wittwer, D.J.H.C. Maas, M. Hoffmann, O.D. Sieber, Y. Barbarin, M. Golling, T. Südmeyer, and U. Keller, Opt. Express **18**, 27582–27588 (2010).

[5] B. Rösener, M. Rattunde, R. Moser, S. Kaspar, T. Töpper, C. Manz, K. Köhler, and J. Wagner, Opt. Lett. **36**, 319–21 (2011).

[6] M. Rattunde, N. Schulz, B. Rösener, C. Manz, K. Köhler, J. Wagner, J.-M. Hopkins, and D. Burns, Solid State Lasers XVII: Technology and Devices, Proc. SPIE **6871**, 68710Z-68710Z-12 (2008).

[7] A. Härkönen, J. Paajaste, S. Suomalainen, J.-P. Alanko, C. Grebing, R. Koskinen, G. Steinmeyer, and M. Guina, Opt. Lett. **35**, 4090–4092 (2010).

[8] A. Härkönen, C. Grebing, J. Paajaste, R. Koskinen, J.-P. Alanko, S. Suomalainen, G. Steinmeyer, and M. Guina, Electron. Lett. **47**, 454–456 (2011).

[9] A. L. McKenzie, Phys. Med. Biol. **35**, 1175-1209 (1990).

[10] J. H. V. Price, T. M. Monro, H. Ebendorff-Heidepriem, F. Poletti, P. Horak, V. Finazzi, J. Y. Y. Leong, P. Petropoulos, J. C. Flanagan, G. Brambilla, X. Feng, and D. J.Richardson, IEEE J. Sel. Top. Quantum Electron. **13**, 738 (2007).

[11] R. Herda and O.G. Okhotnikov, Appl. Phys. Lett. 86, 011113 (2005).

[12] S. Gupta, J.F. Whitaker, and G.A. Mourou, IEEE J. Quantum Electron. **28**, 2464–2472 (1992).

[13] M. Haiml, U. Siegner, F. Morier-Genoud, U. Keller, M. Luysberg, P. Specht, and E. R. Weber, Appl. Phys. Lett. **74**, 1269 (1999).

[14] D.A. Firsov, L. Shterengas, G. Kipshidze, V.L. Zerova, T. Hosoda, P. Thumrongsilapa, L.E. Vorobjev, and G. Belenky, Semiconductors **44**, 50–58 (2010).

[15] S. Anikeev, D. Donetsky, G. Belenky, S. Luryi, C. A. Wang, J. M. Borrego, and G. Nichols, Appl. Phys. Lett. **83**, 16 (2003).

[16] G. Rainò, A. Salhi, V. Tasco, R. Intartaglia, R. Cingolani, Y. Rouillard, E. Tournié, and M. De Giorgi, Appl. Phys. Lett. **92**, 101931 (2008).

Appendix E

Publication 5

J. Paajaste, S. Suomalainen, A. Härkönen, U. Griebner, G. Steinmeyer, M. Guina ”Absorption recovery dynamics in 2 μm GaSb-based SESAMs”, *Journal of Physics D*, **Revised October 2013**

Tampereen teknillinen yliopisto
PL 527
33101 Tampere

Tampere University of Technology
P.O.B. 527
FI-33101 Tampere, Finland

ISBN 978-952-15-3193-4
ISSN 1459-2045